NASA/TM–20260000913

Calibrating a 3-Axis Accelerometer Instrument with a Less Accurate Calibration Device: Part 2

Hector L. Soto
Langley Research Center, Hampton, Virginia

January 2026

NASA STI Program . . . in Profile

Since its founding, NASA has been dedicated to the advancement of aeronautics and space science. The NASA scientific and technical information (STI) program plays a key part in helping NASA maintain this important role.

The NASA STI program operates under the auspices of the Agency Chief Information Officer. It collects, organizes, provides for archiving, and disseminates NASA's STI. The NASA STI program provides access to the NTRS Registered and its public interface, the NASA Technical Reports Server, thus providing one of the largest collections of aeronautical and space science STI in the world. Results are published in both non-NASA channels and by NASA in the NASA STI Report Series, which includes the following report types:

- TECHNICAL PUBLICATION. Reports of completed research or a major significant phase of research that present the results of NASA Programs and include extensive data or theoretical analysis. Includes compilations of significant scientific and technical data and information deemed to be of continuing reference value. NASA counterpart of peer-reviewed formal professional papers but has less stringent limitations on manuscript length and extent of graphic presentations.

- TECHNICAL MEMORANDUM. Scientific and technical findings that are preliminary or of specialized interest, e.g., quick release reports, working papers, and bibliographies that contain minimal annotation. Does not contain extensive analysis.

- CONTRACTOR REPORT. Scientific and technical findings by NASA-sponsored contractors and grantees.

- CONFERENCE PUBLICATION. Collected papers from scientific and technical conferences, symposia, seminars, or other meetings sponsored or co-sponsored by NASA.

- SPECIAL PUBLICATION. Scientific, technical, or historical information from NASA programs, projects, and missions, often concerned with subjects having substantial public interest.

- TECHNICAL TRANSLATION. English-language translations of foreign scientific and technical material pertinent to NASA's mission.

Specialized services also include organizing and publishing research results, distributing specialized research announcements and feeds, providing information desk and personal search support, and enabling data exchange services.

For more information about the NASA STI program, see the following:

- Access the NASA STI program home page at http://www.sti.nasa.gov

- E-mail your question to help@sti.nasa.gov

- Phone the NASA STI Information Desk at 757-864-9658

- Write to:
  NASA STI Information Desk
  Mail Stop 148
  NASA Langley Research Center
  Hampton, VA 23681-2199

NASA/TM–20260000913

Calibrating a 3-Axis Accelerometer Instrument with a Less Accurate Calibration Device: Part 2

Hector L. Soto
Langley Research Center, Hampton, Virginia

National Aeronautics and
Space Administration

Langley Research Center
Hampton, Virginia 23681-2199

January 2026

Nomenclature

Abbreviations

AAD	Angle articulation device
CD	Calibration Device
KM	Kinematics model
NO	Normalized Output
OA	Optimization Algorithm
OOT	Out of Tolerance
ppm	Parts Per Million
RB	Rigid Body in the local frame of reference O*xyz*
SL	Surface level
1xAI	One-axis accelerometer instrument
2xAI	Two-axis accelerometer instrument
3xAI	Three-axis accelerometer instrument

Symbols

CD Symbols

a	Pitch misalignment of the system (as a rigid body)
b	Roll misalignment of the full system (as a rigid body)
d	Yaw misalignment between the two rotary devices
e	Pitch misalignment of the interface x-y plane
f	Roll misalignment of the interface x-y plane
k	Yaw misalignment of the interface x-z plane
p	Pitch angle, calibration first rotary device articulation of the x-y plane
r	Roll angle, calibration second rotary device articulation of the x-y plane
y	Orientation of the x-z plane alignment with x accelerometer pointing forward or backwards
u	Orientation relative to the x-y plane, mount on top or bottom

Instrument Symbols

p_e	Table variable pitch index error
p_w	Pitch accelerometer offset for axis w; w = x, or z
r_w	Roll accelerometer offset for axis w; w = y, or z
y_w	Yaw accelerometer offset for axis w; w = x, or y
B	Instrument bias vector
S	Instrument sensitivity matrix
V_w	Instrument accelerometer voltage output for axis w = x, y, or z
$V_{NO\#}$	Accelerometer voltage Normalized Output for orientation #; # = 1 or 2

Symbols related to the system

ΔB_w	Delta bias which is equals $\bar{B}_w(Estimate) - \hat{B}_w(True); w = x, y\ or\ z$
$\bar{B}_w$	Estimated Bias; w = x, y, or z
$\hat{B}_w$	True Bias; w = x, y, or z

O*xyz*	Local coordinate frame
O*XYZ*	Global coordinate frame
L	Local frame of reference
G	Global frame of reference
Gwg	Global frame of reference with gravity (g) in the –*Z*-axis
g	gravity
g_v	Instrument local frame projected on the global frame Gwg
ΔS_w	Delta sensitivity which is equals $\bar{S}_x - \hat{S}_x; Where\ \lvert\bar{S}_x\rvert \leq \left\lvert\hat{S}_x(True)\right\rvert; w = x, y\ or\ z$
$\bar{S}_w$	Estimated sensitivity; w = x, y, or z
$\hat{S}_w$	True sensitivity; w = x, y, or z
x	*x*-axis local coordinate frame
y	*y*-axis local coordinate frame
z	*z*-axis local coordinate frame
X	*X*-axis global coordinate frame
Y	*Y*-axis global coordinate frame
Z	Z-axis global coordinate frame
prt	3D pitch rotation
rrt	3D roll rotation
yrt	3D yaw rotation

Abstract

This paper is Part 2 of Reference 1. Reference 1 described a full model for the calibration device (CD) and an ideal model for the 3-axis accelerometer instrument (3xAI), with the purpose of showing how the residual misalignments in the CD are transferred to the instrument coefficients when using the conventional calibration methods. In addition, it showed a method to potentially eliminate this transfer by using symmetrical calibration points with additional mounting orientations, regardless of the alignment state of the CD. This paper expands on Part 1 by showing a new math model for the instrument that is congruent with the physics of the measurements, and a very good approximation for the CD equations. With these new models, it is possible to obtain the instrument coefficients with algebra rather than curve fitting. This new method shifts the importance from knowing the angle input to high accuracy in conventional calibrations, to the importance of repeating the same angle setpoints (regardless of the CD misalignments) for each of the instrument mounting orientations.

1 Introduction

Measuring angles with gravity referenced instruments is challenging, especially for very high accuracy measurements. These challenges emanate from the difficulty of aligning the instrument with the angle articulation device (AAD) (which is any object, surface, or plane that is subject to being measured with this instrument or used for calibrating this instrument, CD) reference planes. Where these AAD reference planes must be orthogonal and aligned with the AAD axes of rotations, the AAD global frame of reference (G) must be in alignment with a universal global frame of reference (G_{wg}). This universal global frame refers to a world coordinate system that contains the gravity vector (g_v) in alignment with its *Z*-axis, with context provided in Appendix A.2. To state it differently, the individual math models that represent the AAD and the instruments, are not referenced to the universal global frame of reference, G_{wg}. However, the accelerometers (the sensors used to detect these articulations) are inherently referenced to this G_{wg}. These challenges are exacerbated by the instrument's small form factor and enclosure material. The small form factor makes the instrument susceptible to any small misalignments between instrument reference planes and the AAD reference planes, thus causing large (relative to desired measurement accuracy) angle errors. Another potential source of error is the relative movement of the accelerometers due to the non-uniform expansion and contraction of the enclosure material due to temperature. Appendix F provides more context on how the instrument's small form factor makes it susceptible to biases during calibration, which cause measurement errors that can exceed the instrument accuracy specifications.

One caveat to consider is that the accelerometers used in these derivations closely follow a Sine or Cosine trigonometry function. Other types of accelerometers that deviate from these primitive trigonometry functions, i.e., non-linear devices, are not suitable for the calibration processes described in this paper.

The main distinction between all these devices is the individual kinematics model, which can be chosen by the path that best describes the rotational movements of the AAD reference planes (which are *X-Y* and *X-Z*). The *X-Y* plane (i.e., the top surface of a table) is used for attaching the instrument during the operation, and the *X-Z* plane (orthogonal to the *X-Y* plane) aligns the instrument in yaw. Therefore, what dictates the final accuracy of the instrument after calibration or during measurements is a function of the kinematics model chosen for the CD or AAD, and how well the instrument's own reference planes are aligned with these devices' reference planes. The CD mounting and registration planes shall be flat and smooth, with the top and bottom surface (*X-Y* plane, mounting plane) parallel to each other, and the orthogonal plane (*X-Z*, registration plane) shall have the same orientation when accessed from the top and bottom. These requirements are critical for the method described in Reference 1, and for the one presented in this paper, except for the top and bottom parallelism, which is eliminated by minimizing the required calibration points.

The goal of this paper is to show the best method for obtaining the instrument coefficients with minimal bias from the CD. Appendix B contains several alternative methods for achieving this goal, with pros and cons listed for each method. However, the focus of this paper is on the algebraic solution, which increases the probability of obtaining unbiased coefficients when implemented correctly.

The conventional method for achieving this goal is by providing known angle setpoints of accuracy equal or better than the instrument under calibration, and in some applications requires that the CD be four times more accurate than the instrument under calibration. The accuracy of each angle setpoint is a function of the CD misalignments, the index error and the rotary tables wobble. The CD chosen for calibrating this instrument, shown in Figure 1 and described in more details in Reference 1, shows the CD's internal misalignments relative to its global (G) reference frame, and two additional misalignments that represent the device's G reference frame relative to the G_{wg} reference frame. This model does not include the index and wobble misalignments for each rotary axis, since they are assumed (not proven) to be small and or have a zero mean for the selected calibration points.

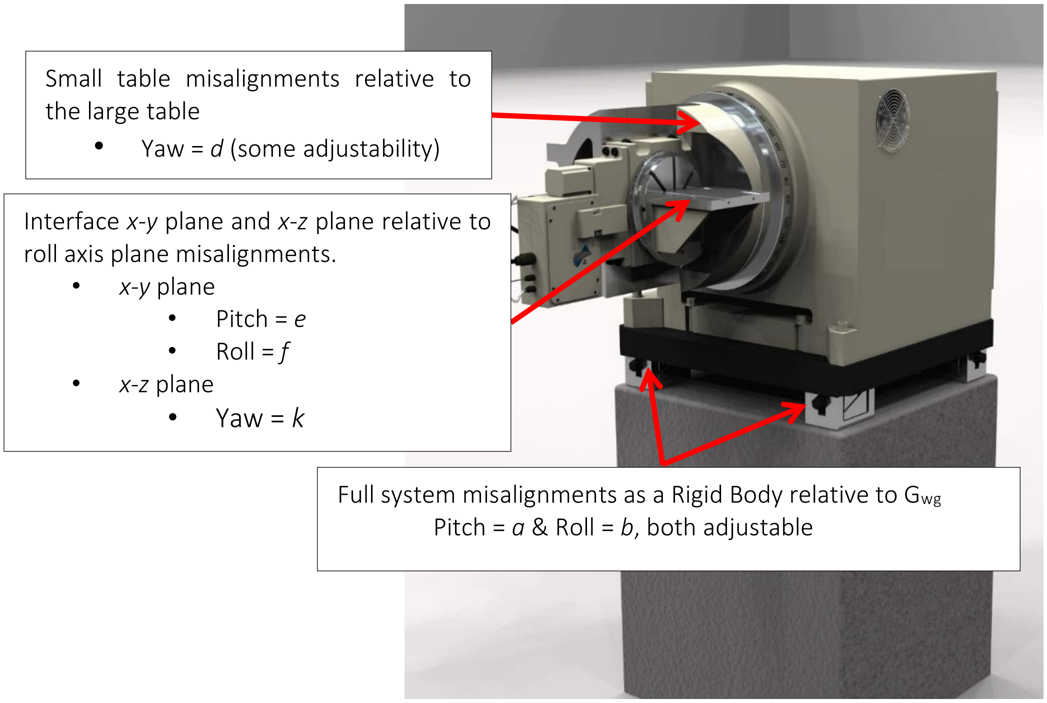

Figure 1. Illustrates the CD, which is a two-axis rotary system. The system is configured to rotate an instrument in pitch and roll starting from a level plane. The labels describe the internal misalignments and their respective locations within the CD, and the two external misalignments of the system as a rigid body relative to G_{wg}.

Another approach for obtaining the instrument coefficients is by an optimization algorithm (OA), which can be designed to find both the instrument coefficients and an estimate of the CD misalignments. This approach converges to a global minimal, regardless of the initial guess, when using the same symmetrical angle setpoints for 4-mounting orientations (Top-Forward, Top-Backwards, Bottom-forward, and Bottom Backwards), presented in Reference 1 for the conventional calibration, and repeated in Appendix B.

The focus of this paper is to demonstrate the best method for obtaining unbiased instrument coefficients. The method solves a minimal set of equations, which are selected to determine these coefficients, and if desired, the CD misalignments. This method was discovered through the process of verifying the OA results using the new math models, derived in Appendix A, for the CD and 3xAI instrument. The simplicity of the method can be difficult to accept without providing background and context. For this reason, this paper will return to basics by building the foundation, starting with the single axis instrument and ending with 3xAI, covered in Appendix A as a multipart math derivation. The first part, Appendix A.1, shows the derivation of the instrument coefficient model starting with the one-axis accelerometer instrument (1xAI), followed by the two-axis accelerometer instrument (2xAI), and finally the three-axis accelerometer instrument (3xAI). Both the 1xAI and 2xAI are designed to measure the angle of an object frame of reference in one axis, while the 3xAI is designed to measure two axes, pitch and roll. Appendix A.2 shows the derivation, including a simplified model, for a few AADs (specifically as CDs). Lastly, Appendix A.3 presents the instrument output as a function of these two models (the instrument coefficients and the CD model). Appendix B shows the various methods for obtaining the instrument coefficients, and Appendix C shows how to solve for the g_v (gravity vector) using these coefficients. The remaining appendices are supportive to these derivations, which were written to avoid confusion.

2 Estimating the Instrument Coefficients with Algebra

The approach described in this section for obtaining the instrument coefficients regardless of the state of the CD alignment, was found to bias the instrument the least relative to the other methods described in Appendix B. This approach solves a minimal set of equations using algebra, where the set of equations are obtained using a few angle setpoints and mounting orientations. In addition, by adding a couple of angle setpoints, it is possible to estimate all the CD misalignments. Although it is possible to calibrate the instrument without knowledge of the CD misalignments, it is advised to have knowledge of the misalignments when performing a calibration. There are two reasons for this knowledge: first, it is important to keep each of the CD misalignments below ±0.1°, as described in Reference 1, and second, it is necessary for computing the accelerometer's sensitivity and bias coefficients/coefficients. The sensitivity and bias coefficients can be estimated without the repeatability requirement; however, it does require that each accelerometer be placed in +1 and –1g fields to within some acceptable range. These positions (+1 and –1g fields) are affected by the CD misalignments and to a lesser extent by the accelerometer offset angles relative to the instrument reference planes. If these misalignments exceed a specified threshold, explained in Section 2.4 "Obtaining the accelerometer sensitivity and bias coefficients", then they could be over or underestimated, which would affect measurement accuracy.

The following three subsections use the models derived as a system shown in Appendix A.3. These models are a combination of the instrument model and the device that articulates this instrument in 1D or 3D space, referred to as the AAD.

2.1 1xAI instrument Coefficients

Equation (1) is the voltage output (V_x) for a single accelerometer tilt instrument. The output is a function of the accelerometer bias (B_x) + gravity vector ([Sin(p) Cos(p)]) * the accelerometer sensitivity (S_x) * the accelerometer position vector ($[1\ p_x]^T$). The gravity vector represents a pure pitch (p) rotation of the AAD reference plane, excluding other potential misalignments in the device. This AAD reference plane/instrument mounting plane is assumed to be orthogonal to the Y-axis of rotation. The accelerometer position vector represents the pitch offset (p_x) of the accelerometer relative to the instrument reference plane, and it is assumed in alignment with the AAD X-axis. The derivation of Equation (1) can be found in Appendix A.3.1.

$$V_x = B_x + [Sin(p) \quad Cos(p)] * S_x * \begin{bmatrix} 1 \\ p_x \end{bmatrix} \tag{1}$$

This equation, although useful for calibrations and measurements, can benefit by expanding it to include the pitch offset angle (S) of the AAD relative to G_{wg}, and from the flexibility of mounting the instrument in two orientations using the parameter y, where y = 0 for forward mount, and y = 180° for backward mount. Equation (2) represents the single axis tilt instrument that is used in this paper for calibration purposes only. However, it can also be used for measurement purposes with y = 0, as the primary mounting orientation.

$$V_x = B_x + [Cos(y)\,Sin(p+S) \quad Cos(p+S)] * S_x * \begin{bmatrix} 1 \\ p_x \end{bmatrix}$$

$$Where\ S = the\ surface\ plane\ misalignment/tilt\ in\ pitch \tag{2}$$

$$y = 0\ or\ Pi\ , for\ forward\ (the\ primary), \\ or\ backward\ mounting\ oriention, respectively$$

With this higher fidelity model, it is easy to obtain the accelerometer offset angle p_x by placing the instrument on a flat and smooth surface. However, this surface may contain an existing pitch angle relative to g_v, S, and a very small roll angle. The roll angle, if small, will not affect this method of calibration. The unknown, p_x, can be determined with two measurements. The first measurement is obtained with the instrument sensitive axis placed in alignment with the surface/plane pitch axis. Then the second measurement is obtained with the instrument rotated by 180° in yaw relative to the first orientation (this can be described as the instrument interface plane rotated relative to the vector normal to this plane, the *Z*-axis). This is identical to the procedure to calibrate a bubble level, described in Reference 1.

The output shall be normalized by using the sensitivity and bias coefficients obtained from Equations (51) and (52), described in the 2.4 "Obtaining the accelerometer sensitivity and bias parameter" section of the paper.

Normalizing Equation (2) and applying trigonometry simplification results in Equation (3):

$$Normalized\ Output\ (NO) = V_{NO} = \frac{V_x - B_x}{S_x} = Sin[Cos(y)(p+S) + p_x] \tag{3}$$

Then, for when p = 0 and y = 0 the resultant, $V_{NO}1$, is

$$V_{NO}1 = S + p_x \tag{4}$$

Then, for when p = 0 and y = 180° the resultant, $V_{NO}2$, is

$$V_{NO}2 = -S + p_x \tag{5}$$

Keep in mind that p = 0 is assumed to be the setpoint angle and S accounts for the misalignment of this setpoint relative to the G_{wg}. Another way to look at this solution is to assume S = 0 and p equals this misalignment of the plane relative the G_{wg}. Both methods shall provide the same result, but, for the purpose of this paper, p = 0 is the method chosen to demonstrate this approach. Therefore, p_x is found by calculating $V_{NO}1 + V_{NO}2$, then dividing the result by 2.

$$p_x = \frac{V_{NO}1 + V_{NO}2}{2} \tag{6}$$

If the desire is to estimate the surface/plane misalignment, then S is found by calculating

$$S = \frac{V_{NO}1 - V_{NO}2}{2} \tag{7}$$

2.2 2xAI instrument Coefficients

The procedure for the 1xAI can be repeated for the 2xAI, except it will require additional points. This can be done with an angle bracket. However, the best method to provide these additional points is by using an AAD composed of a single axis rotary device with a reference plane. The axis of rotation shall be near alignment with the instrument implied Y-axis (this axis is not shown since it is not part of the instrument and CD math model for this instrument). In other words, in 2D, the rotations shown in equation (A.1.5) implies a rotation in 3D relative to the Y-axis. As demonstrated in Appendix A.3.2, the gravity vector (g_v) for this instrument does not change, therefore the voltage output is shown in Equation (8),

$$\begin{bmatrix} V_x \\ V_z \end{bmatrix}^T = \begin{bmatrix} 1 & Sin(\mathrm{p}) & Cos(\mathrm{p}) \end{bmatrix} \begin{bmatrix} B_x & B_z \\ S_x Cos(p_x) & -S_z Sin(p_z) \\ S_x Sin(p_x) & S_z Cos(p_z) \end{bmatrix} \tag{8}$$

The higher fidelity equation (A.3.4) that includes the misalignment and mounting orientation is,

$$\begin{bmatrix} V_x \\ V_z \end{bmatrix}^T = \begin{bmatrix} B_x \\ B_z \end{bmatrix}^T + \begin{bmatrix} Cos(y)\, Sin(p+S) & Cos(p+S) \end{bmatrix} \begin{bmatrix} 1 & -\mathrm{p}_z \\ \mathrm{p}_x & 1 \end{bmatrix} \begin{bmatrix} S_x & 0 \\ 0 & S_z \end{bmatrix} \tag{9}$$

Normalizing equation (9) by accelerometers' bias and sensitivity coefficients yields,

$$\begin{bmatrix} V_{NOx} \\ V_{NOz} \end{bmatrix}^T = \left(\begin{bmatrix} V_x \\ V_z \end{bmatrix} - \begin{bmatrix} B_x \\ B_z \end{bmatrix} \right)^T \begin{bmatrix} \frac{1}{S_x} & 0 \\ 0 & \frac{1}{S_z} \end{bmatrix} = \begin{bmatrix} Cos(\mathrm{y})\, Sin(p+S) & Cos(p+S) \end{bmatrix} \begin{bmatrix} 1 & -\mathrm{p}_z \\ \mathrm{p}_x & 1 \end{bmatrix} \tag{10}$$

For clarity, one can substitute the coefficient matrix (the last matrix in Equation (10) with Equation (A.1.8) and obtain the two outputs, then apply the trigonometry functions' in Equation (A.2.2) to simplify these two equations into Equation (11),

$$\begin{bmatrix} V_{NOx} \\ V_{NOz} \end{bmatrix} = \begin{bmatrix} Sin[Cos[y](p+S)+\mathrm{p}_x] \\ Cos[Cos[y](p+S)+\mathrm{p}_x] \end{bmatrix} \tag{11}$$

The instrument coefficients can be obtained with Equation (11). Table 1 shows the output of Equation (11) for pitch angles 0 and 90° then repeated for the second orientation, y = 180°. At these pitch angles one of the accelerometers is placed in the ±1g field, except the z-axis, which is placed in the +1g field. Therefore, a third point is required to place the z-axis in the -1g field. This can be achieved by rotating the instrument in pitch by 180° or if the CD contains a roll axis, then in roll by 180°. Placing the accelerometers in the ±1g field is necessary for estimating the accelerometers sensitivity and bias parameters, which is covered in Section 2.4.

Table 1. shows the results of Equation (11) for three pitch angles, 0, 90°, and 180° and repeated for the second mounting orientation, y = 180.

Pitch	Matrix NO	1st Orientation y = 0	2nd Orientation y = 180
0	$\begin{bmatrix} V_{NOx} \\ V_{NOz} \end{bmatrix} =$	$\begin{bmatrix} p_x + S \\ +1 \end{bmatrix}$	$\begin{bmatrix} p_x - S \\ +1 \end{bmatrix}$
90°	$\begin{bmatrix} V_{NOx} \\ V_{NOz} \end{bmatrix} =$	$\begin{bmatrix} +1 \\ -p_z - S \end{bmatrix}$	$\begin{bmatrix} -1 \\ p_z - S \end{bmatrix}$
180°	$\begin{bmatrix} V_{NOx} \\ V_{NOz} \end{bmatrix} =$	$\begin{bmatrix} -p_x - S \\ -1 \end{bmatrix}$	N/A

The computation of the instrument coefficients is identical to the 1xAI, with an additional second angle position, p = 90°, required to estimate the second accelerometer offset angle. Therefore, the procedure for obtaining this instrument angle offsets, p_x and p_z require rotating the instrument to p = 0 and p = 90°, with y = 0 (forward orientation), then repeating these angle setpoints with the instrument in y = 180°, which is the second or backward orientation. The equations use the voltages obtained from these two orientations (y = 0 and y = 180°) at one of the two angle setpoints, p = 0 for p_x and p = 90° for p_z. These voltages are first normalized (Table 1) then added together V_{NOx}, and the results are divided by 2.

2.3 3xAI instrument Coefficients

The previous two demonstrations showed the pattern that is repeated in this section. The only difference between the 3xAI derivation versus the previous derivations are that each accelerometer has two angle offsets relative to the two reference planes of the instrument. Equation (12) below, derived in Appendix A.1.4.2, "Derivation of a 3-axis accelerometer instrument (3xAI)", shows the instrument coefficient matrix.

$$\begin{bmatrix} 1 & y_y & -p_z \\ -y_x & 1 & -r_z \\ p_x & r_y & 1 \end{bmatrix} \tag{12}$$

Each column vector represents the accelerometer angle position vector relative to their corresponding axis. This position vector has two parameters representing these offset angles of interest. The parameters in Equation (12) defines *p* is for pitch offset, *r* is for roll offset, and *y* is for yaw offset. These offsets for each accelerometer correspond to the accelerometer angle position relative to the plane that contains the axis for which the accelerometer is aligned. For instance, the first column vector corresponds to the accelerometer that is aligned with the *x*-axis, p_x is the pitch offset of the accelerometer relative to the *x*-*y* plane, and y_x is the yaw offset relative to the *x*-*z* plane. The best approach for obtaining an estimate of these offsets is finding two symmetrical angle setpoints that must include two mounting orientations, which creates two equations with two unknowns. The pattern shows that these symmetrical points place each accelerometer near the zero g field. The selected setpoints are chosen to make one of the offset angles of interest a maximum value, while the second offset is nulled.

Note that obtaining the sensitivity and bias coefficients for this instrument is more complicated than the single axis instruments, as demonstrated in Section 2.4.2. However, the calibration data can be initially normalized, Equation (13), with the sensitivity and bias coefficients estimate using the initial 9 calibration points as shown in Equations (23)-(28). Table 3 shows the required setpoints for this initial sensitivity and bias estimate.

To avoid confusion, the procedure for estimating the instrument coefficients is an iterative process, where the number of iterations is dependent upon the magnitude of the CD misalignments and the accelerometers' offset angles. A detailed procedure is described in Appendix G, which provides multiple numeric examples of this process using different values for CD misalignments and accelerometers' offset angles.

The focus of this section is to demonstrate the approach for obtaining the instrument coefficients with a 9-point calibration. At a minimum, if the CD misalignments are made 0.1° and the accelerometers' offset angles are within 0.1°, then the initial procedure described in this section is all that is required. The examples in Appendix G will show that it is possible to estimate the instrument coefficients with CD misalignments and accelerometers' offset angles that are > 0.1°.

One should note that after assembling the CD and the 3xAI instrument for the first time, the values of these misalignments and offset angles are not known. Obtaining a good instrument calibration when the system misalignments are not known may require multiple iterations and potentially multiple calibrations with additional steps, as covered in Appendix G examples.

The combination of the high-fidelity CD and 3xAI math models results in Equation (13):

$$
\begin{bmatrix} V_{NOx} \\ V_{NOy} \\ V_{NOz} \end{bmatrix}^T = \left(\begin{bmatrix} V_x \\ V_y \\ V_z \end{bmatrix} - \begin{bmatrix} B_x \\ B_y \\ B_z \end{bmatrix} \right)^T \begin{bmatrix} \frac{1}{S_x} & 0 & 0 \\ 0 & \frac{1}{S_y} & 0 \\ 0 & 0 & \frac{1}{S_z} \end{bmatrix} = g_{vm}^T \begin{bmatrix} 1 & y_y & -p_z \\ -y_x & 1 & -r_z \\ p_x & r_y & 1 \end{bmatrix} \tag{13}
$$

The CD model, g_{vm}, in Equation (13) is a very large equation that is simplified, by small angle approximation, in Equation (14), and is explained in Appendix A.2.3:

$$
g_{vm} = \begin{bmatrix} \mathrm{Cos}(y)(\mathrm{Sin}(p) + \big(a + e\,\mathrm{Cos}(r) - k\,\mathrm{Sin}(r)\big)\,\mathrm{Cos}(\mathrm{p})) \\ \mathrm{Cos}(u)\mathrm{Cos}(y)\left(\mathrm{Cos}(p)(\mathrm{Sin}(r) + f\,Cos(r)) + b\,\mathrm{Cos}(r) + \big(k - a\mathrm{Sin}(r) + d\,\mathrm{Cos}(r)\big)\mathrm{Sin}(p)\right) \\ \mathrm{Cos}(u)\left(\mathrm{Cos}(p)(\mathrm{Cos}\big(r\big) - f\,Sin(r)\big) - b\,\mathrm{Sin}(r) - \big(e + a\,\mathrm{Cos}(r) + d\,\mathrm{Sin}(r)\big)\mathrm{Sin}(p)\right) \end{bmatrix} \tag{14}
$$

Equation (15) is the result of simplifying Equations (13) and (14) using trigonometry, the small angle approximation, and rearranging the elements.

$$
\begin{aligned}
V_{NOx} &= Cos(y)\,(Sin(p) + (Cos(y)\,Cos(u)\,p_x\,Cos(r) + a + e\,Cos(r) \\
&\qquad - k\,Sin(r) - Cos(u)\,y_x\,Sin(r))\,Cos(p)) \\
V_{NOy} &= Cos(u)\,Cos(\,y)\,(Cos(p)\,(Sin(r) + (Cos(y)\,r_y + f\,)\,Cos(r)) + b\,Cos(r) \\
&\qquad + (d\,Cos(r) + Cos(u)\,y_y + k - a\,Sin(r))\,Sin(p)) \\
V_{NOz} &= Cos(u)\,(Cos(p)\,(Cos(r) - (f + Cos(y)\,r_z\,)\,Sin(r)) - b\,Sin(r) \\
&\qquad - (d\,Sin(r) + e + a\,Cos(r) + Cos(y)Cos(u)\,p_z\,)\,Sin(p))
\end{aligned} \tag{15}
$$

The constant angles in Equation (14) correspond to the CD internal misalignments, shown in Figure 1 and described in Appendix A.2. To repeat the definition of these angle misalignments, "*a*" (pitch offset) and "*b*" (roll offset) correspond to the CD, as rigid body misalignments with respect to the X-Y plane in G_{wg}. The angle offset "*d*" corresponds to the misalignment between the two rotary tables. The remaining three offsets, *e* (pitch), *f* (roll), and *k* (yaw), correspond to the interface frame of reference misalignments with respect to the roll axis.

Table 2 shows the three accelerometers' normalized output (NO) voltages for each of the selected angle setpoints required to estimate the instrument coefficients. As mentioned above, they are based on selecting two distinctive, symmetrical setpoints that maximize one of the accelerometer offset angles and minimize the value of the second offset angle that makes up each of the accelerometers' position vectors. Choosing the minimal number of symmetrical angle setpoints seems difficult; however, using the following rules can simplify the selection. The optimal symmetrical angles are those that use the same plane and same angle setpoint with two mounting orientations (y = 0 and y = 180°). The rationale for this is that if the setpoint is repeatable, then using the planes that interface each other (CD and instrument) provides the least amount of variation. The CD has one *X-Z* plane (two orifices for accommodating two dowels), and two *X-Y* planes (top and bottom). The instrument has only two individual interface planes (x-y and x-z), which are the three feet to form the *x-y* plane, and one quadrant for each of the two dowels to form the *x-z* plane. It is possible to find other sets of two equations with two unknowns that can solve for the parameter of interest, Appendix E. However, these sets of equations may contain variability that is not accounted for by the model, for instance the index and table wobble variation, which are assumed to have zero mean within the orthogonal setpoints.

Appendix E shows the results of using Equation (15) for the 16 possible orthogonal setpoints for each of the four mounting orientations. The definition of orthogonal points are points where the three axes of the instrument are rotated every 90° to align them with the global frame of reference, G. These are the points where the two axes, pitch and roll of the CD, are rotated by 90°**n*, (for *n* = 0, 1, 2, & 3). The other two parameters, *y* and *u*, are related to the mounting orientations. The instrument mounting surface/plane (top or bottom x-y plane) is specified by *u*, which is defined as *u* = 0 and *u* = 180°, respectively. The second parameter, *y*, specifies the instrument mounting orientation relative to the mounting surface. The two possible orientations are forward or backward, defined as *y* = 0 and *y* = 180°, respectively.

Using these rules, it is possible to calibrate the 3xAI instrument with just three angle setpoints that are repeated for the three mounting orientations, for a total of nine angle setpoints. Table 2 shows the normalized output of the three accelerometers at three angle setpoints represented by (*p*, *r*) as (0, 0), (0, 90°), (90°, 0), which are then repeated for three mounting orientations, represented by (*y*, *u*) as (0, 0), (180°, 0), and (180°, 180°). In addition, it shows two extra angle setpoints, which are used to determine the CD misalignments. The outputs that are not relevant to this process are labeled N/A (not applicable).

Table 2 Required angle setpoint for estimating instrument coefficient and CD misalignments

Angle Setpoints and Mounting Orientations				Normalized Output (NO) Voltages		
p	*r*	*y*	*u*	V_{NOx}	V_{NOy}	V_{NOz}
Bottom Backward						
0	0	180°	180°	*N/A*	*N/A*	*–1*
0	90°	180°	180°	$-a + k - y_x$	*N/A*	*N/A*
90°	0	180°	180°	*N/A*	$b + d + k - y_y$	*N/A*
Top Backward						
0	0	180°	0	$-a - e + p_x$	$-b - f + r_y$	*N/A*
0	90°	180°	0	*N/A*	*–1*	$-b - f + r_z$
90°	0	180°	0	*–1*	*N/A*	$-a - e + p_z$
Top Forward						
0	0	0	0	$a + e + p_x$	$b + f + r_y$	*1*
0	90°	0	0	$a - k - y_x$	*1*	$-b - f - r_z$
90°	0	0	0	*1*	$b + d + k + y_y$	$-a - e - p_z$
Additional Points				For Determining CD Misalignments		
0	180°	0	0	$\mathrm{a - e - p_x}$	N/A	N/A
180°	0	0	0	N/A	$\mathrm{b - f - r_y}$	N/A

Note, to avoid confusion it is simple to show how it is possible to estimate the 12 instrument coefficients (6-angle offsets, 3 sensitivities, and 3 biases) with only 9-angle setpoints. The three accelerometers are independent of each other, therefore, these 9 angle setpoints are technically 27 equations, for which two equations are needed for each of the 12 instrument coefficients. However, observe that a few of the equations in Table 2 have been labeled N/A, thus reducing the equations to 18. Of these 18 equations, 6 place one of the accelerometers in the ±1g field, to obtain the initial estimate for the sensitivity and bias coefficients, shown at the end of this section. For the remaining 12 equations there is a pair of equations that place one of the accelerometers in the zero g field and in two different orientations, which are required to estimate these offset angles, as explained in this section.

Using the following notation, $V_w(p,r,y,u)$ (for $w = x, y$, or z), to identify the selected axis equation, the accelerometers' offset angles can then be estimated using Equations (16)-(21),

$$p_x = \frac{V_{NOx(0,0,0,0)} + V_{NOx(0,0,180^o,0)}}{2} \tag{16}$$

$$y_x = -\frac{V_{NOx(0,90,0,0)} + V_{NOx(0,90,180^O,180^O)}}{2} \tag{17}$$

$$r_y = \frac{V_{NOy(0,0,0,0)} + V_{NOy(0,0,180^O,0)}}{2} \tag{18}$$

$$y_y = \frac{V_{NOy(90,0,0,0)} - V_{NOy(90,0,180^O,180^O)}}{2} \tag{19}$$

$$p_z = \frac{V_{NOz(90,0180^O,0)} - V_{NOz(90,0,0,0)}}{2} \tag{20}$$

$$r_z = \frac{V_{NOz(0,90,180^O,0)} - V_{NOz(0,90,0,0)}}{2} \tag{21}$$

As a reminder, these equations estimate the magnitude and direction of the accelerometers' offset angles relative to their respective frames of reference, as explained in Appendix A. Therefore, when populating the coefficient matrix, Equation (12), with these results, it is important that the three offset angles, y_x, p_z, and r_z, are negated, as shown in this coefficient matrix.

Equation (22) represents the non-normalized voltage output of the 3xAI accelerometers. Table 3 shows the instrument voltage output when placing each accelerometer in the ±1g field, which is an estimate of the bias ± sensitivity or $b_w \pm S_w$. _($w = x, y$ & z) . Equations (23)-(28) demonstrate how to estimate sensitivity and bias parameters for each accelerometer.

$$\begin{bmatrix} V_x \\ V_y \\ V_z \end{bmatrix}^T = \begin{bmatrix} B_x \\ B_y \\ B_z \end{bmatrix}^T + g_{vm}^T \begin{bmatrix} 1 & y_y & -p_z \\ -y_x & 1 & -r_z \\ p_x & r_y & 1 \end{bmatrix} \begin{bmatrix} S_x & 0 & 0 \\ 0 & S_y & 0 \\ 0 & 0 & S_z \end{bmatrix} \tag{22}$$

Table 3. Voltage output for the 3xAI for estimating the sensitivity and bias coefficients

Angle Setpoints and Mounting Orientations				Voltages		
P	R	Y	U	V_x	V_y	V_z
Top Forward						
0	0	0	0	N/A	N/A	$\sim b_z + S_z$
0	90°	0	0	N/A	$\sim b_y + S_y$	N/A
90°	0	0	0	$\sim b_x + S_x$	N/A	N/A
Top Backward						
0	90°	180°	0	N/A	$\sim b_y - S_y$	N/A
90°	0	180°	0	$\sim b_x - S_x$	N/A	N/A
Bottom Backward						
0	0	180°	180°	N/A	N/A	$\sim b_z - S_z$

$$b_x \cong \frac{V_{x(90^o,0,0,0)} + V_{x(90^o,0,180^o,0)}}{2} \tag{23}$$

$$S_x \cong \frac{V_{x(90^o,0,0,0)} - V_{x(90^o,0,180^o,0)}}{2} \tag{24}$$

$$b_y \cong \frac{V_{y(0,90^o,0,0)} + V_{y(0,90^o,180^o,0)}}{2} \tag{25}$$

$$S_y \cong \frac{V_{y(0,90^o,0,0)} - V_{y(0,90^o,180^o,0)}}{2} \tag{26}$$

$$b_z \cong \frac{V_{z(0,0,0,0)} + V_{z(0,0,180^o,180^o)}}{2} \tag{27}$$

$$S_z \cong \frac{V_{z(0,0,0,0)} - V_{z(0,0,180^o,180^o)}}{2} \tag{28}$$

2.4 Obtaining the accelerometer sensitivity and bias coefficients

The first step to obtaining the instrument coefficients using this new approach is by obtaining the instrument sensitivity and bias coefficients. For these two coefficients, it is not critical to repeat the 2-angle setpoints to some accuracy, because placing the accelerometers +1 or -1g fields (tilting the accelerometer to 90° from the 0 g field) within a small angle range relative to these fields has minimal effect on the estimates. Stated differently, there is a small range of angles around the ±1g setpoints that are acceptable for estimating these parameters. This acceptable range is dependent on the instrument resolution and the instrument accuracy specification, with higher measurement accuracy requiring a smaller acceptable range. A full explanation of the effects of over/underestimating the sensitivity and bias parameters for all the instrument types is beyond the scope of this paper. However, the 1xAI instrument is selected to explain how the acceptable range is obtained. To simplify this derivation, assume that the 1xAI instrument is an ideal instrument (in relative terms), with a sensitivity S_x = 1 Volt/g, a bias $B_x \neq 0$, and the offset angle $p_x \neq 0$. In addition, assume the CD has no misalignments, although there is some variable, p_e (this is an index error that is fixed and different for each setpoint). For non-indexable rotary devices this index error becomes a random variable. Equation (1) can be expressed the same as Equation (29), where the instrument output is a function of these parameters.

$$V_x = B_x + S_x\, Sin(p + p_x + p_e); \tag{29}$$

Placing this specific instrument at exactly ± 90° is not feasible since the instrument contains an offset angle, p_x, and the CD has fixed (nonadjustable) angle increments with variable index error, p_e. If the combination of these two angles, $p_x + p_e$, are within some angle threshold, then it is feasible to get a good estimate of the sensitivity and bias parameters with this CD. To estimate this threshold requires understanding of how the over/underestimation of the sensitivity and bias parameters affect the measurement accuracy for this instrument. To demonstrate this effect, assume that $p_x = 0$, and that the remaining index error varies within this desired threshold range. Therefore, rotating the instrument to ±90° results in Equation (30). **Error! Reference source not found.** shows the output of the instrument around ±90°, with the green box representing the acceptable angle threshold. Equation (30), is then simplified using the trigonometry identity, $Sin(\pm 90^{\circ} \pm p_e) = \pm Cos(\pm p_e)$, and then further simplified by obtaining the first two terms of the Taylor series for the Cosine function, around zero angle (not ± 90° for the Sine function).

$$V_{x1} \cong B_x + S_x\, Sin(90^O + p_{e1}) \cong B_x + S_x\, Cos(\pm p_{e1}) = B_x + S_x \left(1 - \frac{(\pm p_{e1})^2}{2}\right) \tag{30}$$

$$V_{x2} \cong B_x + S_x\, Sin(-90^O + p_{e2}) \cong B_x - S_x\, Cos(\pm p_{e2}) = B_x - S_x \left(1 - \frac{(\pm p_{e2})^2}{2}\right)$$

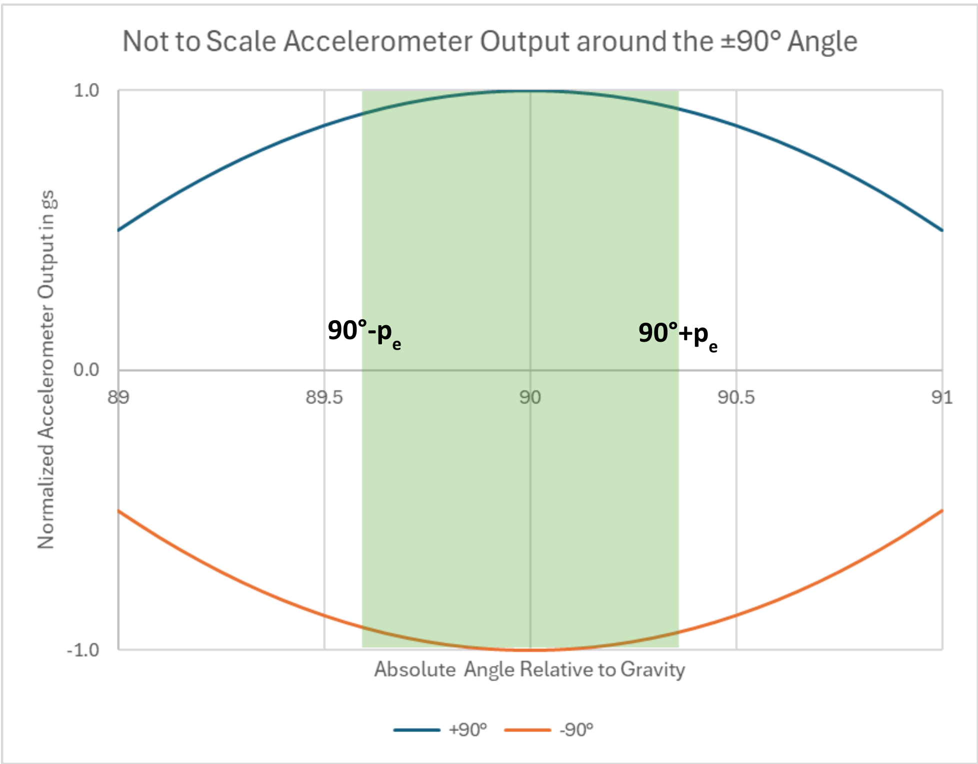

Figure 2 The graph represents the output of the accelerometer, placed around ±90° ±pe

Estimating the bias and sensitivity parameters is achieved by respectively adding or subtracting the two voltages in Equation (30), then dividing by two. The results in Equation (31) show that B_x can be over/underestimated by a maximum of one fourth of the squared index error, $(p_e)^2$ times the true sensitivity of the instrument, specifically when one of the index errors is at zero. The range of this over/underestimation is from $-p_e^2/4\ to\ p_e^2/4$, with a high probability of being very small or near zero.

Figure 2 is a not-to-scale output for the accelerometer placed around ±90°; with top curve for +90° and bottom curve for –90°. The green box represents the angle threshold, $\pm p_e$.

The sensitivity estimate shows that this parameter can only be underestimated when using this process since **Error! Reference source not found.** shows that the voltage output for angles greater o r less than ±90° is lower than the exact ±90° setpoint. Therefore, the range of underestimation in sensitivity is from $-p_e^2/2\ to\ 0$, as shown in Equation (31).

$$B_x \cong \frac{V_{x2}+V_{x1}}{2} \cong B_x + \frac{1}{4}(p_{e2}^2 - p_{e1}^2)S_x\ ;\ \Delta B_x = \frac{1}{4}(p_{e2}^2 - p_{e1}^2)S_x$$
$$S_x \cong \frac{V_{x1}-V_{x2}}{2} \cong S_x\left(1 - \frac{1}{4}(p_{e2}^2 + p_{e1}^2)\right);\ \Delta S_x = -\frac{1}{4}(p_{e2}^2 + p_{e1}^2)S_x \tag{31}$$

Notably, these parameters can change due to other reasons, which are not covered in this paper. Depending on the magnitude of these changes, these two parameters can trigger an Out of Tolerance (OOT) condition after performing a calibration, regardless of the process used.

Determining the bound limits of p_e requires knowledge of the instrument accuracy budget at calibration. For this instrument, the goal is to keep the contribution of each of the estimated parameters/coefficients to within one third to one fourth of the accuracy budget specified by the manufacturer. It is beyond the scope of this paper to demonstrate the effects of the variation of any of the instrument coefficients to measurement accuracy. The challenge with demonstrating these effects is that they are dependent on the angle position of the instrument in 3D space. However, a limited description of the effects of the changes in sensitivity and bias parameters for the 1xAI instrument is provided in the following paragraph.

To simplify this effort, assume that the sensitivity and bias parameters are under/overestimated (keeping in mind that sensitivity can only be underestimated) by some Δ (delta), and expressed in Equation (32) as the voltage output of this accelerometer.

$$\begin{gathered} V_x = \hat{B}_x + \Delta B_x + (\hat{S}_x + \Delta S_x) Sin(p + p_e); Where \\ \Delta B_x = \bar{B}_x(Estimate) - \hat{B}_x(True)\ and \\ \Delta S_x = \bar{S}_x - \hat{S}_x; Where\ |\bar{S}_x| \le |\hat{S}_x(True)| \\ \hat{X}\ represent\ true\ value\ and\ \bar{X}\ represent\ estimate \end{gathered} \tag{32}$$

If we apply the process for estimating the pitch angle for this 1xAI instrument, found in Appendix C, by using the true values for B_x and S_x, as shown in Equation C.2 of the appendix, then the estimated g_x is Equation (33):

$$g_x = \frac{(V_x - \hat{B}_x)}{\hat{S}_x} \cong \frac{\Delta B_x}{\hat{S}_x} + \left(1 + \frac{\Delta S_x}{\hat{S}_x}\right) Sin(p + p_e) \tag{33}$$

where the Δ terms are the result of not placing the instrument exactly at ±1g during calibration. The first term, $\frac{\Delta B_x}{\hat{S}_x}$, has units in g (gravity), and the coefficient of the Sine function, $\frac{\Delta S_x}{\hat{S}_x}$, is unitless. This second term is usually multiplied by one million, due to its small value, and expressed in parts per million (ppm), as shown below in Equation (34).

$$S_x variation\ in\ ppm = \frac{\Delta S_x}{\hat{S}_x} 10^6\ (PPM); \tag{34}$$

The following results use superposition principles since these effects can be viewed independently. To determine the effects of the changes in bias alone, assume that $\Delta S_x = 0$, and the result is Equation (35):

$$\frac{\left(V_x - \hat{B}_x\right)}{\hat{S}_x} \cong \frac{\Delta B_x}{\hat{S}_x} + Sin(p) \tag{35}$$

The estimated pitch angle, *p*, is determined by calculating the ArcSine of Equation (35), which can be approximated with a Taylor series as shown in Equation (36):

$$\begin{gathered} \overline{p} = ArcSin\left(\frac{\Delta B_x}{\hat{S}_x} + Sin(p)\right) \cong Taylor\ Series\ ArcSin[a + Sin(p)] \\ \overline{p} \cong a + \frac{p}{(1-a^2)^{1/2}} + \frac{a\,p^2}{2\,(1-a^2)^{3/2}}; where\ a = \frac{\Delta B_x}{\hat{S}_x} \end{gathered} \tag{36}$$

The error introduced by $\Delta B_x$is determined by subtracting the actual pitch from the estimated pitch in Equation (36). Equation (37) below shows that the error can be further simplified by approximating *a*^2 = 0, then the error in pitch can be expressed as $\overline{p} - p$.

$$\begin{gathered} p\ error \cong \overline{p} - p \cong ArcSin(a) + \frac{a\,p^2}{2} \cong a\left(\frac{2 + p^2}{2}\right); \\ where\ a = \frac{\Delta B_x}{\hat{S}_x}\ and\ a^2 = 0 \end{gathered} \tag{37}$$

This error shows that a delta bias, ΔB_x, results in an error with a parabolic shape (p^2) with a coefficient of $\frac{a}{2}$ and a constant offset of magnitude a.

The same approach can be applied to ΔS_x. Starting with Equation (33) and making $\Delta B_x = 0$, the first two terms are obtained from the Taylor series for the ArcSine, as shown in Equation (38). The results show the first two terms in the Taylor series of the pitch error ($\overline{p} - p$) as a function of ΔS_x and pitch. This derivation of the effects of underestimating the sensitivity parameter is shown in Equation (39).

$$\overline{p} = ArcSin\left(\left(1 + \frac{\Delta S_x}{\hat{S}_x}\right) Sin(p)\right)$$

$$\cong Taylor\ Series\ for\ ArcSin((1+b)Sin(p)) \tag{38}$$

$$\overline{p} \cong (1+b)p;\ where\ b = \frac{\Delta S_x}{\hat{S}_x}$$

The error created by $\Delta S_x$is equal to the estimated pitch minus the actual pitch:

$$p\ error \cong \overline{p} - p \cong \frac{\Delta S_x}{\hat{S}_x}\ p; \tag{39}$$

Equation (39) shows that the error has a slope of $\frac{\Delta S_x}{\hat{S}_x}$, which means the error gets larger as the angle deviates from the zero angle.

To reiterate, determining the acceptable angle range around ±90° that does not increase the measurement error requires knowledge of the instrument error budget at calibration. The total error budget is a function of the measurement angle ranges specified by the manufacturer. For instance, if the 1xAI instrument is specified by the manufacturer to have an accuracy of ±7.2 arcsecs (±0.002) for angles within ±30° then the error contribution for each instrument coefficient (b_x, S_x, p_x), shall be within ±7.2 arcsecs divided by the three or ±2.4 arcsecs/coefficient. To simplify this calculation, one can make the error per coefficient approximately ±2 arcsecs or ±0.0005°. Applying this potential error to Equations (37) and (39), the acceptable errors at the ends of this range (±30°) are ±0.0005° each, for both the bias and sensitivity parameters. To solve for the range, assume S_x = 1 V/g, and that $ArcSin\left(\frac{\Delta B_x}{\hat{S}_x}\right) = \frac{\Delta B_x}{\hat{S}_x}$ for small $\frac{\Delta B_x}{\hat{S}_x}$.

$$p\ error \cong \frac{\Delta B_x}{\hat{S}_x}\left(\frac{2+p^2}{2}\right) = \pm 0.0005^{O}; at\ p = 30^{O}$$

$$\frac{\Delta B_x}{1\ V/g} = \frac{2 * 0.0005 * \frac{Pi}{180}}{\left(2 + \left(30 * \frac{Pi}{180}\right)^2\right)} = 7.675 * 10^{-6} \text{or } 7.68\ \mu g \tag{40}$$

Equation (41), shows the acceptable angle range around ±90° to estimate ΔB_x within ±2 arcsecs:

$$\pm p_e \Rightarrow \frac{1}{4}(p_{e2}^2 - p_{e1}^2) = \Delta B_x\ ; if\ p_{e1}\ or\ p_{e2} = 0; then$$

$$\pm p_e \cong \pm\sqrt{4 * \Delta B_x} \cong \pm\sqrt{4 * 7.675 * 10^{-6}} * \frac{180}{Pi} = \pm 0.3174^{O} \tag{41}$$

Apply the same process to ΔS_x:

$$p\ error \cong \Delta S_x p = -0.0005^O; at\ p = 30^O$$
$$\Delta S_x = -\frac{0.0005}{30} = -1.667 * 10^{-5}\ or\ 16.67 ppm \quad (42)$$

Equation (43), shows the acceptable angle range around ±90° to estimate ΔS_x within ±2 arcsecs:

$$\pm p_e \Rightarrow -\frac{1}{4}(p_{e2}^2 + p_{e1}^2) = \Delta S_x\ ; if\ p_{e1} = p_{e2}; then$$
$$p_e \cong \pm\sqrt{2 * \Delta S_x} \cong \pm\sqrt{2 * 1.667 * 10^{-5}} * \frac{180}{Pi} = \pm 0.331^O \quad (43)$$

The acceptable angle range is approximately 90° for estimating both sensitivity and bias parameters, thus keeping the error contributions of these parameters to maximum allowed measurements' error at the limit of the instrument measurement range, at ±0.3174°. When staying within this range, the ΔB_x shall be within ±7.675 ug, and the $\Delta S_x$is within ±15.3 ppm, if other potential misalignments explained below have near zero values.

This acceptable range is applicable to the 3xAI sensitivity and bias parameter for all three accelerometers, however, in two different directions. Each accelerometer in the 3xAI requires alignment in pitch and roll to reach the ± 1g. Details on how to align each accelerometer with the 1g field are provided in Section 2.4.2 "3xAI Sensitivity and Bias Coefficients".

To summarize this section, it is noted that each parameter in Equation (15) is affected by the other parameters in the system. For instance, Equation (44) shows the *x*-axis accelerometer (normalized output) for the 3xAI instrument without using the small angle approximation for the Cosine functions. What this equation shows is that each individual parameter in the system (instrument coefficients and CD misalignments) can reduce the magnitude of the individual parameters representing this accelerometer output. Although many of these individual parameters are compensated for before calculating the *x*-axis sensitivity coefficient, section 2.4.2, there are two misalignments that cannot be compensated for and may contribute to underestimating this coefficient. These two misalignments are the CD system roll misalignment, *b*, with respect to the G_{wg} and the orthogonal misalignment, *d*, with respect to G. These two misalignments, if not kept within ±0.1° or compensated mathematically as demonstrated in Appendix G: will have an impact on the instrument coefficients. These two misalignments and potential others introduced by mounting misalignments can impact the x-axis sensitivity for the other two tilt instruments 1xAI and 2xAI if they are not kept below the acceptable tolerance.

$$
\begin{aligned}
g_x = {} & \mathrm{Cos}(a)\mathrm{Cos}(b)\mathrm{Cos}(d)\mathrm{Cos}(e)\mathrm{Cos}(k)\mathrm{Cos}(\mathrm{p}_x)\mathrm{Cos}(y_x)\mathrm{Sin}(p) + \\
& \mathrm{Cos}(p)\,\big(a\,\mathrm{Cos}(b)\mathrm{Cos}(d)\mathrm{Cos}(e)\mathrm{Cos}(k)\mathrm{Cos}(\mathrm{p}_x)\mathrm{Cos}(y_x) \\
& + \mathrm{p}_x\,\mathrm{Cos}(r)\mathrm{Cos}(b)\mathrm{Cos}(a)\mathrm{Cos}(g)\mathrm{Cos}(e)\mathrm{Cos}(y_x) \\
& + e\,\mathrm{Cos}(r)\mathrm{Cos}(b)\mathrm{Cos}(a)\mathrm{Cos}(g)\mathrm{Cos}(k)\mathrm{Cos}(\mathrm{p}_x)\mathrm{Cos}(y_x) \\
& - y_x\,\mathrm{Sin}(r)\mathrm{Cos}(b)\mathrm{Cos}(a)\mathrm{Cos}(g)\mathrm{Cos}(k) \\
& - k\,\mathrm{Sin}(r)\mathrm{Cos}(b)\mathrm{Cos}(a)\mathrm{Cos}(g)\mathrm{Cos}(\mathrm{p}_x)\mathrm{Cos}(y_x)\big)
\end{aligned}
\tag{44}
$$

In order to determine what the maximum misalignment of any one or a combination of these specific misalignments, *b*, and *d*, may have on the sensitivity coefficient of the *x*-axis of 3xAI requires several assumptions. The first assumption is that *b* or *d* are small, and the second is when estimating the maximum misalignment of either one, the other is assumed zero. Therefore, Equation (45) shows this effect on g_x if $d \neq 0$, which reduces the magnitude of the *Sin(p)* function, by the *Cos(d)* factor. Then, using the first two terms of the Taylor series for $Cos(d) = \left(1 - \frac{d^2}{2}\right)$ to substitute in the equation shows the error introduced by this misalignment as a function of the pitch angle.

$$
\begin{aligned}
g_x &= \mathrm{Cos}(d)\mathrm{Sin}(p) \cong \left(1 - \frac{d^2}{2}\right)\mathrm{Sin}(p) \\
\overline{p} &= ArcSin\left(\left(1 - \frac{d^2}{2}\right)\mathrm{Sin}(p)\right) \cong \left(1 - \frac{d^2}{2}\right)p \therefore the\ error\ \cong\ -\frac{d^2}{2}p
\end{aligned}
\tag{45}
$$

Estimating the error in pitch when *b* and *d* are $\neq 0$, assume both misalignments have similar magnitude; therefore, the error can be approximated by Equation (46):

$$
\begin{aligned}
g_x &= \mathrm{Cos}(b)\mathrm{Cos}(d)\mathrm{Sin}(p) \cong Cos^2(d)Sin(p) \cong (1 - d^2)\mathrm{Sin}(p) \\
\overline{p} &= ArcSin\big((1 - d^2)\mathrm{Sin}(p)\big) \cong (1 - d^2)p \therefore the\ error\ \cong\ -d^2 p
\end{aligned}
\tag{46}
$$

The result of both scenarios is a reduction of the estimate in pitch since the *Cos(±x)* < 1 for *x* around the 0° angle. To find the angle tolerance for one or both angles, assume that the error in pitch is within the max allowable at the ends of the pitch range, i.e., if ±30° is less than -0.0005°, then *d* must be within.

$$
\begin{aligned}
for\ d \neq 0\ and\ b\ = 0\ then\ d &= \pm\sqrt{\frac{2 * 0.0005}{30}} * \frac{180}{Pi} = \pm 0.331^{O} \\
for\ d \neq 0\ and\ b\ = d\ then\ d &= \pm\sqrt{\frac{0.0005}{30}} * \frac{180}{Pi} = \pm 0.234^{O}
\end{aligned}
\tag{47}
$$

The angle ranges for these two misalignments are only available if the other contributors to ΔS_x, i.e., p_e (pitch index error 1 and 2) in Equation (43), are near zero. If the other contributors are not zero, then it is important to determine the impact of b and d misalignments to the sensitivity coefficient first and then determine the acceptable range for p_e using Equation (43). The misalignments, b and d, are fixed, or not cancelable, as the other contributors mentioned before are during a calibration. The goal is to minimize the effect of all misalignments to these sensitivity and bias coefficients. More details are covered in Section 2.4.2.

Note that the explanation in this section only applies to the 3xAI instrument. For the other two types of single axis tilt instruments, 1xAI and 2xAI, it is advised to nullify these two misalignments before any calibration, since this will affect the estimate to the sensitivity and bias coefficients. In addition, this explanation extends to the inherent yaw misalignment, y_x, for the *x*-axis accelerometer in these single axis tilt instruments. This yaw misalignment is not accounted for in the mathematical equations, which can affect the estimate in the sensitivity coefficient. Broadening this topic, each individual accelerometer, regardless of the type of single axis tilt instrument, has a second angle offset, which can affect the sensitivity estimate. For the 1xAI and 2xAI instruments, this second offset only comes into play if the accelerometer is rotated relative to its own sensing axis (*x*-axis or roll rotation), which they are not designed to measure.

For clarification, the 1xAI offset angle, y_x, relative to the *X-Z* plane, has been ignored because it doesn't impact the single axis tilt instrument math model. This offset can be compounded by any yaw misalignment, *k* (misalignment with respect to the *X-Z* plane), of the instrument relative to the primary axis of rotation (pitch) during installation. If this misalignment is large, it affects the magnitude of the sensitivity which introduces a measurement error in pitch. Again, the y_x offset angle does not impart a measurement error since its effects are calibrated out. However, the effect of a mounting misalignment in yaw that is different from calibration and introduced during measurements may cause a pitch error (for high pitch angles), even when not rotated relative to the *x*-axis (roll). This last statement is true regardless of the calibration method.

2.4.1 Sensitivity and Bias Estimate For the 1xAI and 2xAI

2.4.1.1 Math method of calculating sensitivity and bias for the single pitch instruments,

$$instrument\ output\ in\ Volts\ \mathrm{V}_x[p] = B_x + S_x * Sin(p + S + p_x); \qquad (48)$$

If $S + p_x < \pm 0.3174°$, then obtaining V1 and V2 using Equations (49) and (50) is unnecessary; therefore, V1 is obtained by setting the instrument to $p = 90°$ and V2 at $p = -90°$. However, if $S + p_x > \pm 0.3174°$, then correcting for these parameters is necessary. The +1g position is found by setting the instrument to $p = 90 - S - p_x \pm 0.3174°$, for V1, as shown in Equation (49) below:

$$\mathrm{V1} = \mathrm{V}_x[\,p = 90^{O} - \mathrm{S} - \mathrm{p}_x\ \pm\ 0.3174^{O}] = B_x + S_x \qquad (49)$$

Then the -1g position is found by setting the instrument to $p = -90 - S - p_x \pm 0.3174°$ to obtain the second measurement, V2, show in Equation (50):

$$\mathrm{V2} = \mathrm{V}_x[p = -90^O - \mathrm{S} - \mathrm{p}_x \ \pm\ 0.3174^O] = \ B_x - S_x \qquad (50)$$

The bias is found by calculating V1 plus V2 then dividing the result by 2,

$$B_x = \frac{V1 + V2}{2} \qquad (51)$$

The sensitivity is found by calculating V1 minus V2 then dividing the result by 2,

$$S_x = \frac{V1 - V2}{2} \qquad (52)$$

The sensitivity and bias coefficients for the *z*-axis accelerometer in the 2xAI instrument requires $p = 0$ and $p = 180°$ or if the AAD has a roll axis, then roll ($r = 180°$). As described for the *x*-axis accelerometer above, Equations (54) and (55) are necessary if $S + p_z > \pm 0.3174°$.

$$instrument\ output\ in\ Volts\ V_z[p] = \ B_z + S_z * Cos(p + S + p_z); \qquad (53)$$

In other words, at $p = 0$ (implied $r = 0$) the accelerometer voltage is V1,

$$V1 = V_z[\ p = 0 - S - p_z \pm\ 0.3174^O] = \ B_z + S_z \qquad (54)$$

Repeat for p =180° (implied $r = 0$), or $p = 0$ and $r = 180°$ angle articulation,

$$V2 = V_z[p = 180^O - S - p_z \pm\ 0.3174^O] = \ B_z - S_z \qquad (55)$$

The bias is found by calculating *V1* plus *V2* then dividing the result by 2,

$$B_z = \frac{V1 + V2}{2} \qquad (56)$$

The sensitivity is found by calculating V1 minus V2 then dividing the result by 2,

$$S_z = \frac{V1 - V2}{2} \tag{57}$$

2.4.2 3xAI Sensitivity and Bias Coefficients

Estimating the sensitivity and bias coefficients for each accelerometer within this instrument is less straight forward than with the 1xAI instrument. The reason is that each accelerometer contains two offset angles, and finding the ±1g field requires rotating the accelerometer in two angle directions. These rotations require knowledge of the CD misalignments and the individual accelerometer position vector. The goal is to place the accelerometer near the 1g field within ±0.3174° from the required angle. The equations in Appendix E show that this angle is ±90° regardless of the alignment state of the CD and the position vector. This is due to simplified expression of equations, which means that presenting the equations in a different expression will render a slightly different result at these ±1g positions. This section will use the alternative expression of the system (CD and instrument combined) equations to estimate the accelerometers' sensitivity and bias parameters. To clarify, the intent of this section is to estimate the absolute value of sensitivity that approximates the true value. This estimate can be used as the basis of comparison for a calibration that is performed with only a 9-point calibration.

It is possible to estimate the accelerometers' absolute sensitivity to within tolerance with the first estimate from the 9-point calibration if CD misalignments and accelerometers' offset angles are less than 0.1°. However, it is good practice to estimate these parameters using the method in this section, since at a minimum these corrected parameters are much closer to the true value, and thus can be used as the basis for comparison for these first estimates. Keep in mind, the true value of these parameters is never fully known throughout the life of the accelerometer. These coefficients' true values depend on the local gravity, environmental temperature, the state of the internal magnets' strength, and forces placed on the accelerometer body during instrument assembly and or handling during operations. On the other hand, if the CD misalignments or the accelerometer offset angles are larger than 0.1°, then the method in this section is more critical not only for estimating these two coefficients (sensitivity and bias), but also for the other six coefficients, and to a lesser extent the CD misalignments.

There are two CD misalignments, the system roll angle, *b*, and the orthogonal angle between the pitch and roll rotary tables, *d*, that are not correctable using the method in this section. If they are too large, then they can affect the *x*-axis sensitivity and bias estimates. Equation (44) shows the effects of the CD misalignments on all the elements in $g_{x,}$ which is the first element in Equation (58). This element, g_x, is the normalized result of the *x*-axis voltage output using an estimate of the sensitivity and bias coefficients. Equation (71) at the end of this section is a simplified representation of the *x*-axis voltage output affected by these two misalignments, when the other CD misalignments have been canceled by the method described in this paper.

Equation (58) uses the general voltage output (normalized) representation of the full system (instrument and CD), shown in Equation (A.3.5) in Appendix A.3.3. Equation (A.2.18) from

Appendix A.2.3, is selected to represent the CD g_{vm}, and only the top and forward mounting orientation is needed (the mounting orientation parameters, y & u = 0) for this section.

$$g_{vm} = \begin{bmatrix} \mathrm{Sin}\big(p + a + (e + \mathrm{p}_x)\mathrm{Cos}(r] - (k + y_x)\mathrm{Sin}(r)\big) \\ \mathrm{Cos}(p)\mathrm{Sin}\big(r + f + r_y\big) + b\ \mathrm{Cos}(r) + \mathrm{Sin}(p)\left(k + y_y + d\ \mathrm{Cos}(r) - a\ \mathrm{Sin}(r)\right) \\ \mathrm{Cos}(p)\mathrm{Cos}(r + f + r_z) - b\ \mathrm{Sin}(r) - \mathrm{Sin}(p)\big(e - p_z + d\ \mathrm{Sin}(r) + a\ \mathrm{Cos}(r)\big) \end{bmatrix} \quad (58)$$

Equation (58) is the instrument and CD combined into a system or the new g_{vm}. A calculus minimum/maximum method is used to find the exact 1g field for each accelerometer. Finding the x-axis accelerometer 1g field using Equation (58), g_{xm} or (g_{vm}[[1]]), requires a pitch angle that maximizes or minimize g_{xm}, which is known to be near 90°. However, before finding this exact pitch angle it is important to find the roll angle that maximizes the argument of g_{xm}.

The roll angle that minimizes/maximizes g_{xm} is obtained by deriving it with respect to roll and making it equal to zero. Equation (59) shows two elements that make this equation zero, with the second term providing the best estimate for estimating the roll angle. Then, using this roll angle, one can estimate the pitch angle that makes the first term in Equation (59) equal to zero.

$$\frac{dg_{xm}}{dr} = \mathrm{Cos}\big(p + a + (e + p_x)\mathrm{Cos}(r) - (k + y_x)\mathrm{Sin}(r)\big) * \big(-(e + p_x)\mathrm{Sin}(r) - (k + y_x)\mathrm{Cos}(r)\big) \quad (59)$$

Find the roll angle which makes the second term in Equation (59) equal to zero, shown here in Equation (60):

$$\begin{gathered} -(e + p_x)\mathrm{Sin}(r) - (k + y_x)\mathrm{Cos}(r) = 0 \\ r_{max} = ArcTan\left(\frac{-\left(k + y_x\right)}{\left(e + p_x\right)}\right) \end{gathered} \quad (60)$$

This r_{max} value does not include the CD misalignment of the reference plane in roll, f. To account for this misalignment, subtract it from r_{max} from Equation (60).

$$r'_{max} = ArcTan\left(\frac{-\left(k + y_x\right)}{\left(e + p_x\right)}\right) - f \quad (61)$$

The pitch angle which makes the first term in Equation (59) equal to zero, is also the same pitch angle in combination with the roll angle from Equation (61), which makes g_{xm} equal to ±1g, shown in Equation (62).

$$\mathrm{Sin}\big(p + a + (e + \mathrm{p}_x)\mathrm{Cos}(r] - (k + y_x)\mathrm{Sin}(r)\big) = \pm 1$$
$$when\ p + a + (e + p_x)\mathrm{Cos}(r'_{max}) - (k + y_x)\mathrm{Sin}(r'_{max}) = \pm 90^0; \tag{62}$$
$$Therefore, p = \pm 90^0 - a - (e + p_x)\mathrm{Cos}(r'_{max}) + (k + y_x)\mathrm{Sin}(r'_{max})$$

The procedure is to set roll to r'_{max} and then to set the pitch angle from Equation (62). While it is not imperative to dial this exact value, it is important to dial it to within ±0.3174° from this exact 1g value. The instrument itself will be used to assist with dialing these two angles.

This process can be repeated for the other two accelerometers. However, it is easier to return to the nonconsolidated version of the g_{vm} shown as Equation (15). This formulation is shown in Equation (63) with y & u = 0. The rational here is that estimating these two coefficients only requires a single mounting orientation, thus the primary mount is chosen.

$$g_{vm} = \begin{bmatrix} \mathrm{Sin}(p) + \mathrm{Cos}(p)(a + (e + \mathrm{p}_x)\mathrm{Cos}(r) - (k + y_x)\mathrm{Sin}(r)) \\ \mathrm{Cos}(p)\mathrm{Sin}(r) + \mathrm{Cos}(r)\big(b + \big(f + r_y\big)\mathrm{Cos}(p)\big) + \mathrm{Sin}(p)\big(k + y_y - a\ \mathrm{Sin}(r) + d\ \mathrm{Cos}(r)\big) \\ \mathrm{Cos}(p)\mathrm{Cos}(r) - \mathrm{Sin}(r)\ (b\ + (f + r_z)\mathrm{Cos}(p)) - \mathrm{Sin}(p)(e - p_z + a\ \mathrm{Cos}(r) + d\ \mathrm{Sin}(r)) \end{bmatrix} \tag{63}$$

Derive the g_{ym}[[2]] in Equation (63), relative to pitch, then set the result equal to zero with r = 90°, and solve for p.

$$\frac{dg_{ym}[[2]]}{dp} = -\mathrm{Sin}(p)\mathrm{Sin}(r) + \mathrm{Cos}(r)\big(d\mathrm{Cos}(p) - \big(f + r_y\big)\mathrm{Sin}(p)\big) + Cos(p)\big(k + y_y - a\mathrm{Sin}(r)\big) = 0 \tag{64}$$

At r = 90° the accelerometer is near the 1g field, therefore getting it closer to this field requires finding the pitch angle that makes $\frac{dg_{ym}}{dp} = -\mathrm{Sin}(p) + Cos(p)\big(k + y_y - a\big) \cong Sin(-p + k + yy - a) = 0$. Thus, the angle is:

$$p = k + y_y - a \tag{65}$$

Repeating for r = -90°, makes $\frac{dg_{ym}}{dp} = \mathrm{Sin}(p) + Cos(p)\big(k + y_y + a\big) \cong Sin(p + k + y_y + a) = 0$

$$p = -k - y_y - a \tag{66}$$

After canceling the pitch misalignment for this accelerometer for the two roll angles (±90°), then one finds the roll angle that cancels the system misalignments and sets the accelerometer in the ±1g field using Equation (67),

$$
\begin{aligned}
g_{ym}[\mathrm{p}=k+yy-a] &= \mathrm{Sin}(r)+\mathrm{Cos}(r)\left(b+f+r_y\right) \cong \mathrm{Sin}\left(r+b+f+r_y\right)=1 \\
g_{ym}[\mathrm{p}=-k-yy-a] &= \mathrm{Sin}(r)+\mathrm{Cos}(r)\left(b+f+r_y\right) \cong \mathrm{Sin}\left(r+b+f+r_y\right)=-1
\end{aligned}
\tag{67}
$$

which equals +1 at $r = 90^{O} - b - f - r_y$ and –1 at $r = -90^{O} - b - f - r_y$

The process is repeated for g_{zm},

$$
\begin{aligned}
\frac{dg_{zm}}{dp} = {} & -\mathrm{Sin}(p)\mathrm{Cos}(r) - b\mathrm{Sin}(r) - Cos[p](e+p_z+a\mathrm{Cos}(r)+d\mathrm{Sin}(r)) \\
& + (f+r_z)Sin(p)\mathrm{Sin}(r) = 0
\end{aligned}
\tag{68}
$$

This accelerometer is near the ±1g field at r = 0 and Pi; therefore, to find the pitch angle that cancels the system misalignments, use the derivative of g_{zm} with respect to p and make it equal to zero,

$$
\begin{aligned}
\frac{dg_{zm}}{dp}[r=0] &= -\mathrm{Sin}[p] - Cos[p](e+p_z+a) \cong -\mathrm{Sin}[p+e+p_z+a] = 0 \\
\frac{dg_{zm}}{dp}[r=Pi] &= \mathrm{Sin}[p] - Cos[p](e+p_z-a) \cong -\mathrm{Sin}[p-e-p_z+a] = 0
\end{aligned}
\tag{69}
$$

The accelerometer is near the +1g field, when $p = -e - p_z - a$, and -1g field, when $p = e + p_z - a$. The result is shown in Equation (70). The roll angle that places the accelerometer in ±1g field is found by canceling the roll misalignments, as shown in Equation (70).

$$
\begin{aligned}
g_{zm}[\mathrm{p}=-e-p_z-a] &= \mathrm{Cos}(r) - (b+f+r_z)\mathrm{Sin}(r) \cong \mathrm{Cos}(r+b+f+r_z) = 1 \\
g_{zm}[\mathrm{p}=e+p_z-a] &= \mathrm{Cos}(r) - (b+f+r_z)\mathrm{Sin}(r) \cong \mathrm{Cos}(r+b+f+r_z) = -1
\end{aligned}
\tag{70}
$$

Therefore, g_{zm} equals +1 at $r = 0 - b - f - r_z$ and -1 at $r = Pi - b - f - r_z$

Table 4 summarizes the pitch and roll angles described above for estimating the sensitivity and bias coefficients. These coefficient estimates are near absolute values; therefore, it is good practice to follow this process to increase instrument measurements confidence levels.

Table 4. Recalculating the 3xAI sensitivity and bias coefficients after correcting for the CD misalignments and the accelerometers' offset angles.

<table>
<tr><td colspan="4">Angle Setpoints and Mounting Orientations</td><td colspan="3">3xAI Instrument Voltage Output</td></tr>
<tr><td>p</td><td>r</td><td>y</td><td>u</td><td>V_x</td><td>V_y</td><td>V_z</td></tr>
<tr><td colspan="4">Top Forward</td><td colspan="3">After Correcting for Accelerometers and CD Misalignments</td></tr>
<tr><td>p_{1x}</td><td>r_{1x}</td><td>0</td><td>0</td><td>$b_x + s_x$</td><td>N/A</td><td>N/A</td></tr>
<tr><td>p_{2x}</td><td>r_{2x}</td><td>0</td><td>0</td><td>$b_x - s_x$</td><td>N/A</td><td>N/A</td></tr>
<tr><td>p_{1y}</td><td>r_{1y}</td><td>0</td><td>0</td><td>N/A</td><td>$b_y + s_y$</td><td>N/A</td></tr>
<tr><td>p_{2y}</td><td>r_{2y}</td><td>0</td><td>0</td><td>N/A</td><td>$b_y - s_y$</td><td>N/A</td></tr>
<tr><td>p_{1z}</td><td>r_{1z}</td><td>0</td><td>0</td><td>N/A</td><td>N/A</td><td>$b_z + s_z$</td></tr>
<tr><td>p_{2z}</td><td>r_{2z}</td><td>0</td><td>0</td><td>N/A</td><td>N/A</td><td>$b_z - s_z$</td></tr>
<tr><td colspan="5">$r_{1x} = ArcTan\left(-\frac{\overline{k} + \overline{y_x}}{\overline{e} + \overline{p_x}}\right) - \overline{f}$</td><td colspan="2">$p_{1x} = \frac{Pi}{2} - \overline{a} - (\overline{e} + \overline{p_x})\ Cos(r_{1x}) + (\overline{k} + \overline{y_x})\ Sin(r_{1x})$</td></tr>
<tr><td colspan="5">$r_{2x} = r_{1x}$</td><td colspan="2">$p_{2x} = -\frac{Pi}{2} - \overline{a} - (\overline{e} + \overline{p_x})\ Cos(r_{2x}) + (\overline{k} + \overline{y_x})\ Sin(r_{2x})$</td></tr>
<tr><td colspan="5">$p_{1y} = \overline{k} + \overline{y_y} - \overline{a}$</td><td colspan="2">$r_{1y} = \frac{Pi}{2} - \overline{f} - \overline{r_y} - \overline{b}$</td></tr>
<tr><td colspan="5">$p_{2y} = -\overline{k} - \overline{y_y} - \overline{a}$</td><td colspan="2">$r_{2y} = -\frac{Pi}{2} - \overline{f} - \overline{r_y} - \overline{b}$</td></tr>
<tr><td colspan="5">$p_{1z} = -\overline{e} - \overline{p_z} - \overline{a}$</td><td colspan="2">$r_{1z} = -\overline{f} - \overline{r_z} - \overline{b}$</td></tr>
<tr><td colspan="5">$p_{2z} = \overline{e} + \overline{p_z} - \overline{a}$</td><td colspan="2">$r_{1z} = Pi - \overline{f} - \overline{r_z} - \overline{b}$</td></tr>
</table>

The following Equations (72)-(77) use the information tabulated in Table 4 for estimating the accelerometers' sensitivity and bias coefficients. In addition, Equations (72) and (73) show how to correct the *x*-axis sensitivity and bias coefficients for the two CD misalignments: system roll, *b*, and orthogonal angle between rotary tables, *d*. This is only necessary if these two misalignments are large or > 0.1°. Equation (71) shows the effects of these two misalignments on the voltage output after the other CD misalignments have been canceled, as described in Equations (72) and (73).

$$V_x = b_x - S_x\ Sin(b)\ \ Sin(d) + S_x\ Cos(b)\ \ Cos(d)\ \ Sin(p) \tag{71}$$

Equation (71) shows the bias element is reduced by S_x *Sin(b)Sin(d)* and the sensitivity, S_x, magnitude is lowered by *Cos(b)Cos(d)*. To reverse these effects, first correct the sensitivity estimate by dividing the rightmost element by *Cos(b) Cos(d)*, then with this result, correct the bias estimate by adding S_x *Sin(b)Sin(d)*.

$$S_x = \frac{V_{x(\mathrm{p}_{1x}, r_{1x}, 0,0)} - V_{x(\mathrm{p}_{2x}, r_{2x}, 0,0)}}{2};$$
$$Correcting\ \ S_x\ when\ CD\ misalignment\ b_e\ \&\ d_e > 0.1^O$$
$$S_x = \frac{V_{x(\mathrm{p}_{1x}, r_{1x}, 0,0)} - V_{x(\mathrm{p}_{2x}, r_{2x}, 0,0)}}{2\ \mathrm{Cos}[b_e] Cos[d_e]} \tag{72}$$

$$b_x = \frac{V_{x(\mathrm{p}_{1x}, r_{1x}, 0,0)} + V_{x(\mathrm{p}_{2x}, r_{2x}, 0,0)}}{2}$$
$$Correcting\ \ b_x\ when\ CD\ misalignment\ b_e\ \&\ d_e > 0.1^O$$
$$b_x = \frac{V_{x(\mathrm{p}_{1x}, r_{1x}, 0,0)} - V_{x(\mathrm{p}_{2x}, r_{2x}, 0,0)}}{2} + \ S_x\ Sin[b_e]\ Sin[d_e] \tag{73}$$

$$b_y = \frac{V_{\mathrm{y}(\mathrm{p}_{1y}, r_{1y}, 0,0)} + V_{\mathrm{y}(\mathrm{p}_{1y}, r_{1y}, 0,0)}}{2} \tag{74}$$

$$S_y = \frac{V_{\mathrm{y}(\mathrm{p}_{2y}, r_{2y}, 0,0)} - V_{\mathrm{y}(\mathrm{p}_{2y}, r_{2y}, 0,0)}}{2} \tag{75}$$

$$b_z = \frac{V_{\mathrm{z}(\mathrm{p}_{1z}, r_{1z}, 0,0)} + V_{\mathrm{z}(\mathrm{p}_{1z}, r_{1z}, 0,0)}}{2} \tag{76}$$

$$S_z = \frac{V_{\mathrm{z}(\mathrm{p}_{2z}, r_{2z}, 0,0)} - V_{\mathrm{z}(\mathrm{p}_{2z}, r_{2z}, 0,0)}}{2} \tag{77}$$

2.5 Obtaining an estimate of the CD misalignments

There are multiple ways to obtain the CD misalignments. Depending on the type of CD, each estimate will vary slightly from the other. The proposed calculations, Equations (78)-(83), for obtaining these estimates use the same process for obtaining the instrument coefficients, which is the process of using the same setpoint with two mounting orientations to render two equations with two unknowns. This rule is eliminated for obtaining the system misalignments, *a* and *b*, Figure 1. These two parameters require one single mount and two angle setpoints, where the angle setpoints keep the axis of interest in a fixed position, while rotating the second axis, which is not of interest. For instance, in order to obtain the system pitch misalignment, *a*, the setpoint pitch angle is kept at zero, while the roll table is rotated from zero to 180°. The process is repeated for the system roll misalignment, *b*, where the roll angle is kept at zero, while the pitch axis is rotated from zero to 180°.

Estimating these two system misalignments, *a* and *b*, requires two additional setpoints found at the bottom of Table 2. With these two misalignments, it is feasible to obtain the other misalignments using the same equations in Table 2 for estimating the instrument coefficients. Again, these are estimates of the CD misalignments and the goal of this approach is to obtain them with the minimal number of setpoints. Although it is possible to obtain some of them with a single setpoint, it is best to keep the process demonstrated here, since it reduces the probability of other elements in the CD contributing to the estimate.

$$a = \frac{V_{x(0,0,0,0)} + V_{x(0,180^{\text{o}},0,0)}}{2} \tag{78}$$

$$b = \frac{V_{y(0,0,0,0)} + V_{y(180^{\text{o}},0,0,0)}}{2} \tag{79}$$

Estimate the reference planes' misalignments, *e*, *f*, and *k*, with Equations (80)-(82),

$$e = \frac{V_{x(0,0,0,0)} - V_{x(0,0,180^{\text{o}},0)}}{2} - a \tag{80}$$

$$f = \frac{V_{y(0,0,0,0)} - V_{y(0,0,180^{\text{o}},0)}}{2} - b \tag{81}$$

$$k = \frac{V_{x(0,90^{\text{o}},180^{\text{o}},180^{\text{o}})} - V_{x(0,90^{\text{o}},0,0)}}{2} + a \tag{82}$$

The orthogonal angle, *d*, is estimated with Equation (83),

$$d = \frac{V_{y(90^{\mathrm{o}},0,0,0)} + V_{y(90^{\mathrm{o}},0,180^{\mathrm{o}},180^{\mathrm{o}})}}{2} - b - k \tag{83}$$

2.6 Coefficient bias from variation in angle setpoints with different mounting orientation

In practice, if the interface surface (plane) is not flat and smooth, there is a chance that the second instrument orientation may introduce a slightly different misalignment. In addition, if no attachment force (using fasteners or magnets) is required for this instrument, then we can model the system with different AAD misalignments for each instrument orientation. The reason for assuming "no attachment force" is because there is a possibility for the accelerometer position relative to the enclosure to shift when a force is applied to the instrument while fastening it to the test article or CD interface plane. This is more likely when the enclosure and the test article interface/reference planes are not flat and smooth. Another possibility for introducing this second misalignment can occur with a rotary system with setpoint repeatability that is less than the instrument specifications (this is known as position hysteresis or index error). In order to avoid this issue for the 1xAI, it is best to use a rigid table with a flat and smooth surface, i.e., a large granite table on a stable stand.

Demonstrating this effect for the 1xAI instrument requires some assumptions: assume that the misalignment of the AAD with respect to G_{wg} is $S1$ for the primary mounting orientation, and $S2$ for the symmetrical orientation. Therefore, for $y = 0$ in Equation (3), substituting $S1$ for S, then normalizing the output, the measurement can be represented with Equation (84),

$$V_{NO}1 = \mathrm{Sin}(p + S1 + \mathrm{p}_x) \tag{84}$$

The second measurement, $V_{NO}2$, is for $y = 180°$ and the instrument experiences a slightly different pitch misalignment, $S = S2$,

$$V_{NO}2 = \mathrm{Sin}(-(p + S2) + \mathrm{p}_x) \tag{85}$$

where $S2$ can occur from surface deformations or low setpoint repeatability. This can be expressed in terms of $S1$ by Equation (86),

$$\begin{gathered} S2 = S1 + \Delta S_{21} \\ \text{where,} \\ \Delta S_{21} = S2 - S1 \end{gathered} \tag{86}$$

Then, at pitch $p = 0$, and using small angle approximation,

$$V_{NO}1 = S1 + \mathrm{p}_x \tag{87}$$

$$V_{NO}2 = -S2 + \mathrm{p}_x = -(S1 + \Delta S_{21}) + \mathrm{p}_x$$

Solving for p_x and for S, using the process in Section 2.1, “1xAI instrument Coefficients” results in,

$$p_x = \frac{V_{NO}1 + V_{NO}2}{2} = \mathrm{p}_x - \frac{\Delta S_{21}}{2}$$
$$S = \frac{V_{NO}1 - V_{NO}2}{2} = \mathrm{S} + \frac{\Delta S_{21}}{2} \tag{88}$$

What this solution shows is that the effect of having different reference misalignment for the second reading is a biased instrument coefficient. The bias is one half of the delta between the two reference misalignments. In addition, this bias affects the estimate of the surface misalignment by the same magnitude. This explains the requirement for high angle setpoint repeatability, where the variability shall be less than the accuracy specifications of the instrument. The reference surface shall be flat and smooth for all interface planes (for both the AAD (or CD) and instrument reference/interface plane).

The same analysis applies to a shift of the accelerometer position relative to the enclosure, which can occur when users accidentally tug on the cables after the instrument is installed on the AAD, or users bumping the instrument against a hard surface during installation or handling, assuming the sensors are robust enough to handle such an event.

3 Conclusions

The algebraic solution presented in this paper for estimating the coefficients for any tilt instrument (with accelerometers that follow a single trigonometric function) has a few advantages over the conventional calibration methods. The advantages of this method are that it does not require a high accuracy angle standard (a CD with known angle setpoints with accuracy equal or higher than the instrument under calibration), and that it can estimate the coefficients with zero or minimum biases from the CD and installation misalignments. The basic requirements for the CD are that it is capable of setting three repeatable near orthogonal angle setpoints, replicated for three mounting orientations for a total of nine angle setpoints. It is feasible to estimate the instrument coefficients with these nine angle setpoints, unless the system misalignments are large thus affecting the sensitivity and bias coefficient estimates. Therefore, to mitigate these large system misalignments the CD must allow for setpoint adjustability (without the repeatability requirement), which is required for placing the accelerometers near the ±1g fields.

Other advantages are that although it is not required to align the CD with g_v, as it is required for conventional methods, this method with an additional two angle setpoints, it can provide an estimate of the CD misalignment relative to G and G_{wg}. Appendix G provides a procedure on how to achieve this alignment. The algebraic method and alignment procedures can be applied in the field with the right equipment and by a trained person. The ability to calibrate at the measurement site has the advantages of improving measurement accuracy by calibrating at the operating temperature (this reduces the potential errors from the instrument temperature compensation algorithm), by calibrating with the local gravity magnitude, and by verifying that the instrument is operating within tolerance before and after measurements. Lastly, field calibrations can eliminate long lead times from sending the instrument out for calibration.

4 References

1. Soto, H. L, “Calibrating a 3-Axis Accelerometer Instrument with a Less Accurate Calibration Device Part 1: Mathematical Methodology”, NASA/TM-2020-5005041, July 2020
2. Tripp, J. S. and Tcheng, P., “Uncertainty Analysis of Instrument Calibration and Application," NASA TP-1999-209545, 1999.
3. Marshall, R., and Landman, D., “An Improved Method for Determining Pitch and Roll Angles Using Accelerometers,"21st AIAA Advanced Measurement Technology and Ground Testing Conference, Denver, Colorado, AIAA 2000-2384, June 2000.
4. Strang, G., “Introduction to Linear Algebra," Wellesley Cambridge Press, Chapter 4.3, Fifth Edition
5. Jazar, R.N., “Theory of Applied Robotics," Springer, Chapter 2 and 3, Second Edition
6. Alfonso Croeze, Lindsey Pittman, and Winnie Reynolds; “Solving Nonlinear Least-Square Problems with the Gauss-Newton and Levenberg-Marquardt Methods”
7. Menezes Filho, R. P.; Silva, F. O.; Cavalho, G. S.; Vieira , L. A. ”Triaxial accelerometer calibration using an extended two-step methodology”, 2020 Latin American Robotics Symposium (LARS), 2020 Brazilian Symposium on Robotics (SBR) and 2020 Workshop on Robotics in Education (WRE)
8. Gheorghe , M. V., “Advanced calibration method for 3-axis MEMS accelerometers”, 2016 International Semiconductor Conference (CAS)
9. Geist, J. and Gaitan, M. “Type B Uncertainty Analysis of Gravity-Based Determinations of Triaxial-Accelerometer Properties by Simulation of Measurement Errors”, Volume 126, Article No. 126038 (2021), Journal of Research of National Institute of Standards and Technology
10. Geist, J.; Yaqub Afridi ,M.; McGray ,C. D.; and Gaitan, M. “Gravity-Based Characterization of Three-Axis Accelerometers in Terms of Intrinsic Accelerometer Parameters”, Volume 122, Article No. 32 (2017), Journal of Research of National Institute of Standards and Technology
11. Gaitan, M.; López Bautista, I. M.; Geist, J. “Reduction of calibration uncertainty due to mounting of three-axis accelerometers using the intrinsic properties model”, Open Access IOP Publishing, Bureau International des Poids et Mesures
12. Parker, P. A, Finley, T. D, “Advancements in Aircraft Model Force and Attitude Instrumentation by Integrating Statistical Methods”, JOURNAL OF AIRCRAFT Vol. 44, No. 2, DOI: 10.2514/1.23060, March–April 2007
13. Crawford, B. L, “Angle Measurement System (AMS) for Establishing Model Pitch and Roll Zero, and Performing Single Axis Angle Comparisons”, 45th AIAA Aerospace Sciences Meeting and Exhibit, Reno, NV, AIAA 2007-1162, January 2007

Appendix A: Calibration of a Gravity referenced instrument

Gravity referenced instruments are traditionally calibrated using an L^2 norm approach. Reference 1 showed how this approach can bias the instrument coefficients if any residual misalignments in the CD are not nulled below the instrument accuracy specifications. It also demonstrated an approach that cancels the CD misalignments if the CD meets several requirements. The primary requirement is that the reference planes or interface planes shall be flat, smooth, parallel for the top and bottom *X*-*Y* planes, and the *X*-*Z* plane shall be orthogonal to the *X*-*Y* plane. In addition, the *X*-*Z* plane shall be accessible from the top and bottom planes with near zero misalignment. Another requirement is the CD index and wobble errors are assumed to have an average of zero mean, specifically for the selected angle calibration points. If any or all of the afore mentioned requirements are not met, then each adds a different bias to the instrument, which can cause the instrument accuracy specification to be lower than desired.

A.1: Gravity referenced instrument math model

The goal of this section is to share a general derivation of the math model for any gravity referenced instruments. Although the focus of this paper is on the derivation of the 3-axis accelerometer instrument (3xAI) and the calibration device (CD), this paper will cover two additional configurations: a single axis tilt instrument with one and two accelerometers, and the corresponding CD. The strategy detailed in this section is to start with the derivation of the single axis tilt instrument for its simplicity and build up to the more complex 3xAI instrument.

The instrument output is a function of the kinematics model chosen for the instrument and the kinematics model for the AAD (i.e., CD).

The following derivations are a step-by-step approach to understanding the geometric mechanics of a tilt instrument and CD. Although this approach is identical to kinematics, the intent is not as a substitute, but a basic approach to provide the reader context for the derivations to follow.

A.1.1: General derivation of a 1-axis tilt instrument

There is a need to measure the angle of an object's chosen frame of reference relative to another object's chosen frame of reference.

Figure 3 shows two frames of reference, in 2D, aligned at their points of origin (OXZ and Oxz), with one frame rotated by an angle α relative to the other frame. The blue frame (x-z) represents the local frame of reference (L), and the red frame (X-Z) represents the global frame of reference (G).

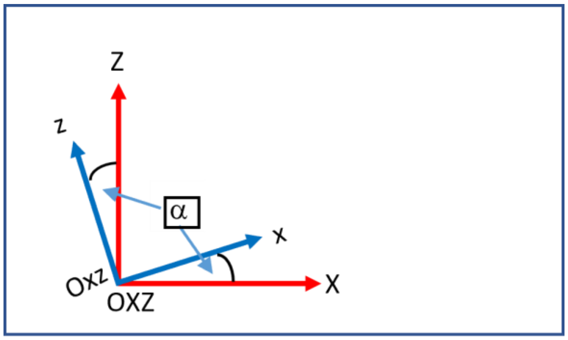

Figure 3. The local frame of reference in blue is aligned at the point of origin with the global frame in red, and then rotated by an angle α.

One method to track the L rotations with respect to the G reference frame is to determine the length of the projections of each axis of L onto the two axes of G, Figure 4.

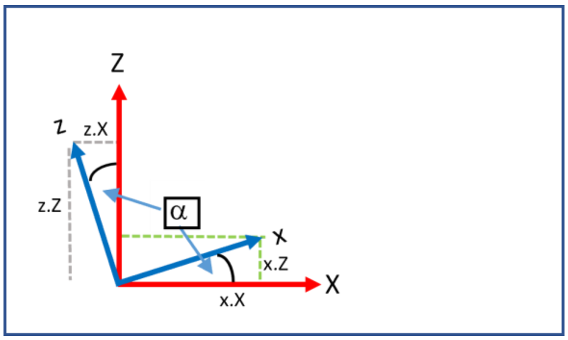

Figure 4. The dotted lines in this figure represent the projection of each axis in the local frame onto the two axes in the global frame.

The length of the projections for the L *x*-axis onto the G two axes are the dot product of *x*-axis with both axes in G, represented by *x.X* and *x.Z*, and the same goes for the *z*-axis, which are *z.X* and *z.Z*. All these axes have magnitude of one.

Projecting the local *x*-axis on to both *X*-axis and *Z*-axis of the G is shown in equations (A.1.1) and (A.1.2):

$$x.X = \| x \| \| X \| \, Cos(\alpha) \qquad \text{(A.1.1)}$$

$$x.Z = \| x \| \| Z \| \, Cos(90^{O} - \alpha) = \| x \| \| Z \| \, Sin(\alpha) \qquad \text{(A.1.2)}$$

Projecting the local *z*-axis on to both *X*-axis and *Z*-axis of G is shown in equations (A.1.3) and (A.1.4):

$$z.X = \| z \| \| X \| \, Cos(90^O + \alpha) = -\| x \| \| Z \| \, Sin(\alpha) \tag{A.1.3}$$

$$z.Z = \| z \| * \| Z \| \, Cos(\alpha) \tag{A.1.4}$$

Placing the results from Equation (A.1.1)-(A.1.4) in a matrix is the basis for kinematics. From this demonstration the matrix rotation is,

$$\begin{bmatrix} x.X & z.X \\ x.Z & z.Z \end{bmatrix} = \begin{array}{cc} \begin{array}{cc} \quad x & \qquad\quad z \end{array} & \\ \begin{bmatrix} Cos(\alpha) & -Sin(\alpha) \\ Sin(\alpha) & Cos(\alpha) \end{bmatrix} & \begin{array}{c} X \\ Z \end{array} \end{array} \tag{A.1.5}$$

Equation (A.1.5) is referred to as a 2D rotation or transformation matrix by an angle α. From this point on in this paper, this rotation matrix describes the relationship, in 2D, of rotating L relative to G.

This matrix is orthonormal, thus the inverse for this matrix is the transpose, which is identical to a rotation in opposite direction or - α. In addition, the inverse matrix itself is used as a rotation of G relative to L, which is not covered in this paper (ref. 5).

To clarify the notation for most of the equations/matrices in Appendix A:, the letters above the column vector(s) and the letters to the right of the rows of the matrices are for keeping track of components of the L frame of reference (the *x*, *y* and *z*-axis elements) relative to the G frame of reference (*X*, *Y*, and *Z*-axis). For instance, Equation (A.1.5) shows that first element in the first column is Cos(α), which is the *x*-axis component in L projected onto the G *X*-axis, and the second element in the first column is Sin(α), which is the *x*-axis component in L projected onto the G *Z*-axis.

A.1.2: Derivation of a 1-axis accelerometer instrument (1xAI)

A single axis instrument can be composed of one or two accelerometers in one enclosure. Ideally, the instrument is assembled using an enclosure manufactured to high tolerances and the accelerometer sensitive axis is in alignment with the enclosure reference plane. Unfortunately, this is not feasible without incurring high manufacturing costs, and in the end aligning the accelerometer to the desired position. Figure 5 shows a non-ideal 1xAI, where the accelerometer sensitive axis is not in alignment (parallel) with the enclosure reference plane or bottom surface.

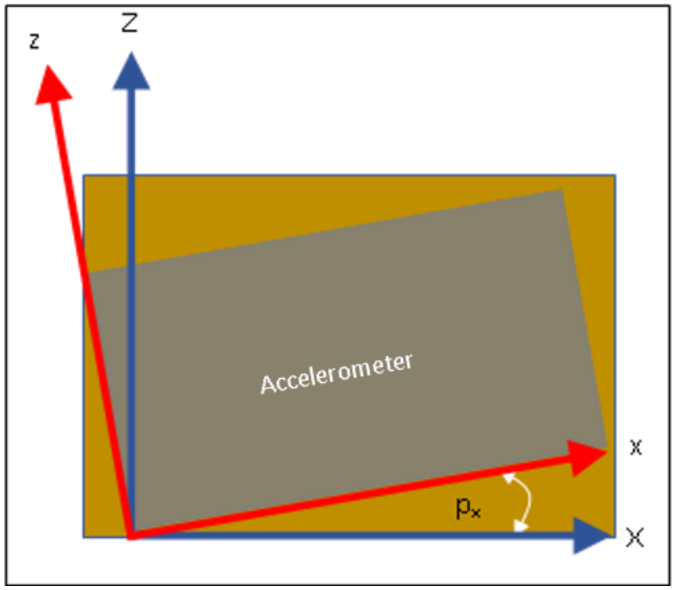

Figure 5 . Graphical representation of a single axis tilt instrument frames of reference

Figure 5 shows a single axis tilt instrument, composed of an accelerometer (in grey) and an enclosure (in gold). The enclosure represents the global frame, G, with the *X*-axis aligned with the interface plane. The accelerometer sensitive axis is aligned with the *x*-axis local frame. The angle p_x represents the misalignment between the two frames of references or the sensor relative to the enclosure reference frame. Equation (A.1.5) can be used to describe the instrument in Figure 5, except the instrument has only one accelerometer to track the rotation of L relative G, meaning Equation (A.1.5) has two column vectors representing the two axes of the local frame of reference, L. For this configuration, the accelerometer angle position is modeled by the first column vector in Equation (A.1.5).

1xAI Coefficient Matrix

$$Instrument\ Model = \begin{array}{cc} x & \\ \begin{bmatrix} Cos(p_x) \\ Sin(p_x) \end{bmatrix} & \begin{array}{c} X \\ Z \end{array} \end{array} \quad (A.1.6)$$

It is possible to simplify this vector using small angle approximation, Equation (A.1.7). The result from using either Equations (A.1.6) or (A.1.7) is, depending of the accuracy budget of the instrument, imperceptible for small offset angles (i.e., <± 0.5°), but in some situations one form provides a cleaner result over the other. This applies to the other instruments, and it will become clear at different stages of the development of the instrument math equations.

Simplified using small angle approximation

$$Instrument\ Model = \begin{array}{cc} x & \\ \begin{bmatrix} 1 \\ p_x \end{bmatrix} & \begin{array}{c} X \\ Z \end{array} \end{array} \tag{A.1.7}$$

A.1.3: Derivation of a 2-axis accelerometer instrument (2xAI)

This configuration is rarely used, except for a few organizations. The reasons for including it in this paper are because it is an extension of the derivatives shown above for the 1xAI instrument and it serves as a bridge when explaining the 3xAI instrument, which is more challenging to explain and cover all the characteristics of that instrument.

Figure 6 shows a 2xAI instrument, composed of an enclosure (in gold) and two sensors (in grey) with their respective angles relative to the enclosure reference frame. The enclosure represents the global frame, G, with the X-axis aligned with the interface plane. Both sensors' sensitivity axes are aligned with one of the axes of the individual local frames, red and green, assigned to each accelerometer. The offset angles for both sensors are pitch offset with different magnitude and direction, px and pz.

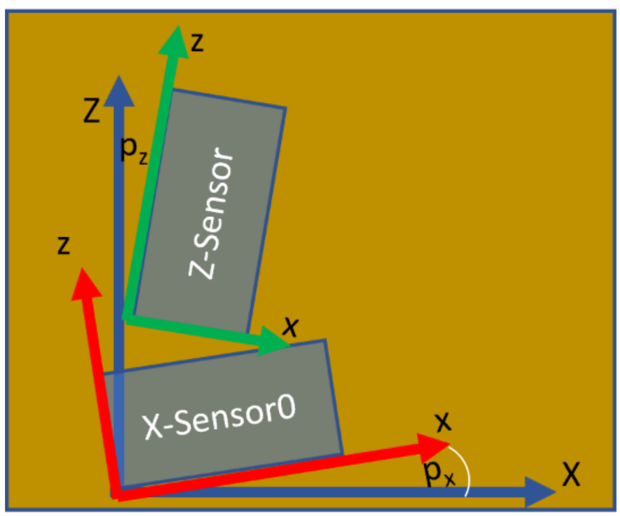

Figure 6. Graphical representation of a 2xAI tilt instrument frames of reference

This configuration has a few advantages over the single accelerometer. The advantages are that it can measure a wider range of angles, and it may reduce the impact from temperature effects and parameter drift, since the angle is obtained by the ratio of the two accelerometers. The disadvantage of this configuration is discussed at the end of this section.

Returning to the derivation of the 1xAI, the vector that best represented that accelerometer was the first column vector of Equation (A.1.5) since it was aligned with the *x*-axis of the local frame of reference. This second accelerometer, Figure 6, is aligned with the *z*-axis of L, thus the second vector in Equation (A.1.5) is selected. The difference is that both accelerometers in this instrument have different offset angles, p_x and p_z, respectively. Finally, the instrument coefficient matrix goes from a single vector for the 1xAI to a two-vector (column vector) matrix for the 2xAI, shown in Equation (A.1.8).

2xAI Coefficient Matrix

$$Instrument\ Model = \begin{array}{cc} \begin{array}{cc} x & z \\ \begin{bmatrix} Cos(p_x) & -Sin(p_z) \\ Sin(p_x) & Cos(p_z) \end{bmatrix} & \begin{array}{c} X \\ Z \end{array} \end{array} \end{array} \tag{A.1.8}$$

Simplified using small angle approximation

$$Instrument\ Model = \begin{array}{cc} \begin{array}{cc} x & z \end{array} & \\ \begin{bmatrix} 1 & -p_z \\ p_x & 1 \end{bmatrix} & \begin{array}{c} X \\ Z \end{array} \end{array} \tag{A.1.9}$$

There are a few issues with the 1xAI and 2xAI instruments. When either instrument is placed on a flat table that is not leveled in two axes (pitch and roll), then the angle measured with this instrument will depend on the orientation of the instrument relative to the table G. If the instrument is aligned with one of the two axes of rotation, then the output of the instrument is a function of that axis alone. However, if the instrument is aligned with the pitch axis and then rolled, the measurement error increases as the roll angle increases, reaching max value at roll = 90^o.

This action is not possible with a normal table or without the instrument sliding off the table after it is rolled. However, it is possible with a two-axis rotary table when the instrument is clamped as it is currently managed. Keep in mind that a clamp will bias the instrument during calibration and this bias will change after each clamping application, during calibration or measurement.

The reason for the measurement errors is due to the instrument model which does not account for the offset angle, y_x shown in Figure 7. Figure 7 shows the accelerometer offset angle, y_x, relative to G frame of reference X-Z plane. This offset angle is not accounted for in the instrument math model and it is a source of error when the instrument is rolled. As the instrument is rolled the accounted offset angle, p_x in Figure 6, contributes less to the measured angle, thus creating an error in Equation (C.3) and Equation (C.4) of Appendix C when canceling p_x from the estimate of the AAD pitch angle.

This gets more complicated for the 2xAI since the accelerometer that is aligned with the local *z*-axis will move out of the G *X-Z* plane. This tilt will underestimate the magnitude of this vector and thus cause a measurement error. The measured angle with a 2xAI instrument is a function of ArcTan2(gx/gz), Appendix C.2, and gz shall remain within the X-Z plane. If it does not, the magnitude of the projected vector *z.Z* is reduced, changing the estimated angle. These effects are not significant for small rotation in roll, but the error increases as roll reaches ±90°.

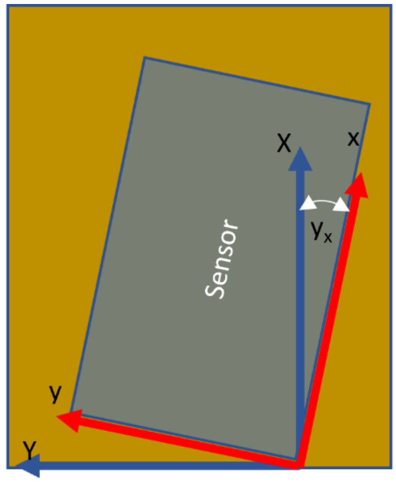

Figure 7. The x-axis Accelerometer offset angle, y_x, not accounted for in the instrument math model

The 3xAI instrument was developed to alleviate some of these issues; however, this instrument comes with another set of challenges that affect the measurement accuracy.

A final point about these single axis tilt instruments: even if the instrument is used to measure one axis rotation, i.e., pitch with zero roll, the math model does not account for placing the instrument with a yaw rotation relative to the G *Z*-axis. Therefore, if the instrument is placed at a yaw angle relative to one of the two axes of rotation (pitch or roll), then the output of the instrument will have an error that is a function of this yaw angle. However, this is not a concern for small yaw misalignments, and if pitch angles are within a small range of angles around zero g-field or level plane.

A.1.4: Derivation of a 3-axis accelerometer instrument (3xAI)

The derivation of the 3xAI instrument requires three matrices to represent each possible rotation in 3D. The next section shows these matrices and the chosen signs (+/-) for the trigonometric Sine function, which are chosen based on the right-hand rule and a positive angle rotation.

A.1.4.1: The common matrix rotations in 3D

The rotation matrices for 3D frames of reference are well established in math, science, and engineering textbooks. The overall structures of these matrices are identical no matter which way the positive direction of the rotation is chosen, or whether it uses the right-hand or left-hand rule. The only thing that changes is the sign of the elements for each column vector, depending on the characteristics of the rotations, i.e., positive right-hand rule rotation. This section will present three rotation matrices (which represent a rotation of L relative to G) that are right-hand rule and use aircraft convention. The aircraft convention means that a positive pitch is for the nose of the aircraft to be higher than the tail, a positive roll angle is the left wing to be higher than the right wing, and a positive yaw angle is for the aircraft nose, looking from the top, rotating clockwise relative to a pivot point.

Equations (A.1.10), (A.1.11), and (A.1.12) correspond to aircraft convention pitch, roll, and yaw 3D rotation matrices, using the right-hand rule.

Pitch Rotation (*prt*):

$$prt(\alpha) = \begin{bmatrix} Cos(\alpha) & 0 & -\mathrm{Sin}(\alpha) \\ 0 & 1 & 0 \\ \mathrm{Sin}(\alpha) & 0 & \mathrm{Cos}(\alpha) \end{bmatrix} \tag{A.1.10}$$

Roll Rotation (*rrt*):

$$rrt(\beta) = \begin{bmatrix} 1 & 0 & 0 \\ 0 & \mathrm{Cos}(\beta) & -\mathrm{Sin}(\beta) \\ 0 & Sin(\beta) & \mathrm{Cos}(\beta) \end{bmatrix} \tag{A.1.11}$$

*Yaw Rotation (*yrt):

$$yrt(\gamma) = \begin{bmatrix} \mathrm{Cos}(\gamma) & Sin(\gamma) & 0 \\ -\mathrm{Sin}(\gamma) & \mathrm{Cos}(\gamma) & 0 \\ 0 & 0 & 1 \end{bmatrix} \tag{A.1.12}$$

A.1.4.2: Derivation of the instrument sensors positions:

For the 3xAI instrument, each accelerometer contains two offset angles which are relative to the two planes the accelerometer local frame axes are nearest to. For instance, the *x*-axis for the 1xAI and 2xAI was modeled with a single offset angle p_x, which is the pitch offset of the *x*-axis relative to the enclosure G, *X*-*Y* reference plane. There is a second offset angle that was ignored during the derivation of the single axis tilt instruments, shown in Figure 7. This offset angle is the angle of the accelerometer *x*-axis relative to the enclosure orthogonal plane, *X*-*Z* plane (which is the *Z*-axis, implied in Figure 7). This offset angle is a yaw angle, and it only comes into play if the instrument is rotated in roll (which is a rotation of the instrument L relative to the G *X*-axis).

The following sections will describe these angle offsets for each accelerometer in the 3xAI instrument. The accelerometer sensitive axis position relative to the enclosure G can be found by a minimal of two angle rotations, which can be found by any combination of the three matrices in equations (A.1.10), (A.1.11), and (A.1.12). Reference 2 shows a different selection of rotation vis à vis this paper. These selected rotations in Reference 2 create a perceived nonlinearity to the system math model. The advantage of the combination of rotations chosen in this paper for each axis make the model congruent with the physics of the measurement, thus facilitating the algebraic solution.

Derivation of the accelerometer aligned with the x-axis

The position vector for the *x*-axis accelerometer is derived by obtaining the matrix product of a pitch rotation matrix times a yaw rotation matrix, and then selecting from this result the *x*-axis vector. Again, as mentioned for the 1xAI instrument, the best vector that represents this accelerometer is the *x*-axis.

$prt(p_x)yrt(y_x)$ =

$$\begin{array}{cc} \begin{array}{ccc} x & y & z \end{array} & \\ \begin{bmatrix} \mathrm{Cos}(p_x)\mathrm{Cos}(y_x) & \mathrm{Cos}(p_x)Sin(y_x) & -Sin(p_x) \\ -Sin(y_x) & \mathrm{Cos}(y_x) & 0 \\ Sin(p_x)\mathrm{Cos}(y_x) & Sin(p_x)Sin(y_x) & \mathrm{Cos}(p_x) \end{bmatrix} & \begin{array}{c} X \\ Y \\ Z \end{array} \end{array} \quad (A.1.13)$$

The *x*-axis accelerometer position is the first column vector,

$$\begin{bmatrix} \mathrm{Cos}(p_x)\mathrm{Cos}(y_x) \\ -Sin(y_x) \\ Sin(p_x)\mathrm{Cos}(y_x) \end{bmatrix} \quad (A.1.14)$$

Derivation of the accelerometer aligned with the y-axis

The position is derived by the matrix product of a roll rotation times a yaw rotation, and selecting the *y*-axis column vector:

$rrt(r_y)yrt(y_y)$ =

$$\begin{array}{cc} \begin{array}{ccc} x & y & z \end{array} & \\ \begin{bmatrix} Cos(y_y) & Sin(y_y) & 0 \\ -Sin(y_y)Cos(r_y) & Cos(y_y)Cos(r_y) & -Sin(r_y) \\ -Sin(y_y)Sin(r_y) & Cos(y_y)Sin(r_y) & Cos(r_y) \end{bmatrix} & \begin{array}{c} X \\ Y \\ Z \end{array} \end{array} \quad (A.1.15)$$

The *y*-axis column vector, is the second column vector,

$$\begin{bmatrix} Sin(y_y) \\ Cos(y_y)Cos(r_y) \\ Cos(y_y)Sin(r_y) \end{bmatrix} \tag{A.1.16}$$

Derivation of the accelerometer aligned with the z-axis

The position is derived by the matrix product of a pitch rotation times a roll rotation, and selecting the *z*-axis column vector

$prt(p_z)rrt(r_z) =$

$$\begin{array}{cc} \begin{array}{ccc} x & y & z \end{array} & \\ \begin{bmatrix} Cos(p_z) & -Sin(p_z)Sin(r_z) & -Sin(p_z)Cos(r_z) \\ 0 & Cos(r_z) & -Sin(r_z) \\ Sin(p_z) & Cos(p_z)Sin(r_z) & Cos(p_z)Cos(r_z) \end{bmatrix} & \begin{array}{c} X \\ Y \\ Z \end{array} \end{array} \tag{A.1.17}$$

The *z*-axis column vector, is the third column vector,

$$\begin{bmatrix} -Sin(p_z)Cos(r_z) \\ -Sin(r_z) \\ Cos(p_z)Cos(r_z) \end{bmatrix} \tag{A.1.18}$$

To construct the new math model for the 3xAI, the three independent column vectors are combined into one 3x3 matrix

3xAI Coefficient Matrix

$$\begin{array}{cc} \begin{array}{ccc} x & y & z \end{array} & \\ \begin{bmatrix} \mathrm{Cos}(p_x)\mathrm{Cos}(y_x) & Sin(y_y) & -Sin(p_z)Cos(r_z) \\ -Sin(y_x) & Cos(y_y)Cos(r_y) & -Sin(r_z) \\ Sin(p_x)\mathrm{Cos}(y_x) & Cos(y_y)Sin(r_y) & Cos(p_z)Cos(r_z) \end{bmatrix} & \begin{array}{c} X \\ Y \\ Z \end{array} \end{array} \tag{A.1.19}$$

Simplified using small angle approximation,

$$\begin{bmatrix} 1 & y_y & -p_z \\ -y_x & 1 & -r_z \\ p_x & r_y & 1 \end{bmatrix} \tag{A.1.20}$$

Equation (A.1.20) is an effective approximation to equation (A.1.19). A name for this type of matrix is a "near orthonormal matrix". In other words, the other two components of each column vector are very small numbers, thus the magnitude of each vector is near unity, and the angle between any pair of two column vectors is near 90°.

For instance, the *x*-axis vector magnitude is:

$$\left\| \left| \begin{bmatrix} 1 \\ -y_x \\ p_x \end{bmatrix} \right\| \right| = (1^2 + y_x^2 + p_x^2) \cong 1; where\ \left|y_x\right| \ \&\ \left|p_x\right| < 0.1^O \tag{A.1.21}$$

One property observed from working with this matrix is that it is possible to find the inverse matrix for Equation (A.1.20) by a very simple operation, which is presented in Appendix D.

However, if one or both accelerometer angle offsets are > 0.1°, then the element (= 1) in the column vector may require adjustment. The adjustment is based on using the Taylor series for Cos(Offset 1)*Cos(Offset2) shown in diagonal elements in Equation (A.1.19). For the *x*-axis accelerometer example, the element = 1 can be approximated by Equation (A.1.22),

$$\mathrm{Cos}(y_x)\mathrm{Cos}(p_x) \cong \left(1 - \frac{y_x^2}{2}\right)\left(1 - \frac{p_x^2}{2}\right) \cong 1 - \frac{y_x^2}{2} - \frac{p_x^2}{2} < 1\ for\ |y_x| \ \&\ |p_x| > 0.1^O \tag{A.1.22}$$

Equation (A.1.23) verifies that the magnitude of this column vector is near 1 for angle > 0.1°; the upper limit depends on the accuracy requirements for the instrument. In this paper the goal is to estimate the sensitivity of the accelerometer within ±16.7 PPM, therefore the upper limit for the offset angles is the approximate average of both angles that is below ±3.65° (e.g., p_x = 4°, y_x=3°, average 3.5°). Keep in mind that for a well-constructed instrument, it is unusual to have large accelerometer offset angles.

$$\left\| \left| \begin{bmatrix} 1 - \frac{y_x^2}{2} - \frac{p_x^2}{2} \\ -y_x \\ p_x \end{bmatrix} \right\| \right| = \left(\left(1 - \frac{y_x^2}{2} - \frac{p_x^2}{2}\right)^2 + y_x^2 + p_x^2 \right) \cong 1 + \frac{(y_x^2 + p_x^2)^2}{4} \cong 1; \tag{A.1.23}$$

$$\text{for } \frac{|y_x| + |\ p_x|}{2} \cong 3.65^O > \ |y_x|\ \&\ |p_x| > 0.1^O$$

A.2: Angle articulation device (AAD) math model

The instrument output is a function of the position of the accelerometer within the enclosure and the apparatus which rotates the instrument in its respective space. For instance, the output for the 1xAI is a function of the offset angle between the accelerometer and the enclosure reference plane, and the device which rotates this instrument relative to the global frame of reference with gravity aligned with *Z*-axis (G_{wg}). By keeping both the instrument position vectors and AAD math models separate, it is possible to apply the instrument output model to more complex AAD math models. However, estimating pitch and roll angles may not be straight forward unless all the parameters in the equations are well known, which makes this topic beyond the scope of this paper.

The common use for the 3xAI instrument is to always rotate it in alignment with the AAD orthogonal planes. Any misalignment of the instrument interface planes with AAD interface planes causes a measurement error, which is a function of the rotation axes of the AAD times the magnitude of the misalignments. Appendix A.3.3 will provide additional explanation of this effect.

A.2.1: Single axis angle articulation device

A single axis AAD (e.g., the Calibration Device (CD) or Test article) contains an interface plane where its rotational movement, as per kinematics, can be represented by Equation (A.1.5). Equation (A.1.5) represents each axis (*x* and *z*) of the local frame (L) projected onto each axis (*X* and *Z*) of the global frame (G). However, the only elements of interest are the individual axes in L (*x* and *z*) projected on to the G *Z*-axis since the accelerometers in the instrument can only track the projections of their respective position vectors (equations for 1xAI (A.1.6) or 2xAI (A.1.8)) projected onto the G_{wg} *Z*-axis. Therefore, the vector which best represents this AAD interface plane is the second row of Equation (A.1.5), presented in Equation (A.2.1) and substituting α with p.

$$g^T\ vector = [g_x \quad g_z] = [x.Z \quad z.Z] = \ [Sin(p) \quad Cos(p)] \tag{A.2.1}$$

For the method described in this paper, it is critical that Equation (A.2.1) either nullifies the misalignment or accounts for it as illustrated in Figure 8. Figure 8 illustrates the accelerometer local reference frame (in blue) tilted by p_x relative to G (in red), G is the AAD reference frame, which is tilted by *S* relative to the G_{wg}. If G is not aligned to Gwg then the angle *S* becomes an unaccounted residual misalignment.

Equation (A.1.5) represents a rotation of L relative to G, which may or may not be aligned with G_{wg}. More specifically, representing L relative to G_{wg} requires G and G_{wg} to be in complete alignment. There are three different misalignments of G with respect to G_{wg}, namely pitch, roll, and yaw. The single tilt instrument ignores roll and yaw, where yaw does not play a role in the calibration since the instrument is insensitive to rotation of the instrument relative to the normal vector or Z_{wg}. However, a yaw misalignment with respect to the G *Z*-axis can play a role in the measurement error. This error is a function of the magnitude of this yaw misalignment, which is not part of the model, and is proportional to the pitch range. Note that with today's technology, it is not yet feasible to estimate this yaw misalignment after mounting the instrument to any AAD reference plane.

The pitch misalignment between the two frames of reference (G and G_{wg}) can be modeled, and it is very easy to show how this misalignment can bias the instrument coefficients that pertain to pitch. For the standard calibration process, this misalignment does transfer again to the instrument coefficients unless it is accounted for or nullified before calibration. The new approach for estimating the instrument coefficients, which is the focus of this paper, does not transfer this misalignment. Note that there are specific circumstances where this misalignment magnitude can affect estimating the sensitivity and bias coefficients demonstrated in Section, 2.4.

This pitch misalignment can be modeled using Equation (A.1.5) with $\alpha = p$ and then multiply the same matrix for $\alpha = S$.

The following two trigonometric identities in Equation (A.2.2) are transformed by assuming that δ is a small angle,

$$\begin{aligned} Sin(p+\delta) &= Sin(p)Cos(\delta) + Sin(\delta)Cos(p) = Sin(p) + \delta\, Cos(\mathrm{p}) \\ Cos(p+\delta) &= Cos(p)Cos(\delta) - Sin(\delta)Sin(p) = Cos(p) - \delta\, Sin(\mathrm{p}) \end{aligned} \tag{A.2.2}$$

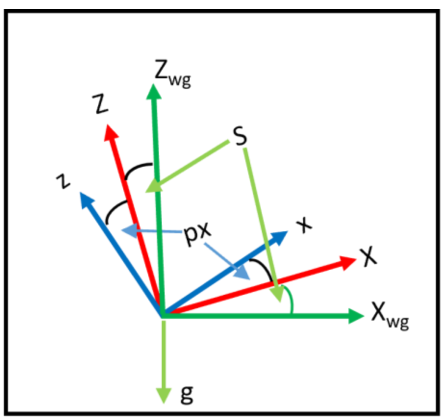

Figure 8. The accelerometer frame of reference frame relative to the enclosure and relative to a global frame of reference.

Figure 8 illustrates the accelerometer frame of reference frame (in blue) relative to the enclosure frame of reference (in red), which is relative to G_{wg}.

The right hand side of Equation (A.2.3) is simplified using Equation (A.2.2) in reverse (S is a small angle),

$$\begin{bmatrix} Cos(p) & -Sin(p) \\ Sin(p) & Cos(p) \end{bmatrix} \begin{bmatrix} 1 & -S \\ S & 1 \end{bmatrix} = \begin{bmatrix} Cos(p+S) & -Sin(p+S) \\ Sin(p+S) & Cos(p+S) \end{bmatrix} \tag{A.2.3}$$

Only the second row is relevant to the instrument, since the instrument accelerometer output changes with a rotation of the instrument L relative to G_{wg} Z-axis.

Equation (A.2.4) works for the 1xAI and 2xAI.

$$g_v^T \; vector \; with \; misalignment = \; g_{vm}^T = [Sin(p+S) \quad Cos(p+S)] \tag{A.2.4}$$

The math model for the 3xAI CD was demonstrated in Reference 1, which contains the misalignments and different mounting orientations. To duplicate a similar model for the single axis instruments that provides different mounting orientations requires a kinematics matrix rotation for 2D models, described in the next paragraph. Keep in mind that unlike the 3xAI, which requires a minimum of three mounting orientations, for the single axis tilt instruments, only two mounting orientations are required. These mounting orientations are the primary orientation (chosen for standard calibration and for measurements) and the opposite orientation (instrument rotated 180° in yaw relative to the interface plane normal vector or G *Z*-axis).

The first 2D rotation matrix, described in Equation (A.1.5), is a rotation of L relative to G *Y*-axis. In 2D this *Y*-axis is not shown, however, imagine the 2D graphical representation as 3D system where the *Y*-axis is either pointing into the page or out of the page. The *Y*-axis direction depends on the selected right-hand or left-hand rule, as mentioned in Appendix A.1. It is possible to extract the AAD math model in 2D with two mounting orientations using the 3xAI instrument math model in Equation (A.3.5). This can be achieved by deleting the second column and row vectors in 3D and setting $r = 0$ and $u = 0$. The deleted vectors pertain to the L *y*-axis and G *Y*-axis. This same strategy can be applied to the 3D yaw rotation in Equation (A.1.12) by deleting the same two aforementioned vectors in order to obtain the 2D rotation in yaw, Equation (A.2.5).

The correct way to derive the yaw rotation matrix is to apply the same approach used to derive kinematics Equation (A.1.5), which showed a rotation of L relative to G *Y*-axis (not mentioned during the derivation). A yaw (y) rotation is a rotation of L relative to the G *Z*-axis, which means that L *z*-axis does not change with this rotation, while L x-axis (for single axis), and L y-axis (including x-axis for 3xAI) do change. The result is Equation (A.2.5), where the first column vector represents the x-axis and second column vector represents the z-axis.

It is noted that this matrix is intended to change the sign of the output of the instrument *x*-axis for the two mounting orientations of interest. The only two values for this yaw are exactly 0 and 180°;

however, if there is any residual yaw angle relative to these two values, then this may become a source for bias. This is an especially important consideration for the 3xAI instrument.

The yaw rotation in 2D is given by Equation (A.2.5),

$$yrot[y] = \begin{bmatrix} \mathrm{Cos}(y) & 0 \\ 0 & 1 \end{bmatrix} \tag{A.2.5}$$

Obtaining the angle articulation math model that includes this mounting orientation matrix requires finding the matrix product of Equation (A.2.3) with Equation (A.2.5), as shown in Equation (A.2.6), and then selecting the second row vector to obtain Equation (A.2.7).

$$\begin{aligned} &\begin{bmatrix} Cos(p+S) & -Sin(p+S) \\ Sin(p+S) & Cos(p+S) \end{bmatrix} \begin{bmatrix} Cos(y) & 0 \\ 0 & 1 \end{bmatrix} \\ &\qquad = \begin{bmatrix} \mathrm{Cos}(y)Cos(p+S) & -Sin(p+S) \\ \mathrm{Cos}(y)Sin(p+S) & Cos(p+S) \end{bmatrix} \end{aligned} \tag{A.2.6}$$

Therefore, the best model for the AAD/CD is as follows:

$$g_{vm}^{T} = \begin{bmatrix} \mathrm{Cos}(y)Sin(p+S) & Cos(p+S) \end{bmatrix} \tag{A.2.7}$$

A.2.2: Two-axis angle articulation (pitch and roll) device

The kinematic model to describe the motion of any AAD depends on the design of such a device. Given that the need is for measuring angles relative to gravity, most systems can be simplified by a general pitch and roll kinematics model. There are various reasons for not including yaw rotations into a gravity referenced instrument kinematics model. If the yaw articulation happens with respect to the G_{wg} Z_{wg}-axis, then the instrument output does not change. However, if the yaw articulations occur relative to the G *Z*-axis that is normal to the instrument interface plane, then these rotations will add complexity to the measurement and make it challenging to determine the desired angle measurements. The exemption is when these rotations, e.g., 0 and 180°, serve to change the mounting orientation of the instrument.

The math for a gravity-reference instrument is simplified immensely if the instrument is aligned with the AAD reference planes and articulated purely relative to the pitch and/or roll axes. Any or all misalignments (depending on magnitude) in the AAD or introduced during installation of the instrument that are not accounted for or nullified, will be a source for systematic errors. These misalignments are transferred to the instrument during standard calibration as biases, and as measurement errors during operations.

A.2.3: Calibration Device Model

The derivation for the CD math model was presented in Reference 1; however, it was not simplified beyond Equation (A.2.10) shown below. The kinematic model (KM) for a two-axis rotary system used as a calibration device (CD), was determined by Equation (A.2.8), which results in Equation (A.2.9).

$$KM_{3x3} = rrt(b)prt(p)prt(a)yrt(d)rrt(r)rrt(f)prt(e)yrt(k)yrt(y_{fb})rrt(u_{tb}) \tag{A.2.8}$$

$$KM = \begin{array}{cc} \begin{array}{ccc} x & y & z \end{array} & \\ \begin{bmatrix} x.X & y.X & z.X \\ x.Y & y.Y & z.Y \\ x.Z & y.Z & z.Z \end{bmatrix} & \begin{array}{c} X \\ Y \\ Z \end{array} \end{array} \tag{A.2.9}$$

As mentioned in the single-axis AAD, Appendix A.2.1 above, the only components of interest are the local frame axes projected onto the G *Z*-axis. These components are found in the third row of Equation (A.2.9), which is the gravity vector (g_{vm} with misalignments) in 3D. The vector components can be defined as a function of the mounting orientations, fixed misalignment (constants), and the pitch and roll angle articulations (variables).

$$g_{vm}^T = [x.Z \quad y.Z \quad z.Z] = \mathrm{g}[p,r,b,a,d,f,e,k,y,u]^T \tag{A.2.10}$$

Variables:

p = pitch angle

r = roll angle

Fixed Misalignments:

b = system (as a rigid body) roll misalignment

a = system (as a rigid body) pitch misalignment

d = orthogonal misalignment between the rotary axes

f = the reference (instrument mounting plane) x-y plane roll misalignment[1]

e = the reference, x-y plane pitch misalignment[1]

k = the reference (dowels reference), x-z plane yaw misalignment[1]

[1] The reference misalignments exclude instrument mounting misalignments.

Mounting Orientation parameters:

y = 0 (Forward mounted) or 180° (Backward mounted)

u = 0 (Top mounted) or 180° (Bottom mounted)

This model can be simplified by using small angle approximations. It is noted that this approximation has shown near identical results vis à vis the full model.

The g_{vm} approximation is given in Equation (A.2.11),

$$g_{vm} = \begin{bmatrix} \text{Cos}(y)(\text{Sin}(p) + \left(a + e\,\text{Cos}(r) - k\,\text{Sin}(r)\right)\text{Cos}(\text{p})) \\ \text{Cos}(u)\text{Cos}(y)\left(\text{Cos}(p)(\text{Sin}(r) + f\,Cos(r)) + b\,\text{Cos}(r) + \left(k - a\text{Sin}(r) + d\,\text{Cos}(r)\right)\text{Sin}(p)\right) \\ \text{Cos}(u)\left(\text{Cos}(p)(\text{Cos}(r) - f\,Sin(r)) - b\,\text{Sin}(r) - \left(e + a\,\text{Cos}(r) + d\,\text{Sin}(r)\right)\text{Sin}(p)\right) \end{bmatrix} \quad \text{(A.2.11)}$$

To demonstrate how Equation (A.2.10) turns to Equation (A.2.11) by using small angle approximation, it is important to evaluate the impact of this approximation to the desired goal of finding the instrument coefficients with a CD with unknown misalignments. To simplify this demonstration, only g_{vx} is shown, since the other two g_v components behave in the same manner. The first step is to substitute each Sin(misalignment) with the misalignment itself (i.e., Sin(x)=x). The result is a g_{vx} that contains elements with a single misalignment and with multiple misalignments multiplied by each other. Any element with two or more misalignments multiplied together can be considered zero, which makes the equation a second order approximation error type equation. For example, if the misalignments are within ±0.1° (1.745e-3 radians) then two misalignments of similar magnitude multiplied by each other will result in $(1.745\text{ mrad})^2 \cong 3\text{E}-6\ (\text{rad})^2 \cong 0$. However, if the misalignments have magnitudes larger than 0.1°, then these second order elements (two misalignment products) will increase the error in the estimates of the instrument coefficients. How this affects the estimates of the instrument coefficients is beyond the scope of this paper. Nevertheless, this subject is covered in Section 2.4.2 of the paper, and in Appendix G, which demonstrates how to correct for system misalignments > 0.1°.

Equation (A.2.12) keeps all the single misalignment elements and it shows that the coefficients in front of each of the remaining parameters have $(\text{Cos(misalignment)})^N$, where N is the number of misalignments (which is different for each parameter). Although $Cos(x) \cong 1$, $Cos(x)^N < 1$, which is not a concern if x is within ±0.1°. To show more granularity, if x = 0.2°, then $Cos(0.2^o)^5 = 0.9999695$, which can reduce the sensitivity calculation by (1-0.9999695) *10^6 = 31ppm. This delta in sensitivity reduces the pitch angle accuracy as pitch is increased, thus it has no effect at pitch near 0 degree and it reaches approximately 0.002° or 7.2 arcsecs error at pitch = 30°, which is the max error budget at calibration, hence maintaining the misalignments with ±0.1° is preferred.

$$g_x = \text{Sin}(p)\ \text{Cos}(a)\text{Cos}(b)\text{Cos}(d)\text{Cos}(e)\text{Cos}(k) \quad \text{(A.2.12)}$$

$$
\begin{aligned}
&+ \mathrm{Cos}(p)(a\ \mathrm{Cos}(b)\mathrm{Cos}(d)\mathrm{Cos}(e)\mathrm{Cos}(k) \\
&+ e\ \mathrm{Cos}(r)\ \mathrm{Cos}(a)\mathrm{Cos}(b)\mathrm{Cos}(g)\mathrm{Cos}(k) \\
&- k\ \mathrm{Sin}(r)\ \mathrm{Cos}(a)\mathrm{Cos}(b)\mathrm{Cos}(g))
\end{aligned}
$$

Returning to Equation (A.2.11), there are a few ways to dissect this gravity vector that can provide clarity to the reader of what this equation means. In summary, the gravity vector components contain a set of CD misalignments where each of them will dominate the component value depending on where the system is within the 360^{o} pitch x 360^{o} roll space.

The purpose of the following equation is to provide clarity for Equation (A.2.11), and is not intended to be a substitute.

Using Equation (A.2.2) with the *x*-axis component of g_{vm} and grouping the misalignment into $\delta = a + e*\mathrm{Cos}(r) - k*\mathrm{Sin}(r)$ results in Equation (A.2.11) transforming into Equation (A.2.13).

$$
\begin{aligned}
g_{vmx} &= \mathrm{Cos}(y)\mathrm{Sin}\big(p + a + e\ \mathrm{Cos}(r) - k\ \mathrm{Sin}(r)\big) \text{ or} \\
g_{vmx} &= \mathrm{Sin}\Big(\mathrm{Cos}(y)\big(p + a + e\ \mathrm{Cos}(r) - k\ \mathrm{Sin}(r)\big)\Big)
\end{aligned}
\tag{A.2.13}
$$

What Equation (A.2.13) shows is that the dominant misalignments for the *x*-axis component of the g_{vm} vector are *a*, *e*, and *k* (system pitch, reference *x-y* plane pitch and *x-z* plane yaw). These misalignments are offset angles of the reference plane for which "*a*" is a constant offset for all pitch angles, and the magnitude of the other two offset angles are a function of roll. With one misalignment, *e* or *k* dominates this component depending on the angle position in roll.

For $r = 0$, then the g_{vm} in Equation (A.2.13) is identical to the first component in (A.2.7) for $S = a + e$.

The same strategy can be applied to other two component of the g_{vm} vector.

$$
\begin{aligned}
g_{vmy} = \mathrm{Cos}(u)\mathrm{Cos}(y)\Big(&\mathrm{Cos}(p)\mathrm{Sin}(\mathrm{r} + b\ Sec(\mathrm{p}) + f + d\ Tan(p)) \\
&+ \big(k - a\mathrm{Sin}(r)\big)\mathrm{Sin}(p)\Big)
\end{aligned}
\tag{A.2.14}
$$

For $p = 0$ the equation simplifies to (A.2.15), which shows that for all roll the error = $b + f$.

$$
g_{vmy} = \mathrm{Cos}(u)\mathrm{Cos}(y)\mathrm{Sin}(\mathrm{r} + b + f) \tag{A.2.15}
$$

$$
g_{vmz} = \mathrm{Cos}(u)\Big(\mathrm{Cos}(p)\mathrm{Cos}[\mathrm{r} + b\ Sec(p) + f + d\ Tan(p)] - \big(e + a\mathrm{Cos}(\mathrm{r})\big)\mathrm{Sin}(p)\Big) \tag{A.2.16}
$$

Again, for $p = 0$ or $r = 0$, then g_{vmz} simplifies to Equation (A.2.17),

$$p = 0 \; then \; g_{vmz} = \mathrm{Cos}(u)\mathrm{Cos}(\mathrm{r} + b \; + f)$$
$$r = 0 \text{ then } g_{vmz} = \mathrm{Cos}(u)\mathrm{Cos}(p + e + a) \tag{A.2.17}$$

Equation (A.2.17) confirms the roll error when $p = 0$. In addition, when $r = 0$ and if $S = e \; + a$ then it is identical to the second component in g_{vm} in Equation (A.2.7) for the 1xAI and 2xAI instruments, which it is only mounted on the top plane, thus $u = 0$.

As demonstrated above, the elements at the end of Equations (A.2.14) and (A.2.16), including the orthogonal misalignment, have little effect for low pitch angle ranges. The effect of these elements will depend on the magnitude of the misalignments, the pitch angle value (max effect at $p = \pm 90^{o}$), and the instrument specifications. This implies that the higher the accuracy of the instrument, the higher the probability they will play a larger role. The other misalignments, b and f, dominate these two equations, (A.2.14) and (A.2.16), for roll angles. These misalignments are unaccounted offset angles, which most likely get transferred to the instrument coefficients. This last statement is dependent on the calibration procedure and the angle setpoints chosen as inputs. The f misalignment is a constant offset for all roll angles, and the magnitude of the b misalignment gets larger as pitch angle increases. Although this interpretation is not congruent with observations, Equation (A.3) in Appendix A of Reference 1 showed the instrument coefficients being biased by this misalignment, b Sec(p). Keep in mind that this was the result of performing a symbolic least square regression using only pitch angle setpoints on the right side of the sphere. However, if additional pitch angle setpoints from the left side of the sphere are added to input, then this bias is canceled when performing any L^2 norm calibration. For gravity reference instruments, symmetry can be achieved in different ways. The simplest are shown in Section 2 "Estimating the Instrument Coefficients with Algebra".

This new way of representing Equation (A.2.11), as Equation (A.2.18), may help explain other incongruencies. These incongruencies have to do with estimating the accelerometers sensitivity and bias coefficients. If Equation (A.2.11) is used to model the effect of placing each accelerometer in the 1g field by rotating the accelerometer by ±90° from the level plane, then it will show that the misalignments are zeroed out, indicating that they have no effect at this angle position. However, when using Equation (A.2.18), these misalignments are not zeroed out, thus making it easier to find the optimal 1g field, especially if the misalignments in the system are large. This topic is discussed in the main portion of Section 2.4 "Obtaining the accelerometer sensitivity and bias coefficients" of this paper. Both Equations (A.2.11) and (A.2.18) are trigonometrically identical. However, caution should be used when preferring one set of equations over others at different angle position in the 360° x 360° angular space.

$$g_{vm} = \begin{bmatrix} \mathrm{Cos}(y)\mathrm{Sin}(p + a + e\,\mathrm{Cos}(r) - k\,\mathrm{Sin}(r)) \\ \mathrm{Cos}(u)\mathrm{Cos}(y)\left(\mathrm{Cos}(p)\mathrm{Sin}\big(\mathrm{r} + b\,Sec(p) + f + d\,Tan(p)\big) + \big(k - a\mathrm{Sin}(r)\big)\mathrm{Sin}(p)\right) \\ \mathrm{Cos}(u)\left(\mathrm{Cos}(p)\mathrm{Cos}\big(\mathrm{r} + b\,Sec(p) + f + d\,Tan(p)\big) - \big(e + a\mathrm{Cos}(r)\big)\mathrm{Sin}(p)\right) \end{bmatrix} \tag{A.2.18}$$

A.3: Instrument output models for 1xAI, 2xAI, and 3xAI

The instrument output model presented in Equation (A.3.1) is a generic model and the units can be voltage (V) or current (Amp). To simplify the derivation, the output units are in volts. Therefore, B_x is the bias output in Volts, and S_x is the scale factor (referred in this paper as sensitivity) in V/g. The g_v^T is found in Equations (A.2.1) and (A.2.11) and the instrument coefficient matrix from Equations (A.1.7), (A.1.9), or (A.1.20); which selection is dependent on the number of accelerometers in the instrument.

$$Instrument\ output = B_x + g_{vm}^T * S_x * coefficient\ matrix \qquad (A.3.1)$$

There are a few caveats about the sensitivity parameter. The estimate for S_x is independent of the method used to obtain it. However, each method presents this sensitivity parameter in a different way. For instance, the method demonstrated in this paper obtains this estimate directly, Section 2.4 "Obtaining the accelerometer sensitivity and bias coefficients." On the other hand, the least square solution demonstrated in Appendix B.1 presents this parameter as vector, $S_w * coefficient\ matrix$, thus requiring the calculation of the magnitude of this accelerometer column vector to estimate S_w, where $w = x, y,$ and or z . In addition, this parameter is the amplitude of the trigonometry function that represents the output of each axis. The correct sensitivity for each accelerometer is the derivative of this trigonometry function. For instance, the most basic function to represent a 1xAI is found in Equation (A.3.3), where $p_x = 0$, therefore $V_x = B_x + S_x Sin[p]$. The sensitivity of this accelerometer is the slope of the curve or $S_x Cos[p]$. What this shows is that the accelerometer sensitivity is relatively constant for a range of angles around $p = 0$ and the sensitivity starts to decrease, reaching zero sensitivity, as p approaches ±90°. What this indicates is that the real sensitivity of the accelerometers is variable, peaking around the zero g field and reducing to zero at the ±1g fields. The marginal voltage output change of the accelerometer decreases to zero, as the pitch get closer to ±90°.

The sensitivity magnitude is dependent of the local gravity magnitude. Therefore, estimating this parameter at two location with vastly different gravity magnitudes will provide two different results. The method for correcting for local gravity is to multiply the sensitivity by the local (measurement location) gravity magnitude and divide by the gravity magnitude at the calibration location. The Global Information System (GIS) is a source for the average gravity magnitudes by geographical area. Earth gravity magnitude varies by the local geographical density and distance to the center of the earth; therefore, there is a difference between the magnitude at the equator and the poles, and with elevation relative to the surface.

The reason why a single row vector (which represents the gravity vector) is to the left of each instrument coefficient matrix is because the instruments are sensitive to the G *Z*-axis of a kinematic model of the AAD. The G *Z*-axis is the last row of this AAD kinematic model. For the 1xAI and 2xAI this is the last row of a 2 X 2 kinematic model. This is particularly obvious for the 3xAI, where Equation (A.2.10) is the last row of Equation (A.2.9), which is the full kinematics model of the CD with misalignments. The top two rows of this model are not trackable with these gravity referenced instruments, thus not part of the equation. Instead of using Equation (A.3.2) to represent the instrument, which is an accurate representation but not practical, Equation (A.3.5) in the below section is used. The rational for this explanation is to avoid confusion for those with linear algebra knowledge.

$$\begin{bmatrix} 0 & 0 & 0 \\ 0 & 0 & 0 \\ V_x & V_y & V_z \end{bmatrix} = \begin{bmatrix} 0 & 0 & 0 \\ 0 & 0 & 0 \\ B_x & B_y & B_z \end{bmatrix} + \begin{bmatrix} 0 & 0 & 0 \\ 0 & 0 & 0 \\ x.Z & y.Z & z.Z \end{bmatrix} \begin{bmatrix} S_x & y_y S_y & -p_z S_z \\ -y_x S_x & S_y & -r_z S_z \\ p_x S_x & r_{yS_y} & S_z \end{bmatrix} \qquad \text{(A.3.2)}$$

A.3.1: The output model for 1xAI

The equations below will use the full model for the AAD developed in the previous section. This is critical for determining the real instrument coefficients, whether using conventional or algebraic methods.

$$V_x = B_x + [Cos(y)\,Sin(p+S) \quad Cos(p+S)] * S_x * \begin{bmatrix} 1 \\ p_x \end{bmatrix} \qquad \text{(A.3.3)}$$

A.3.2: The output model for 2xAI

$$\begin{bmatrix} V_x \\ V_z \end{bmatrix}^T = \begin{bmatrix} B_x \\ B_z \end{bmatrix}^T + [Cos(y)\,Sin(p+S) \quad Cos(p+S)] \begin{bmatrix} 1 & -\mathrm{p}_z \\ \mathrm{p}_x & 1 \end{bmatrix} \begin{bmatrix} S_x & 0 \\ 0 & S_z \end{bmatrix} \qquad \text{(A.3.4)}$$

A.3.3: The output model for 3xAI

$$\begin{bmatrix} V_x \\ V_y \\ V_z \end{bmatrix}^T = \begin{bmatrix} B_x \\ B_y \\ B_z \end{bmatrix}^T + g_{vm}^T \begin{bmatrix} 1 & y_y & -p_z \\ -y_x & 1 & -r_z \\ p_x & r_y & 1 \end{bmatrix} \begin{bmatrix} S_x & 0 & 0 \\ 0 & S_y & 0 \\ 0 & 0 & S_z \end{bmatrix} \qquad \text{(A.3.5)}$$

Where g_{vm}^T is equation (A.2.11)

To reiterate, the models in this section were derived with the assumption that the accelerometers' offset angles have magnitudes < 0.1°. If the accelerometers' offset angles were larger than 0.1°, this information doesn't change the model, except for the diagonal elements, in the second to last matrix, which pertain to the sensitivity coefficients. These elements will change by the product of the Cosine of other elements in the column vector that represents the respective accelerometer. For instance, for the 3xAI the *x*-axis accelerometer column vector is composed of $[1 \quad -y_x \quad p_x]$, which under this circumstance the new column vector is $\left[(1 - \frac{y_x^2}{2} - \frac{p_x^2}{2}) \quad -y_x \quad p_x\right]$. This new element is derived from Taylor series for the $Cos(y_x)Cos(p_x) \cong (1 - \frac{y_x^2}{2})(1 - \frac{p_x^2}{2}) \cong (1 - \frac{y_x^2}{2} - \frac{p_x^2}{2})$. The full matrix is found in example 6 in Appendix G.

Appendix B: Other Methods for Obtaining Instrument Coefficients

Solving for the instrument coefficients

As mentioned in the introduction, there are various procedures for obtaining the instrument coefficients, References 1, 3, 7, 8, 9, 10, 11, and 12. The conventional method is to perform a least square regression. This process requires knowledge of the angle setpoints to an accuracy equal to or greater than the instrument under calibration. Unfortunately, the estimate of the angle setpoints can contain residual misalignments of the calibration device (CD) that change depending on the angle position in the 3D space. The practical approach to obtaining an unbiased estimate of the instrument coefficients is to nullify the misalignments in the CD. In addition, it assumes that the rotary device index and wobble variations have a zero mean for the selected calibration angle points. Otherwise, the misalignments and other variations get partially or fully transferred to the estimate of the instrument coefficients. This transfer is a function of the selected angle setpoints. The orthogonal points only transfer the misalignments of the reference planes, while angle setpoints that are within one side of the full sphere (as demonstrated in Appendix A of Reference 1) transfer all the CD misalignments to the instrument coefficients. On the other hand, if using the orthogonal positions with different mounting orientations, then it is possible to cancel out the reference plane misalignments. This assumes that the reference planes meet requirements, which is not easy to achieve.

Another approach for estimating the instrument coefficients and the CD misalignments is by using an optimization algorithm (OA). For documentation purposes, Appendix B.2 will demonstrate that the OA finds the global minimum for all parameters if the input angle setpoints have full symmetry. As mentioned in the introduction, the importance of this OA is that it opened the door for finding the method presented in this paper.

To share how verifying the OA results influenced the discovering of the algebraic solution needs more context. After reducing the CD math model to Equation (A.2.11) and using the 16 orthogonal angle setpoints times 3 accelerometers times all 4 mounting orientations, this creates 192 equations, which are found in Appendix E. These tables show 16 angle setpoints per mounting orientation, including the accelerometers +1g or -1g (used to determine the sensitivity and bias coefficients). The equations are separated out into a group that place the accelerometers near the zero g field, and then they are matched into symmetrical pairs, using the rules explained in Section 2 “Estimating the instrument coefficients with algebra”. Using these pairs, it is possible to obtain multiple replicates for each of the parameters (instrument coefficients and CD misalignments). The average of these replicates shows near identical results to the OA results. In addition, this work shows that the average of the instrument coefficients can be skewed by the mounting/reference planes when such reference planes do not meet the requirements that the top and bottom planes are flat, smooth, and parallel. In addition, the *X-Z* orthogonal plane is in the same plane when accessing it from the top and bottom planes. Therefore, to reduce the probability of introducing other biases to any of the L^2 norm solutions, the algebraic solution showed the best probability of estimating the coefficient without any biases. It is noted that this algebraic solution reduces the many requirements for any of the L^2 norm solutions. The algebraic solution does **not** require that the reference top and bottom *x-y* planes be parallel, the *x-z* plane be orthogonal to the *x-y* plane or that multiple angle setpoints be known to an accuracy equal to or better than the instrument accuracy specification. However, in addition to the other requirements for L^2 norm methods, this algebraic solution does require some flexibility in dialing the angle setpoints for obtaining the accelerometers' sensitivity and bias coefficients, as explained in Section 2.4 "Obtaining the accelerometer sensitivity and bias coefficients."

There are a few challenges with these approaches including the algebraic solution. For instance, practice has shown that it is challenging to nullify the CD misalignments to below the instrument accuracy specifications, although the methods shown in this paper have improved the probability of achieving this nullification. Other challenges come from the mounting variation from calibration to calibration, which is relatively small for pitch and roll (within ± 2 arcsecs). This result is from using the same calibrator and on the same reference plane, and it is suspected that it may be different for other references. The hypothesis is challenging to verify without other references that meet requirements and having multiple calibrators, not to mention resources. For the *x-z* plane or yaw, this variability is currently relatively high (within ±50 arcsecs or higher). The reason for the large yaw variation is due to the instrument form factor, the short distance of the contact points for the dowels or *X-Z* plane, and the use of fasteners to secure the instrument. The sequence of tightening of the fasteners can cause variation in pitch and roll, when interfacing the instrument to a surface that is not flat, especially if the instrument's own interface plane is not flat. Other effects are rotational forces from torquing these fasteners, which can cause yaw rotation (most likely) and torsional forces (impossible to verify) to the instrument enclosure. The hypothesis is that these torsional forces can move the sensors position relative to the enclosure reference planes.

A method within L^2 norm, which showed promise in estimating the CD misalignments, is the OA demonstrated in the next section. This method can provide an estimate for the misalignments, although they can be biased by the variation of each parameter and other factors. One observation found when nullifying the CD misalignments with the results of the OA is that, for the standard mounting orientation, the residual errors for the other 3 mounting orientations are not zero and they may exceed the instrument accuracy specifications. In other words, favoring one mount for standard calibrations after nullifying the misalignments with these estimates can potentially bias the instrument coefficients.

In addition, each L^2 norm has its pros and cons. The standard method, least square regression, has an advantage that it only requires installing the instrument in one orientation. The disadvantage is that if there are any residual misalignments in the CD, these are transferred to the instrument coefficients. The OA has the advantage that it does not require a CD with nullified or known misalignments to determine the desired parameters. The disadvantage is that it requires high repeatable angle setpoints for each mounting orientation and that the reference meets all the requirements.

B.1: Least square regression for instrument calibration

There are two L^2 norm methods described in this appendix for obtaining the instrument calibration coefficients. The first method, the least square regression, requires known (to an accuracy equal to or better than the instrument under calibration) angle setpoints, and the second method, an OA does not require known angle setpoints. The first method, which is the current method of choice (albeit for a single mount), is applied to all three instruments discussed in this paper. The second method has only been investigated as an approach for obtaining the instrument coefficients of the 3xAI instrument and the CD misalignments.

The selected angle setpoints for these two methods can have an impact to the coefficient estimates. The region chosen within 360° pitch x 360° roll, the number of points, and the symmetry of the points and repeatability of these points can have an impact if multiple mounting orientations are used. For the least square regression, using multiple mounting orientations was discussed in Reference 1. For the OA, to find the global minimum, regardless of initial guess, requires total symmetry between the selected angle setpoints. Total symmetry requires the full region within 360° pitch x 360° roll, and the 4 mount orientations described at the top of this Appendix B:

The generic equation to solve for the coefficients using a least square regression was described in Equation (A.3.1). To apply least square regression requires *n* angle setpoints to place the instrument in different angular positions and record the output at each input value. Afterwards, the following linear algebra operations are applied to the data.

B.1.1: 1xAI coefficient vector

When estimating the coefficient matrix for the 1xAI instrument using a least square regression, the assumption is that the CD has zero misalignments, Equation (A.2.1), and the instrument is mounted in the standard orientation. Rearrange Equation (A.3.3) and then apply a least square regression for *n* angle setpoints, Equation (B.1),

$$V_{x(nx1)} = \begin{bmatrix} 1 & g^T \end{bmatrix}_{nx3} \begin{bmatrix} B_x \\ S_x \\ S_x p_x \end{bmatrix}; \; where \; g_v^T = Sin(p) \quad Cos(p) \tag{B.1}$$

Note, it is possible to obtain the instrument coefficient with the g_{vm}^T if the misalignment(s) are known, Equation (A.2.4). If the misalignment(s) are not known, then it requires two mounting orientations, thus requiring Equation (A.2.7).

This is most likely an overdetermined system; therefore, this regression can be obtained with this simple matrix operation, from Reference 4, Equation (B.2).

$$\begin{bmatrix} B_x \\ S_x \\ S_x p_x \end{bmatrix} = \left[\begin{bmatrix} 1 & g_v^T \end{bmatrix}_{3xn}^T \begin{bmatrix} 1 & g_v^T \end{bmatrix}_{nx3} \right]^{-1} \begin{bmatrix} 1 & g_v^T \end{bmatrix}_{3xn}^T V_{x(nx1)} \tag{B.2}$$

The correct method to obtain the absolute value for S_x when using least square regression is to obtain the magnitude of the accelerometer position vector, in this representation $S_x[1\ p_x]$. Equation (B.2), which is a simplified expression of the *x*-axis accelerometer coefficient vector, shows that S_x can be estimated from the first element in the position vector, which in this representation is the second element. This is valid if $p_x < \pm 0.1°$. If $p_x > \pm 0.1°$, then S_x is best found by obtaining the magnitude of the position vector, which are elements below the bias parameter. This applies to the following two instruments, 2xAI and 3xAI described below. There is more nuance to this subject, in Appendix A.1.4.2: “3xAI Coefficient Matrix,” which shows in Equation (A.1.23) how to correct the position vector for the *x*-axis in a 3xAI when the accelerometers' offset angles are > ± 0.1°.

B.1.2: 2xAI coefficient matrix

When estimating the coefficient matrix for the 2xAI instrument, rearrange Equation (A.3.4) and then apply a least square regression for *n* angle setpoints, Equation (B.3),

$$\begin{bmatrix} V_x \\ V_z \end{bmatrix}_{nx2}^{T} = [1 \quad g_v^T]_{nx3} \begin{bmatrix} B_x & B_z \\ S_x & -S_z \mathrm{p}_z \\ S_x \mathrm{p}_x & S_z \end{bmatrix} \tag{B.3}$$

$$\text{Where} \quad g_v^T = [Sin[p] \quad Cos[p]]$$

Solving for the coefficient matrix, Equation (B.4)

$$\begin{bmatrix} B_x & B_z \\ S_x & -S_z \mathrm{p}_z \\ S_x \mathrm{p}_x & S_z \end{bmatrix} = [[1 \quad g_v^T]_{3xn}^T [1 \quad g_v^T]_{nx3}]^{-1} [1 \quad g_v^T]_{3xn}^T \begin{bmatrix} V_x \\ V_z \end{bmatrix}_{nx2}^{T} \tag{B.4}$$

$$\text{Where} \quad g_v^T = [Sin(p) \quad Cos(p)]$$

B.1.3: 3xAI coefficient matrix

When estimating the coefficient matrix for the 3xAI instrument, rearrange Equation (A.3.5) and then apply a least square regression for *n* angle setpoints, Equation (B.5),

$$\begin{bmatrix} V_x \\ V_y \\ V_z \end{bmatrix}_{nx3}^{T} = [1 \quad g_v^T]_{nx4} \begin{bmatrix} B_x & B_y & B_z \\ S_x & S_y y_y & -S_z p_x \\ -S_x y_x & S_y & -S_z r_z \\ S_x p_x & S_y r_y & S_z \end{bmatrix} \tag{B.5}$$

$$where\ g_v^T = [Sin(p) \quad Sin(r)Cos(p) \quad Cos(r)Cos(p)]$$

Solving for the coefficient matrix, one obtains Equation (B.6),

$$\begin{bmatrix} B_x & B_y & B_z \\ S_x & S_y y_y & -S_z p_x \\ -S_x y_x & S_y & -S_z r_z \\ S_x p_x & S_y r_y & S_z \end{bmatrix} = [[1 \quad g_v^T]_{4xn}^T [1 \quad g_v^T]_{nx4}]^{-1} [1 \quad g_v^T]_{4xn}^T \begin{bmatrix} V_x \\ V_y \\ V_z \end{bmatrix}_{nx3}^T \tag{B.6}$$

The gravity vector g_v chosen is for a CD with nullified misalignments. In addition, it is possible to achieve the same estimate with a CD that contains known misalignments (not nullified) by using Equation (A.2.11) and with a single mount, by making y and u = 0. In theory, this approach does provide an unbiased instrument coefficient matrix. The disadvantage of this approach is that it requires conducting the algebraic solution to obtain the estimate of these misalignments, which makes the approach redundant. On the other hand, if the CD misalignment is stable for a period of time, then batch calibrations can benefit from this approach since it only requires a single mount.

B.2: By Optimization Algorithm (OA)

Another method for estimating the instrument coefficients is an L^2 norm OA, specifically the Gauss-Newton and Levenberg-Marquardt Method, Reference 6. The method used today, Reference 3, as the standard calibration process was selected due to the perceived nonlinearity of the instrument math model derived in Reference 2. What this means is that the least square regression, demonstrated in the previous section, would have found near identical coefficients. Contrary to the OA described below, the OA in Reference 3 does not find an estimate of the CD misalignments, since it assumes that they are zero, and it is applied to an individual axis versus the method described below, which is applied simultaneously to all 3 axes.

The following OA finds the global minimum when the input contains symmetrical angle inputs that encompasses the full 360°x360° sphere and the 4 mounting orientations.

This approach was tested with the full model for g_{vm}, Equations (A.3.5) or (A.2.10), and with the approximate model for g_{vm}, Equation (A.2.11) with indiscernible differences.

Using Equation (A.3.5) with g_{vm} Equation (A.2.10) obtains the instrument voltage model. Then, the partial derivate is found for each of the 18 parameters (which do not include the input variables p, r, y, and u) for this model, and creates a vector for each accelerometer. Next, a matrix is formed with these 3 vectors to form a 3x18 Jacobian matrix $J(x_k,\ Wi)$ or Equation (B.7), where x_k is a vector of the unknown parameters, and W_i are the input variables.

The results from this OA are the average instrument coefficients and an estimate of the CD average misalignments that minimizes the residual errors. The issue with this approach is that the instrument coefficients are biased by the state of the reference planes. Thus, if the reference does not meet requirements, then the average of the reference planes' misalignments is transferred to the instrument coefficients. In addition, any variation of the accelerometer offsets relative to the G_{wg} for each mounting orientation is transferred to the CD estimated misalignments (see the Appendix B.3.3 "Demonstration of misalignments transfer to the 3xAI instrument coefficients"). All things considered, if the instrument and CD reference planes are in alignment, and other mounting errors are kept below the instrument accuracy specifications, it is a reasonable approach for obtaining all the desired parameters (instrument coefficients and CD misalignments).

B.2.1: Algorithm

1. Create an initial guess for the x_k vector

2. Obtain a set of the instrument output using all the orthogonal angle setpoints in Appendix E for W (Measured values or calibration data).

3. Generate a set of estimated voltages, using Equation (A.3.5) with the x_k vector and the same W (estimated/calculated values).

4. Calculate the first residual delta, $r\ (x_k, W_i)$, between the calibration data and estimated voltages. The Sum (residual delta) may reach tolerance before convergence since it contains positive and negative residuals, therefore obtaining $\mathrm{r}(x_k,\ Wi).\mathrm{r}(x_k,\ Wi)$ or sum of the squares, assures that convergency has a higher probability of occurring. The adjustment to the parameters is based on the following Equation (B.7),

$$J[x_k,\ Wi]^T J[x_k,\ Wi] s_k = -J[x_k,\ Wi]^T.\mathrm{r}[x_k,\ Wi]$$

$$J[x_k,\ Wi] = \begin{bmatrix} \frac{\partial V_x}{\partial b_x}, \frac{\partial V_x}{\partial S_x}, \frac{\partial V_x}{\partial p_x}, \frac{\partial V_x}{\partial y_x}, 0,0,0,0,0,0,0,0,0, \frac{\partial V_x}{\partial a}, 0,0, \frac{\partial V_x}{\partial e}, \frac{\partial V_x}{\partial k} \\ 0,0,0,0, \frac{\partial V_y}{\partial b_y}, \frac{\partial V_y}{\partial S_y}, \frac{\partial V_y}{\partial r_y}, \frac{\partial V_y}{\partial y_y}, 0,0,0,0, \frac{\partial V_y}{\partial b}, \frac{\partial V_y}{\partial a}, \frac{\partial V_y}{\partial d} \frac{\partial V_y}{\partial f}, 0, \frac{\partial V_y}{\partial k} \\ 0,0,0,0,0,0,0,0, \frac{\partial V_z}{\partial b_z}, \frac{\partial V_z}{\partial S_z}, \frac{\partial V_z}{\partial p_z}, \frac{\partial V_z}{\partial r_z}, \frac{\partial V_z}{\partial b}, \frac{\partial V_z}{\partial a}, \frac{\partial V_z}{\partial d} \frac{\partial V_z}{\partial f}, \frac{\partial V_z}{\partial e}, 0 \end{bmatrix} \quad \text{(B.7)}$$

$$x_k = b_x, s_x, p_x, y_x, b_y, s_y, r_y, y_y, b_z, s_z, p_z, r_z, b, a, d, f, e, k$$

$$W_i = p_i, r_i, y_i, u_i$$

Algorithm:

$x_k = Initial\ Guess$

$\mathrm{r}[x_k,\ Wi]$ = 3xAI$[x_k,\ Wi]$ – Data$[Wi]$;

LevMqt = 1; "Levenberg Marquardt first value"

While ($\mathrm{r}[x_k,\ Wi].\mathrm{r}[x_k,\ Wi]$) $> 1E^{-7}$,

$ata = J[x_k,\ Wi]^T.J[x_k,\ Wi]$; "ata means A^TA in Linear Algebra"

$s_k = Phseudo\ Inverse[ata + LevMqt\ .I].J[x_k,\ Wi]^T.\mathrm{r}[x_k,\ Wi]$; "$I$ is the identity matrix"

$x_k = x_k + s_k$

If $\left[\sqrt{\mathrm{Max}\left[\mathrm{Diagonal}[\mathrm{ata.ata}]\right]} < .05\ then\ \mathrm{LevMqt} = \mathrm{LevMqt} * 10\ else\ \mathrm{LevMqt} = \mathrm{LevMqt}/10\right]$

$\mathrm{r}[x_k,\ Wi]$ = 3xAI$[x_k,\ Wi]$ – Data$[Wi]$ (this final bracket closes the While Loop)

Print$[x_k]$

After convergence x_k can be rearranged to obtain an estimate of the coefficients, Equation (B.8) and CD misalignments, Equation (B.9),

$$\text{3xAI coefficients} = \begin{bmatrix} B_x & B_y & B_z \\ S_x & S_y y_y & -S_z p_x \\ -S_x y_x & S_y & -S_z r_z \\ S_x p_x & S_y r_y & S_z \end{bmatrix} = \begin{bmatrix} x_1 & x_5 & x_9 \\ x_2 & x_6 x_8 & x_{10} x_{11} \\ x_2 x_3 & x_6 & x_{10} x_{12} \\ x_2 x_4 & x_6 x_7 & x_{10} \end{bmatrix} \tag{B.8}$$

$$\text{CD Misalignments } [\text{b}, \text{a}, \text{d}, \text{f}, \text{e}, \text{k}] = [x_{13} \quad x_{14} \quad x_{15} \quad x_{16} \quad x_{17} \quad x_{18}] \tag{B.9}$$

B.3: Potential CD misalignment transfer when using a standard calibration process

B.3.1: Demonstration of misalignments transfer to the 1xAI and 2xAI instrument coefficients

The demonstration will show how the instrument coefficients are biased by the misalignments of the CD when using conventional calibration methods. In addition, it will demonstrate what is wrong with verifying the instrument calibration on the same device using calibration angle setpoints that are the same or within the pitch and roll ranges. These verifications always result in near zero residual errors. The best approach for verifying the instrument calibration when only one CD exists is to mount the instrument in the opposite direction to the mounting orientation chosen during the calibration. The residual error calculations are first performed with the 1xAI, due to its simplicity, and then followed with the other instruments.

To provide the instrument with multiple angle setpoints for conventional calibration procedures, as it is currently implemented, requires a rotary device with zero misalignment (ideal CD). In addition, it is important that the primary reference plane is flat and smooth and that the rotary tables have zero wobble and index error.

For the single axis instruments, a two axes CD may contain two potential residual misalignments which are transferred to these single axis instrument coefficients, again when using conventional calibration methods. These two misalignments are the mounting/reference plane, which has a tilt in pitch (*e*) relative to the roll rotary table, and the full device as a rigid body, which has a tilt in pitch (*a*) relative to the G_{wg}. For a two-axes rotary system, the model that represents this device is the 3D g_{vm}. Then, the desire is to calibrate the single axis tilt instruments (1xAI and 2xAI) with this CD. This demonstration uses Equation (A.2.4) to represent the pitch misalignment.

There is a reason that the residual misalignments are near zero for the current verification approach, which is easier to demonstrate mathematically and or graphically than to explain in written form.

Figure 8, in Appendix A.2.1, illustrates graphically why the residual errors are near zero for conventional calibrations. The process starts with an unbalanced system/equation. The instrument output, the left side of the equation, is referenced to G_{wg}, and the instrument math model, and the right side of the equation, is referenced to G, which assumes zero misalignments.

Expressing this mathematically in Equation (B.10), where the left side of the equation is $S \neq 0$, and the right side assumes $S = 0$,

$$B_x + [Sin(p+S) \quad Cos(p+S)] * S_x * \begin{bmatrix} 1 \\ p_x \end{bmatrix} = B_x + [Sin(p) \quad Cos(p)] * S_x * \begin{bmatrix} 1 \\ p_x \end{bmatrix} \tag{B.10}$$

The same is applied to the 2xAI output, Equation (B.11),

$$\begin{bmatrix} B_x \\ B_z \end{bmatrix}^T + [Sin(p+S) \quad Cos(p+S)] \begin{bmatrix} 1 & -\mathrm{p}_z \\ \mathrm{p}_x & 1 \end{bmatrix} \begin{bmatrix} S_x & 0 \\ 0 & S_z \end{bmatrix} = \begin{bmatrix} B_x \\ B_z \end{bmatrix}^T + [Sin(p) \quad Cos(p)] \begin{bmatrix} 1 & -\mathrm{p}_z \\ \mathrm{p}_x & 1 \end{bmatrix} \begin{bmatrix} S_x & 0 \\ 0 & S_z \end{bmatrix} \tag{B.11}$$

Performing a least square regression for these two scenarios results in a biased instrument:

Biased 1xAI, Equation (B.12),

$$\begin{bmatrix} 1 \\ p_x' \end{bmatrix}; where\ p_x' = p_x + S \tag{B.12}$$

Biased 2xAI, Equation (B.13),

$$\begin{bmatrix} 1 & -p_z' \\ p_x' & 1 \end{bmatrix}; where\ p_x' = p_x + S\ and\ p_z' = p_z + S \tag{B.13}$$

For these two instruments there are other misalignments that the models do not account for; however, they can play a role in the measurement error, especially if the range of angles measured is beyond a certain limit. For instance, the 1xAI instrument is usually limited to ±60° in pitch with accuracy specifications for different ranges, with higher accuracy around zero and lower accuracy for the wider ranges. On the other hand, the 2xAI instrument is designed for angles above ±60°. At the max angles, both instruments are susceptible to relatively large misalignments in roll and yaw with respect to the reference/mounting plane. These two instruments are not designed to maintain pitch accuracy if they are rotated in roll with zero yaw.

B.3.2: Verification of a biased instrument

This section describes a method to verify if the instrument has been biased during calibration.

The simple method to determine bias is to perform the process used to check a bubble level, which is to rotate the instrument in yaw (rotate it with respect to the *Z*-axis that is normal to the interface plane) by 180°.

After obtaining the biased instrument coefficients with the process described in the previous section, these biased coefficients are applied to the CD/instrument math model Equation (A.3.3) to obtain Equation (B.14).

$$V_x = B_x + S_x \begin{bmatrix} Sin(p) & Cos[p] \end{bmatrix} \begin{bmatrix} Cos(p'_x) \\ Sin(p'_x) \end{bmatrix} = B_x + S_x Sin(p + p'_x) \tag{B.14}$$

Take the left side of Equation (B.14) and substitute it with Equation (B.15), which is the real output of the instrument for each angle setpoint. The output is V_{nb} (nb is no bias), for voltage output with no-bias.

$$\begin{aligned} V_{nb} &= B_x + S_x \begin{bmatrix} Sin(p+S) & Cos(p+S) \end{bmatrix} \begin{bmatrix} Cos(p_x) \\ Sin(p_x) \end{bmatrix} \\ &= B_x + S_x Sin(p + S + p_x) \end{aligned} \tag{B.15}$$

Flip the equations and solve (B.14) = (B.15), shown in Equation (B.16), for *p*, as demonstrated in Appendix C, Equation (B.17).

$$B_x + S_x Sin(p + p'_x) = B_x + S_x Sin(p + S + p_x) \tag{B.16}$$

$$Sin(p + p'_x) = \frac{V_{nb} - B_x}{S_x} = \frac{(B_x + S_x Sin(p + S + p_x)) - B_x}{S_x} \tag{B.17}$$

$$\begin{gathered} p = ArcSin\big(Sin(p + S + p_x)\big) - p'_x = p \\ Where\ p'_x = S + p_x \end{gathered} \tag{B.18}$$

Exactly as expected, the residual error is equal to zero, as shown in Equation (B.18), because the biased coefficient cancels the device misalignment. Returning to the bubble level analogy, this calibration is identical to zeroing a bubble level indicator on a surface plane that is assumed to be leveled but contains a residual $p = S$. Not checking the bubble reading by rotating it 180° relative to the surface plane after the bubble level has been zeroed, as per procedure would show that the bubble will read p = -2S, hence a biased bubble level.

Moving from the bubble analogy to the instrument verification point, rotating the instrument by 180° with respect to the Z-axis, results in the following. Using Equation (A.3.3) to represent the left side of the equation, where g_x term is updated with Cos(y), shown below as Equation (B.19).

$$\begin{aligned} V_{nb} &= B_x + S_x \left[Cos(y)Sin(p+S) \quad Cos(p+S)\right] \begin{bmatrix} Cos(p_x) \\ Sin(p_x) \end{bmatrix} \\ &= B_x + S_x Sin[Cos(\mathrm{y})(p+S) + p_x] \end{aligned} \tag{B.19}$$

Now solve Equation (B.14) = (B.19) for p, Equation (B.20), using y = 180° to account for rotating the instrument by this quantity:

$$Sin(p + p'_x) = \frac{V_{nb} - B_x}{S_x} = \frac{(B_x + S_x Sin(-p - S + p_x)) - B_x}{S_x} \tag{B.20}$$

$$p = ArcSin\big(Sin(-p - S + p_x)\big) - p'_x = -p - 2S \tag{B.21}$$

The expected value is –p, however the result is –(p+2S), Equation (B.21), which means that the measurement contains 2x the unaccounted CD misalignment, S. Using a biased instrument on a test article results in measurement error equal to this bias. Another method for checking the instrument bias is with a calibrated level plane, where the output will be -S in both orientations.

B.3.3: Demonstration of misalignments transfer to the 3xAI instrument coefficients

It is noted that the 3xAI instrument is susceptible to misalignments from mounting, depending on how it is referenced to the angle articulation device (AAD), excluding the CD. As mentioned before, there are ways to mitigate these misalignments when calibrating the instrument. However, methods to mitigate misalignments during measurements has not been studied, thus further research is required.

Demonstration of how the 3xAI instrument is biased by the CD when using a least square regression, depends on a few things: the condition of the reference planes, and the selected angle setpoints for calibration. To simplify this demonstration, the selected angle setpoints are the orthogonal points (p & r = –90, 0, 90, and 180) for a total of 16 points. The interface/reference planes are flat and smooth; however, the top and bottom planes are not parallel, and the X-Z plane does not have the same orientation when accessed from the top and bottom planes. The magnitude and direction for these misalignments in the reference planes are not known. Also, the dowels from the instrument can misalign the instrument in yaw for the remaining mounting orientations, as explained in Appendix F.

The following demonstration will show the instrument coefficients obtained using least square regression for 4 individual mounting orientations relative to the interface/reference planes. The only parameters that can vary amongst mounting orientations are the reference planes and the potential misalignments introduced during the instrument installation.

Table 5 shows the symbolic least square regression results when using a CD with the misalignments that are assumed to be zero in Equation (B.5). However, since the CD most likely has residual misalignments, then obtaining the results in Table 5 requires substituting the left side (voltage vector) with the same equation but using g_{vm}^T (Equation (A.2.11)) instead of g_v^T (gravity vector with zero misalignment). This is computed symbolically for each individual mounting orientation. In addition, the table shows that canceling out the reference misalignment requires a reference with parallel top and bottom planes and the X-Z plane with the same alignment when accessed from the top and bottom planes. The average results, shown in the last three rows, are identical to performing a least square regression using the data for all four mounting orientations.

The first mounting orientation is the top (u = 0) and forward (y = 0), which is the selected orientation for the conventional calibration and for measuring the angle of any AAD. The reference misalignments are $f1$ (reference roll), $e1$ (reference pitch), and $k1$ (reference yaw). The remaining mounting orientations are captured in Table 5.

Mounting Orientation	Matrix Result	y_x'	p_x'	y_y'	r_y'	p_z'	r_z'
Top-Forward (y = 0 and u = 0)	$\begin{bmatrix} 1 & y_y' & -p_z' \\ -y_x' & 1 & -r_z' \\ p_x' & r_y' & 1 \end{bmatrix}$	$y_x + k_1$	$p_x + e_1$	$y_y + k_1$	$r_y + f_1$	$p_z + e_1$	$r_z + f_1$
Top-Backward (y = 180° and u = 0)		$y_x + k_2$	$p_x - e_2$	$y_y + k_2$	$r_y - f_2$	$p_z - e_2$	$r_z - f_2$
Bottom-Forward (y = 0 and u = 180°)		$y_x - k_3$	$p_x - e_3$	$y_y - k_3$	$r_y + f_3$	$p_z - e_3$	$r_z + f_3$
Bottom-Backward (y = 180° and u = 180°)		$y_x - k_4$	$p_x + e_4$	$y_y - k_4$	$r_y - f_4$	$p_z + e_4$	$r_z - f_4$
Average = Least Square Regression using All Mounting Orientations							
x axis		$y_x + \frac{1}{4}(k_1 + k_2 - k_3 - k_4)$			$p_x + \frac{1}{4}(e_1 - e_2 - e_3 + e_4)$		
y axis		$y_y + \frac{1}{4}(k_1 + k_2 - k_3 - k_4)$			$r_y + \frac{1}{4}(f_1 - f_2 + f_3 - f_4)$		
z axis		$p_z + \frac{1}{4}(e_1 - e_2 - e_3 + e_4)$			$r_z + \frac{1}{4}(f_1 - f_2 + f_3 - f_4)$		

Table 5: The 3xAI instrument coefficients biased by the reference and the potential instrument installation misalignments.

In summary, if only one set of orthogonal angle setpoints are provided to the instrument during calibration, then the minimal bias transferred to the instrument is shown in Table 5 for each mounting orientation. If a different set of angle setpoints are provided that are within a small range of pitch from level pitch (example $-30 \leq p \leq 30$) and level roll (examples $-30 \leq r \leq 30$ and $150 \leq r \leq 210$), then other misalignments in the CD can be transferred to the instrument, as demonstrated in Reference 1. To cancel the reference misalignments, it is important that the reference meets requirements, as explained in previous sections of this paper. This reference shall make the individual misalignments magnitude equal for each of the mounting orientations, thus canceling when using the four mounting orientations. It is easy to observe that the 4-mount is superior to just 1-mount (current method) since it results in adding a fourth of each of the reference misalignments with near identical magnitude and direction. However, to machine a reference plane that meets requirements, and installing the two dowels in the 3xAI instrument to be normal to the X-Y plane, is both challenging and expensive.

The reader is referred to Appendix F for more details on how the instrument form factor affects measurement accuracy.

Appendix C: Solving for the gravity vector, g_v

This section is intended to demonstrate a very good approximation for estimating g_v, which is then used for estimating the angles of interest, pitch, or pitch and roll.

C.1: 1xAI

For the 1xAI instrument, there is no direct method for estimating g_v. For this instrument, it is easier to use Equation (A.2.2) to simplify Equation (A.3.3) in order to obtain Equation (C.1). Equation (C.2) normalizes Equation (C.1). Pitch is estimated with Equation (C.3).

$$V_x = B_x + S_x Sin(p + p_x) \tag{C.1}$$

$$g_x = Sin(p + p_x) = \frac{V_x - B_x}{S_x} \tag{C.2}$$

$$p = ArcSin(g_x) - p_x \tag{C.3}$$

C.2: 2xAI

$$g^T = [Sin(p) \quad Cos(p)] = \left(\begin{bmatrix} V_x \\ V_z \end{bmatrix} - \begin{bmatrix} B_x \\ B_z \end{bmatrix}\right)^T \begin{bmatrix} \frac{1}{S_x} & 0 \\ 0 & \frac{1}{S_z} \end{bmatrix} \begin{bmatrix} 1 & \mathrm{p}_z \\ -\mathrm{p}_x & 1 \end{bmatrix} \tag{C.4}$$

Please note the last matrix is an approximation for the inverse of the instrument coefficient matrix, Equation (A.1.9). Appendix D will demonstrate how to obtain this inverse matrix for 2D and 3D near orthonormal systems.

$$p = ArcTan2(g_z, g_x) = ArcTan2\left(\frac{g_x}{g_z}\right) \tag{C.5}$$

C.3: 3xAI

Assume that the AAD has zero misalignments and that the instrument is installed in complete alignment with the interface/reference planes.

$$g^T = [Sin(p) \quad Sin(\mathrm{r})Cos(p) \quad Cos(\mathrm{r})Cos(p)]\left(\begin{bmatrix} V_x \\ V_y \\ V_z \end{bmatrix} - \begin{bmatrix} B_x \\ B_y \\ B_z \end{bmatrix}\right)^T \begin{bmatrix} \frac{1}{S_x} & 0 & 0 \\ 0 & \frac{1}{S_y} & 0 \\ 0 & 0 & \frac{1}{S_z} \end{bmatrix} \begin{bmatrix} 1 & -y_y & p_x \\ y_x & 1 & r_z \\ -p_x & -r_y & 1 \end{bmatrix} \tag{C.6}$$

Again, the last matrix uses the inverse for a near orthogonal matrix, Appendix D, for the instrument coefficient matrix in Equation (A.1.20). Equation (C.7) estimates pitch and roll from the result in (C.6).

$$\begin{aligned} p &= ArcSin(g_x) \\ r &= ArcTan2(g_z, g_y) = ArcTan2\left(\frac{g_y}{g_z}\right) \end{aligned} \tag{C.7}$$

Appendix D: The inverse of a near-orthonormal matrix

D.1: 2D Inverse of Near Orthonormal Matrix

$$\begin{bmatrix} 1 & -p_z \\ p_x & 1 \end{bmatrix}^{-1} \cong \begin{bmatrix} 1 & p_z \\ -p_x & 1 \end{bmatrix} \tag{D.1}$$

Prof:

$$\begin{bmatrix} 1 & -p_z \\ p_x & 1 \end{bmatrix}^{-1} \cong$$
$$\begin{bmatrix} \frac{\mathrm{Cos}(p_z)}{\mathrm{Cos}(p_x)\mathrm{Cos}(p_z) + \mathrm{Sin}(p_x)\mathrm{Sin}(p_z)} & \frac{\mathrm{Sin}(p_z)}{\mathrm{Cos}(p_x)\mathrm{Cos}(p_z) + \mathrm{Sin}(p_x)\mathrm{Sin}(p_z)} \\ -\frac{\mathrm{Sin}[p_x]}{\mathrm{Cos}(p_x)\mathrm{Cos}(p_z) + \mathrm{Sin}(p_x)\mathrm{Sin}(p_z)} & \frac{\mathrm{Cos}[p_x]}{\mathrm{Cos}(p_x)\mathrm{Cos}(p_z) + \mathrm{Sin}(p_x)\mathrm{Sin}(p_z)} \end{bmatrix} \tag{D.2}$$

Small angle approximation,

$$\begin{bmatrix} \frac{1}{1 + p_x p_z} & \frac{p_z}{1 + p_x p_z} \\ -\frac{p_x}{1 + p_x p_z} & \frac{1}{1 + p_x p_z} \end{bmatrix} \cong \begin{bmatrix} 1 & p_z \\ -p_x & 1 \end{bmatrix} \tag{D.3}$$

Multiplying an orthonormal matrix by its inverse equals the identity matrix. Thus, using the approximation matrices,

$$\begin{bmatrix} 1 & -p_z \\ p_x & 1 \end{bmatrix}\begin{bmatrix} 1 & p_z \\ -p_x & 1 \end{bmatrix} \cong \begin{bmatrix} 1 + p_x p_z & 0 \\ 0 & 1 + p_x p_z \end{bmatrix} \cong \begin{bmatrix} 1 & 0 \\ 0 & 1 \end{bmatrix} \tag{D.4}$$

Using small angle approximation results in the identity matrix.

Using small angle approximation: to exaggerate the approximation, assume the angle is 0.1° for each of the non-unity elements. To illustrate, 0.1° = 0.0017 radians, therefore 0.0017^2 = 3E-6 radians^2 or about 600x smaller, therefore the second order or higher terms can be approximated to zero, therefor $p_x p_z \cong 0$ and the diagonal terms, $1 - \mathrm{Cos}(0.1°)^2 \cong 1 - 3\mathrm{E} - 6 \cong 1$

To avoid any doubts of Equation (D.4) being a good approximation to the inverse, let's revisit the non-approximation matrices and this time negate the off-diagonal elements:

$$\begin{bmatrix} \mathrm{Cos}(p_x) & -\mathrm{Sin}(p_z) \\ \mathrm{Sin}(p_x) & \mathrm{Cos}(p_z) \end{bmatrix} \begin{bmatrix} \mathrm{Cos}(p_x) & \mathrm{Sin}(p_z) \\ -\mathrm{Sin}(p_x) & \mathrm{Cos}(p_z) \end{bmatrix}$$
$$= \begin{bmatrix} \mathrm{Cos}(p_x)^2 + \mathrm{Sin}(p_x)\mathrm{Sin}(p_z) & \big(\mathrm{Cos}(p_x) - \mathrm{Cos}(p_z)\big)\mathrm{Sin}(p_z) \\ \big(\mathrm{Cos}(p_x) - \mathrm{Cos}(p_z)\big)\mathrm{Sin}(p_x) & \mathrm{Cos}(p_z)^2 + \mathrm{Sin}(p_x)\mathrm{Sin}(p_z) \end{bmatrix} \tag{D.5}$$
$$\cong \begin{bmatrix} 1 & 0 \\ 0 & 1 \end{bmatrix} \; for\; p_x \approx p_z$$

D.2: 3D Near Orthonormal Matrix

$$\begin{bmatrix} 1 & y_y & -p_z \\ -y_x & 1 & -r_z \\ p_x & r_y & 1 \end{bmatrix}^{-1} \cong \begin{bmatrix} 1 & -y_y & p_z \\ y_x & 1 & r_z \\ -p_x & -r_y & 1 \end{bmatrix} \tag{D.6}$$

Proof:

$$\begin{bmatrix} 1 & y_y & -p_z \\ -y_x & 1 & -r_z \\ p_x & r_y & 1 \end{bmatrix}^{-1} =$$

$$\begin{bmatrix} \frac{1 + r_y r_z}{1 + p_x p_z + r_y r_z + p_z r_y y_x - p_z r_z y_y + y_x y_y} & \frac{-p_z r_y - y_y}{1 + p_z p_z + r_y r_z + p_z r_y y_x - p_z r_z y_y + y_x y_y} & \frac{p_z - r_z y_y}{1 + p_z p_z + r_y r_z + p_z r_y y_x - p_z r_z y_y + y_x y_y} \\ \frac{-p_z r_z + y_x}{1 + p_z p_z + r_y r_z + p_z r_y y_x - p_z r_z y_y + y_x y_y} & \frac{1 + p_z p_z}{1 + p_z p_z + r_y r_z + p_z r_y y_x - p_z r_z y_y + y_x y_y} & \frac{r_z + p_z y_x}{1 + p_z p_z + r_y r_z + p_z r_y y_x - p_z r_z y_y + y_x y_y} \\ \frac{-p_z - r_y y_x}{1 + p_z p_z + r_y r_z + p_z r_y y_x - p_z r_z y_y + y_x y_y} & \frac{-r_y + p_z y_y}{1 + p_z p_z + r_y r_z + p_z r_y y_x - p_z r_z y_y + y_x y_y} & \frac{1 + y_x y_y}{1 + p_z p_z + r_y r_z + p_z r_y y_x - p_z r_z y_y + y_x y_y} \end{bmatrix} \tag{D.7}$$

Using the small angle approximation returns Equation (D.6).

Second proof:

$$\begin{bmatrix} 1 & y_y & -p_z \\ -y_x & 1 & -r_z \\ p_x & r_y & 1 \end{bmatrix} \begin{bmatrix} 1 & -y_y & p_z \\ y_x & 1 & r_z \\ -p_x & -r_y & 1 \end{bmatrix}$$
$$= \begin{bmatrix} 1 + p_x p_z + y_x y_y & p_z r_y & r_z y_y \\ p_x r_z & 1 + r_y r_z + y_x y_y & -p_z y_x \\ r_y y_x & -p_x y_y & 1 + p_x p_z + r_y r_z \end{bmatrix} \cong \begin{bmatrix} 1 & 0 & 0 \\ 0 & 1 & 0 \\ 0 & 0 & 1 \end{bmatrix} \tag{D.8}$$

D.2.1: General Application:

The inverse of a matrix with ones as diagonal elements and very small off diagonal elements, can be approximated as the transpose of the sign of the off-diagonal elements in the matrix. This differs from the definition of the orthonormal matrix, where the inverse is the transpose of the matrix elements. The statement that the inverse of the general matrix is the transpose of the sign of the off-diagonal elements may just be a coincidence. To assure a good approximation, it is best to negate all the off-diagonal elements in the array. For instance,

$$\begin{bmatrix} 1 & a & b \\ c & 1 & d \\ e & f & 1 \end{bmatrix}^{-1} \cong \begin{bmatrix} 1 & -a & -b \\ -c & 1 & -d \\ -e & -f & 1 \end{bmatrix} \tag{D.9}$$

only works if the absolute of each of the off-diagonal elements << 1, e.g., Abs(-a) << 1

$$\begin{bmatrix} 1 & a & b \\ c & 1 & d \\ e & f & 1 \end{bmatrix}\begin{bmatrix} 1 & -a & -b \\ -c & 1 & -d \\ -e & -f & 1 \end{bmatrix} = \begin{bmatrix} 1-ac-be & -bf & -ad \\ -de & 1-ac-df & -bc \\ -cf & -ae & 1-be-df \end{bmatrix} \tag{D.10}$$

Appendix E: Orthogonal Angle Setpoints per Mounting Orientation

The following tables are the instrument output created using Equation (15). Each table represents one of the four mounting orientations and orthogonal angle setpoints. These orthogonal setpoints are chosen to place two of the instrument accelerometers in the near zero g field. The mounting orientations are Top-Forward, which is the chosen mount for standard calibrations and when making measurements, and the remaining three symmetrical mounts are Top-Backward, Bottom-Forward, and Bottom-Backward.

For clarification, the ±1 values, which are obtained when aligning each accelerometer with the global G_z axis in the G_{wg} frame of reference, are not an accurate value and are a result of the trigonometry form shown in Equation (15). This value can only be reached if the angle near their respective 1g field cancels the CD misalignments and the accelerometers' offset angles. This can only be achieved with a pitch and roll rotary device with some adjustability. Section 2.4 "Obtaining the accelerometer sensitivity and bias coefficients" and subsequent sections at the beginning of the paper have more details about this subject.

u = 0 (top) and y = 0 (forward)

$$
\begin{array}{c}
\begin{array}{ccccc} \mathrm{p} & \mathrm{r} & \mathrm{gx} & \mathrm{gy} & \mathrm{gz} \end{array} \\
\begin{bmatrix}
-90. & -90. & -1 & -a-k-y_y & b-d+e+p_z \\
-90. & 0. & -1 & b-d-k-y_y & a+e+p_z \\
-90. & 90. & -1 & a-k-y_y & -b+d+e+p_z \\
-90. & 180. & -1 & -b+d-k-y_y & -a+e+p_z \\
0. & -90. & a+k+y_x & -1 & b+f+r_z \\
0. & 0. & a+e+p_x & b+f+r_y & 1 \\
0. & 90. & a-k-y_x & 1 & -b-f-r_z \\
0. & 180. & a-e-p_x & -b-f-r_y & -1 \\
90. & -90. & 1 & a+k+y_y & b+d-e-p_z \\
90. & 0. & 1 & b+d+k+y_y & -a-e-p_z \\
90. & 90. & 1 & -a+k+y_y & -b-d-e-p_z \\
90. & 180. & 1 & -b-d+k+y_y & a-e-p_z \\
180. & -90. & -a-k-y_x & 1 & b-f-r_z \\
180. & 0. & -a-e-p_x & b-f-r_y & -1 \\
180. & 90. & -a+k+y_x & -1 & -b+f+r_z \\
180. & 180. & -a+e+p_x & -b+f+r_y & 1
\end{bmatrix}
\end{array}
$$

u = 0 (top) and y = 180° (backward)

$$\begin{array}{c}
\begin{array}{ccccc} p & r & gx & gy & gz \end{array} \\
\begin{bmatrix}
-90. & -90. & 1 & a+k+y_y & b-d+e-p_z \\
-90. & 0. & 1 & -b+d+k+y_y & a+e-p_z \\
-90. & 90. & 1 & -a+k+y_y & -b+d+e-p_z \\
-90. & 180. & 1 & b-d+k+y_y & -a+e-p_z \\
0. & -90. & -a-k-y_x & 1 & b+f-r_z \\
0. & 0. & -a-e+p_x & -b-f+r_y & 1 \\
0. & 90. & -a+k+y_x & -1 & -b-f+r_z \\
0. & 180. & -a+e-p_x & b+f-r_y & -1 \\
90. & -90. & -1 & -a-k-y_y & b+d-e+p_z \\
90. & 0. & -1 & -b-d-k-y_y & -a-e+p_z \\
90. & 90. & -1 & a-k-y_y & -b-d-e+p_z \\
90. & 180. & -1 & b+d-k-y_y & a-e+p_z \\
180. & -90. & a+k+y_x & -1 & b-f+r_z \\
180. & 0. & a+e-p_x & -b+f-r_y & -1 \\
180. & 90. & a-k-y_x & 1 & -b+f-r_z \\
180. & 180. & a-e+p_x & b-f+r_y & 1
\end{bmatrix}
\end{array}$$

u = 180° (bottom) and y = 0 (forward)

$$\begin{array}{c}
\begin{array}{ccccc} p & r & gx & gy & gz \end{array} \\
\begin{bmatrix}
-90. & -90. & -1 & a+k-y_y & -b+d-e+p_z \\
-90. & 0. & -1 & -b+d+k-y_y & -a-e+p_z \\
-90. & 90. & -1 & -a+k-y_y & b-d-e+p_z \\
-90. & 180. & -1 & b-d+k-y_y & a-e+p_z \\
0. & -90. & a+k-y_x & 1 & -b-f-r_z \\
0. & 0. & a+e-p_x & -b-f-r_y & -1 \\
0. & 90. & a-k+y_x & -1 & b+f+r_z \\
0. & 180. & a-e+p_x & b+f+r_y & 1 \\
90. & -90. & 1 & -a-k+y_y & -b-d+e-p_z \\
90. & 0. & 1 & -b-d-k+y_y & a+e-p_z \\
90. & 90. & 1 & a-k+y_y & b+d+e-p_z \\
90. & 180. & 1 & b+d-k+y_y & -a+e-p_z \\
180. & -90. & -a-k+y_x & -1 & -b+f+r_z \\
180. & 0. & -a-e+p_x & -b+f+r_y & 1 \\
180. & 90. & -a+k-y_x & 1 & b-f-r_z \\
180. & 180. & -a+e-p_x & b-f-r_y & -1
\end{bmatrix}
\end{array}$$

u = 180° (bottom) and y = 180° (backward)

$$
\begin{bmatrix}
p & r & gx & gy & gz \\
-90. & -90. & 1 & -a-k+y_y & -b+d-e-p_z \\
-90. & 0. & 1 & b-d-k+y_y & -a-e-p_z \\
-90. & 90. & 1 & a-k+y_y & b-d-e-p_z \\
-90. & 180. & 1 & -b+d-k+y_y & a-e-p_z \\
0. & -90. & -a-k+y_x & -1 & -b-f+r_z \\
0. & 0. & -a-e-p_x & b+f-r_y & -1 \\
0. & 90. & -a+k-y_x & 1 & b+f-r_z \\
0. & 180. & -a+e+p_x & -b-f+r_y & 1 \\
90. & -90. & -1 & a+k-y_y & -b-d+e+p_z \\
90. & 0. & -1 & b+d+k-y_y & a+e+p_z \\
90. & 90. & -1 & -a+k-y_y & b+d+e+p_z \\
90. & 180. & -1 & -b-d+k-y_y & -a+e+p_z \\
180. & -90. & a+k-y_x & 1 & -b+f-r_z \\
180. & 0. & a+e+p_x & b-f+r_y & 1 \\
180. & 90. & a-k+y_x & -1 & b-f+r_z \\
180. & 180. & a-e-p_x & -b+f-r_y & -1
\end{bmatrix}
$$

Appendix F: Instrument Small Form Factor

The instrument construction and dimensions play a role in the determination of the accuracy specifications. This section will present a few aspects of this instrument that may bias the coefficients during calibrations or reduce measurement accuracy during operations.

The 3-axis accelerometer instrument (3xAI) mentioned in this paper is constructed with an aluminum enclosure. This enclosure contains three feet to form a triangle or a 3-point plane. Each foot contains a hole for a fastener, designed for attaching/mounting the instrument to the reference plane. The instrument's three feet and angle articulation device (AAD) *X-Y* reference planes shall be flat, smooth, and clean. The goal of this requirement is to make the installation independent of the fastening torque levels and sequence. Unfortunately, in practice, this has not been the case. The instrument is highly sensitive to micro small movements, which can be introduced during this installation, Reference 13. Also, the torquing tool and action can have inherent large variation. Another source of error related to these interface planes is the fact that the short distance between the instrument contact points make the instrument susceptible to particle contamination and or the test articles reference plane not meeting the requirements mentioned above.

The enclosure interface plane for the 3xAI is less than 3 inches long from front to back and 1.5 inches wide. Therefore, a particle size of 2.3µm under the front foot and/or a 650nm under any one of the two back feet, can produce a 0.002-degree pitch and or roll error, respectively. If the reference plane is concave or convex, then fastening the instrument to this plane, can cause the position of the accelerometers to change, thus producing a large root sum square (rms) error (defined as $1 - \|g_v\|$). Lastly, the action of torquing the fasteners during mounting can place rotational and torsional forces to the instrument enclosure. The torsional forces can cause the accelerometers' positions to shift relative to the reference planes, and rotational forces can shift the instrument *X-Z* plane registration with AAD *X-Z* plane, thus causing some variations of the measurement from mount to mount. This variation in pitch and roll relative to the level plane is dependent of the user, and it can be large from user to user, or small for the same user (observed to be within ±0.0005° or 2 arcsecs). However, the variation of yaw misalignment, during mounting, is large regardless of the user, which affects the pitch error (can be as large as 0.015° for experience calibrators/operators) as the instrument is rolled. This yaw mounting misalignment peaks at 90° in roll.

The registration of the dowels is affected by the architecture of the AAD *X-Z* plane, which is designed with dowel holes or slots. The orifice is designed to accept multiple 3xAI instruments with slight variation of the dowel diameter and spacing between the two dowels. Therefore, the orifice is designed with a slip fit, which is large enough to facilitate the installation and extraction of the instrument without a large force. However, it is this fit that allows the instrument to shift in yaw and cause the large yaw variation during installation. Therefore, the rotational forces applied during mounting can affect the ability of the user to register the two dowels with the *X-Z* reference plane. If one dowel moves away from this X-Z plane, then for every 500nm move, it is equivalent to 0.0005°error. This registration of two planes, in practice, is not feasible without some mechanical assistance or without changing the clamping method (fasteners vs hold-downs) of the instrument. In practice, an experienced calibrator/operator may register the dowels relative to the *X-Z* plane by 15µm or more, thus generating 0.015° or 54 arcsecs variation or higher. The variations from user-to-user have not been accurately quantified.

One additional requirement not mentioned before, which is specific to the 3xAI reference dowels, is the only section of the dowels that contacts the *X-Z* plane is the right-side quadrant/tangential line on the right side of the instrument. This requires these dowels to be perfectly normal (not bent) to the enclosure *X-Y* plane. Any dowel misalignment will introduce a bias to the yaw coefficients when using a 4-mount OA calibration, since two quadrants of the dowels contact the reference (*X-Z*) plane depending on the mounting orientation. To reiterate, only one quadrant of the dowels shall be used as the instrument reference plane, therefore using 4-mount calibrations requires two *X-Z* reference planes on the CD (not practical or feasible), which shall be parallel. When the instrument orientation is changed on the top surface, the dowel reference plane (the two dowels' quadrants) will contact the other side of the dowel registration plane (*X-Z* plane); if this other side is not parallel to the first plane, then this will introduce a misalignment for 2 of the 4 mounting orientations. On the other hand, if only one *X-Z* plane is used (this is feasible), then this requires that the dowels are normal to the instrument *X-Y* plane, meaning if they are installed with a tilt relative to the instrument *x-z* plane, then this introduces a different yaw for each mounting orientation relative to this AAD single *X-Z* plane. This is the rational for using only 3 mounting orientations described in the paper. As described in this paper, the two top planes, top-forward, and top-backward mounting orientations, are used for obtaining the pitch and roll coefficients, and for the yaw coefficients, the two references are the top-forward and bottom-backward mounting orientations. It is easy to make one surface flat for each of the two reference planes versus all the reference planes, and more difficult to make them parallel and orthogonal to each other.

Another observation made during a temperature calibration of a 3xAI instrument was that the aluminum enclosure will expand and contract more than the accelerometer's steel material, which can cause a few issues when the instrument is exposed to extreme temperatures. The aluminum enclosure can expand and contract in ways that can either place an undue force on the accelerometer body, thus shifting its bias coefficient, or cause the accelerometer itself to shift position, thus changing the accelerometer position vector. These effects cannot be modeled due to their low probability of occurrence. In addition, it does not take much shift/movement to introduce errors. It depends on the type of movement (rotation or shift in position) of the accelerometer relative to the enclosure. For instance, if the accelerometer shifts position where one edge of the accelerometer is placed at a higher point relative to the opposite edge, and if this delta is approximately 900nm, this causes a 7 arcsec error. Lastly, for these expansion/contraction events, the hypothesis is that most of the hysteresis in the temperature data is due to this material movement itself and not the accelerometer design.

Appendix G: 3xAI Calibration Examples using Algebra Method

The following examples are simulated using the full model of the system (Calibration Device (CD) and Instrument (3xAI) shown in Equation (A.2.10). A better demonstration would have been with real data, however the current CDs available do not meet the requirements for this method. There are two important requirements missing for this approach to work and to demonstrate that they are CD independent. The first requirement is that the current CDs do not provide the ability to set specific pitch and roll angles with a higher resolution than 1°; this is needed to place the accelerometers in the ±1g field. The second requirement is that the CD references, specifically the reference yaw misalignment (*x-z* plane, orthogonal to the mounting *x-y* plane) are believed to have a delta error between the top and bottom mounting planes; this delta will bias the yaw coefficients. Note, the value of the lab references yaw misalignment for the top and bottom planes relative to the axis of rotation is not accurately known. The *x-z* reference plane is composed of two holes, and it is not feasible to know exactly where all the instruments' two dowels make contact within these two holes. The holes are larger than the dowels since they need to accommodate different instruments with different distances between dowels. There are other elements to this misalignment that must be considered for this specific architecture, of which a few are mentioned in Appendix F "Instrument Small Form Factor".

The primary goal is to estimate the instrument coefficients to within a desirable tolerance using the method in this paper. Table G-1 describes the acceptable tolerance for the instrument coefficients and the CD misalignments. The secondary goal is to obtain an estimate of the CD misalignments to ensure they are not too large, which may affect the primary goal. The accuracy of the CD misalignments is not critical for the method in the paper.

Table G-1 Describes the acceptable tolerance for the Instrument coefficients and the CD misalignments

Device	Parameters	Tolerance range	Definition
Instrument			
Accelerometers Bias	b_x, b_y, b_z	±7.68 μg	Micro-gs
Accelerometers Sensitivity	s_x, s_y, s_z	±16.7 PPM	Parts per million
Accelerometers Offset Angles	p_x, y_x, r_y, y_y, p_z, r_z	±2 "	~ ±0.0005°
Calibration Device			
Misalignments	a, b, d, f, e, k	Not critical	*
* The process can tolerate larger than the prescribed (0.1°) CD misalignments and accelerometers' offset angles. If the accelerometers' offset angle magnitude is large, then CD misalignments must be smaller relative to the offset angles.			

The robustness of this method depends on the magnitude of the accelerometers' offset angles and the CD misalignments. If the CD misalignments and accelerometers' offset angles are within ±0.1°, then most of the instrument coefficients will be within tolerance, except for the sensitivity coefficients, which require correction as described in Section 2.4.2, "3xAI Sensitivity and Bias Coefficients". However, as the examples will demonstrate, it is still possible to estimate the instrument coefficients with system misalignment larger than this constraint.

What makes any method for estimating the instrument coefficients challenging is that there is no basis for comparison for the instrument coefficients and/or CD misalignments. After a new instrument or a CD unit is assembled, none of these parameters are known. The manufacturer of the accelerometers does provide an estimate for sensitivity and bias parameters; however, these parameters can be affected during assembly and by the local gravity magnitude.

The procedure for applying the method in the paper is described below, and it is selected to simplify the acquisition and computation of all parameters with minimal difficulty. The goal is to increase the probability of estimating the instrument coefficient to near true values. However, there is the probability of biasing the coefficients. These biases come from mounting misalignments to variability in the CD setpoints. On the other hand, Example 5-2 will demonstrate a biased instrument when using a least square regression results with a CD that contains residual misalignments. The effects are that these CD misalignments are transferred to the corresponding coefficients. For instance, the reference pitch misalignment is transferred to the accelerometers with a pitch offset angle (x-axis, p_x, and z-axis, p_z). The derivation for this effect was demonstrated in Reference 1; however, without a numeric example, which is covered in Example 5-2.

On the other hand, what these examples attempt to show is that the method described in the paper is superior to any other method described in Appendix B. Even if installation misalignments are introduced for each mounting orientation, the net contribution of these misalignments ranges from 0 (when they have magnitudes that cancel each other for the two orientations) to less than or equal to the full installation misalignments (which can happen when the magnitudes for the two mounting orientations do not cancel each other), which are completely transferred to the coefficients during a least square regression. Observations show that the pitch and roll installation misalignments are less than one arcsec, but it depends on the surface plane's flatness, cleanliness, and installer idiosyncrasies. However, yaw installation misalignment is significantly higher, and can be 10s of arcsecs. A few reasons for this misalignment are covered in Appendix F.

Table G-2 tabulates a few guidelines for the acceptable system misalignments when using the method in the paper and a least square regression. For the method in the paper, these optimal ranges are not intended as constraints, since as the examples that follow will show, it is feasible to calibrate a 3xAI instrument with system misalignments that exceed these optimal ranges.

Table G-2 Guide of optimal ranges for the system misalignments for method in the paper and least square regression.

Device	Optimal range	Calibration Method
		Algebra Method
Instrument		
Accelerometers' Offset Angles	±360 ArcSecs	For accelerometers' offset angles larger than this range requires addition steps to improve their respective estimates
Calibration Device		
Misalignments	±360 ArcSecs	The algebra method can tolerate large misalignments. Steps like the ones that mitigate large offset angles can do the same for large misalignment. These can be mitigated by reducing their magnitude using the procedure described in the next section
		Single Mount-Least Square Regression Method
Instrument		
Accelerometers' Offset Angles	N/A	This method can estimate these offset angles; however, the magnitude limits have not been determined. The quality of the estimate is dependent on the magnitude of the CD misalignments
Calibration Device		
Misalignments	±2 ArcSecs	This method cannot tolerate higher misalignments unless other steps are taken, Reference 1

The following sections provide guidance for calibrating the instrument and how to minimize or drive the CD misalignments to acceptable levels.

G.1: 3xAI Instrument calibration procedure.

1. Mount the instrument (apply your lab mounting procedure) on the bottom plane and in the backward orientation relative to the CD reference plane, then acquire 3 setpoints (P,R) as (0,0), (0,90°), and (90°,0).
2. Repeat bullet 1 by mounting the instrument on the top plane and in the backward orientation.
3. Repeat again with the instrument mounted on the top plane and in the forward orientation, also known as the standard measuring orientation.
4. Keeping the instrument in this final orientation then acquire two additional setpoints (P,R) as (0,180), and (180,0).
5. Compute the instrument coefficients following Equations (16)-(28) in the paper.
    a. Estimate the sensitivity and bias parameters for each accelerometer with the first nine calibration points using Equations (23)-(28). Although this data is not perfect for estimating these parameters, they can provide a very good estimate, especially under specific conditions. These conditions will become apparent during the examples.
    b. Normalize the instrument voltages by subtracting the accelerometers' corresponding bias and then dividing by the corresponding sensitivity, Equation (13).
    c. Estimate the instrument coefficients using Equations (16)-(22). Note that these estimates are affected by the results from bullet "a".
    d. Estimate the CD misalignment using Equations (78)-(83). This step is only needed after assembling, or after any changes/alignment performed to the CD. If the CD is permanently mounted and aligned, it is good practice to perform this test on some regular interval. However, making it part of the data reduction process and keeping a history of these values is a good option.
    e. Correct the sensitivity and bias coefficients as explained in Section 2.4. Although this step is not critical except under specific circumstances, it is still a good idea to perform it to obtain estimates that are closer to the true value and to compare the results obtain from bullet "a" with these corrected coefficients. If the results from bullet "a" are out of tolerance, then repeat bullets "b"-"e" with these new sensitivity and bias estimates.

G.2: Procedure for reducing the CD internal misalignments

After completing the instrument calibration procedure, the results will provide an estimate for the CD misalignments. Although these estimates may not be perfect, they are still useful during the following procedure. Note that the goal is to reduce them without the need to zero them, which is very challenging. In addition, as the CD misalignments are made smaller, then the estimate for the instrument coefficients and CD misalignments get closer to the true value for the first estimate.

1. Without removing the instrument from its last mounting orientation (top plane and forward mount), update the instrument coefficients' file to prepare the instrument measurements as a guide for this alignment. Note that these measurements may have large errors; however, the goal is to use the instrument in a relative angle measurement versus absolute angle measurements.
    a. Place the CD to the pitch (p) = 0 and roll (r) = 0 position. In this position, tilt the CD device relative to its mounting base to adjust for system pitch and roll (a and b) parameters. Use the estimates obtained in bullet d (3xAI instrument calibration procedure) and adjust the CD such that instrument output changes to subtract the system pitch, a, and system roll, b, from the pitch and roll readings respectively.
2. After reducing system pitch and roll, it is possible from this position to reduce the misalignment of the CD reference plane, or the pitch and roll misalignments (e and f). The yaw (k) alignment requires to a different setpoint, shown in bullet b.
    a. Set the CD to $p = 0$ and $r = 0$ position and attempt to reduce the reference pitch and roll misalignments. The pitch misalignment may require shims or some other method to reduce its magnitude. The roll misalignment only requires rotating the reference plane with respect to the roll table axis (which is the x-axis). Again, using the instrument output to reduce the pitch reading by the pitch reference misalignment, e, and then repeat for roll, by the roll reference misalignment, f.
    b. Rotate the roll table or set the CD to $p = 0$ and $r = 90°$ position and attempt to reduce the CD reference plane yaw (k) misalignment, which shows as a pitch reading. This misalignment may require shims; however, keep in mind that this operation can change the reference plane in pitch and roll. Again, the intent is to reduce the misalignment and not zero them, which is much harder to do simultaneously for these three reference planes.
    c. Finaly place the CD to $p = 90°$ and $r = 0$ and reduce the orthogonal misalignment (d). This is done by placing shims at the top or bottom of the attachment bracket of the roll table base attachment bracket to the pitch rotary table face/plane, only in this position. The instrument readings do not help for adjusting this misalignment. The best approach is to convert the g_y obtained from Appendix C.4 and convert it to angle by calculating the ArcSin(g_y) * 180/Pi. Equation (14) shows that the CD g_y at this pitch and roll angle position is equal to the CD misalignments $b + k + d$. Assuming that b and k were reduced before this alignment, then d plus some residual misalignments remains. Nevertheless, the goal is to reduce the angle calculated with the ArcSin(g_y) by this orthogonal angle, d.

After reducing the CD misalignments, repeat the instrument calibration procedure and compare results. However, as mentioned above, this is not necessary since it is feasible to estimate the instrument coefficients to near true values with a CD with relatively large misalignments, as it is demonstrated in Example 6.

G.3: Examples setup

The inputs to the system math models in the paper are the 6 CD misalignments, the 12 instrument coefficients, and the calibration setpoints. To simplify this demonstration, the instrument's three accelerometer sensitivity and bias coefficients are fixed to a value for all examples. The remaining 12 parameters are varied for the examples but pegged to limits of the ranges to simulate the worst-case scenario. In addition, for demonstration purposes only, the input for a few examples will be exaggerated to stress this process. The results for the instrument coefficients obtained in the first estimate will have large errors relative to the true values; however, it is possible to correct most of these errors after correcting the sensitivity and bias coefficients as described in Section 2.4 of the paper. However, the *x*-axis sensitivity and bias coefficients may still have errors, which can be corrected by introducing second order terms, and the same goes for two accelerometers' offset angles, the *y*-axis yaw offset, and *z*-axis pitch offset.

These coefficients are biased by the two CD misalignments (*b* and *d*) that cannot be canceled using the method in Section 2.4. Some of this, such as the effects of the misalignments system roll, *b*, and orthogonal error between the rotary stages, *d*, to the sensitivity and bias estimates, is discussed in this paper. In addition, the examples will demonstrate how to correct for these two CD misalignments when their magnitude is greater than 0.1°.

Note, an in-depth derivation for these two methods is beyond the scope of this paper. Introducing a procedure as seen in Section 2.4 or showing the second order terms adds complexity to the paper. The main purpose is to show a potential solution for when the system misalignments (CD misalignments and the accelerometers' offset angles) are greater than 0.1°, which is the suggested limit for small angle approximation.

G.4: Brief description for each example

Table G-3 tabulates the input to the full model for each of the examples below. The first example demonstrates what happens if all the CD misalignments and instrument offset angles are exactly 0.1° and in the same direction, which is the worst-case scenario. The second example is a repeat of the first example with the magnitude of the CD misalignments kept at 0.1°and the instrument coefficient increases by a factor of 5 to 0.5°. The third example reduces the CD misalignments to 0.05° and the accelerometer offsets are kept at 0.5°, with the intent to show the improvement to the first estimates for the instrument coefficients. A reminder that the CD misalignments are nullable, but not an easy task to perform, thus attempts to do so can cause angle distortions in the system. Example 4 shows that it is possible to estimate the instrument coefficients within tolerance for the first estimate, when the CD misalignments are at 0.02° and the accelerometers' offset angles are at 0.2°. Example 5 has two parts; the first part demonstrates the results for the algebra solution and the second part is a repeat with the least square regression solution. Note that for this two-part example, the CD misalignments are reduced by a factor of 4 from the previous example, thus no surprises with the algebra solution; however, the magnitude of these misalignments for the least square solution is too large. The purpose is to show the advantage of the algebra solution over the least square solution, which requires the CD misalignments nulled. If the CD misalignments are nulled, then the two methods will result in near identical instrument coefficients. Finally, the last example, 6, exaggerates the system misalignments to 0.5°. This final example is to demonstrate the potential of estimating the instrument coefficients to within tolerance even with a system with large misalignments.

Table G-3 Example Input to the Full Model or Equation (A.2.10)

Example #	**CD Misalignments**	**Accelerometers offset angles**	**Method**
1	0.1°	0.1°	Algebra
2	0.1°	0.5°	Algebra
3	0.05°	0.5°	Algebra
4	0.02°	0.2°	Algebra
5	0.005°	0.2°	5.1 Algebra & 5.2 Least Square Regression
6	0.5°	0.5°	Algebra

G.4.1: Example 1. CD misalignments to 0.1° and accelerometers' offset angles to 0.1°

Table G-4 Table shows the output of the instrument for the 9-point calibration and two additional points to determine the CD misalignments. The table shows the order in which the data was collected, and it is identical to Table 2 in the paper. The voltage out is the result from using equation (A.2.10) with the system misalignments of 0.1°, as shown in the first column in Table G-5

Table G-4 The voltage output of a 3xAI for different p and r, and three mounting orientations

Output Using System Full Model						
Simulated 3xAI Voltage Output						
P^o	R^o	y^o	u^o	V_x(V)	V_y(V)	V_z(V)
Bottom Backwards						
0.	0.	180.	180.	-0.00168334	-0.00212731	-1.26208
0.	90.	180.	180.	0.00291355	1.29433	0.00582975
90.	0.	180.	180.	-1.30713	0.00013938	0.0102363
Top Backwards						
0.	0.	180.	0.	0.00291357	-0.00668447	1.26932
0.	90.	180.	0.	0.00747844	-1.30313	0.00139621
90.	0.	180.	0.	-1.30712	-0.0134687	0.00140776
Top Forwards						
0.	0.	0.	0.	0.0120353	0.00242184	1.26929
0.	90.	0.	0.	0.00287354	1.29432	-0.00302188
90.	0.	0.	0.	1.31748	0.00465688	-0.00303343
Addtional Points						
0.	180.	0.	0.	0.00290556	-0.0112021	-1.26208
180.	0.	0.	0.	-0.00169132	-0.0066845	-1.26208

Table G-5 Shows the input to the full model, and the results. The first column of numbers are the inputs to the model or true values. The second column top 12 parameters are the first estimate of the instrument coefficients using the first 9 points from Table G-4 and the bottom 6 parameters are for the CD misalignments using the 9-point data plus the two additional points in Table G-4. The third column of numbers are the errors of the estimated values relative to the first column (true values). The fourth column are a set of new estimates after normalizing the data with the accelerometers’ sensitivity and bias coefficients corrected for system misalignments as shown in Table G-6.

Table G-5 Example 1, first and second estimates of the 3xAI instrument coefficients and CD misalignments

Algebra Method–3xAI

Input To Model			Output From Algorithm		After Correcting S & B	
Instrument Coefficients			1st Estimted	Error	2nd Estimted	Error
x–axis	b_x	0.005184 V	0.00517599 V	-6.1 ug	0.00518 V	-3. ug
	S_x	1.31234 V/g	1.3123 V/g	-32. PPM	1.31234 V/g	-3. PPM
	p_x	0.1^{0}	0.1004^{0}	1.3"	0.1002^{0}	0.6"
	y_x	0.1^{0}	0.0997^{0}	-1.2"	0.0998^{0}	-0.6"
y–axis	b_y	-0.004398 V	-0.00440593 V	-6.1 ug	-0.004398 V	0. ug
	S_y	1.29874 V/g	1.29872 V/g	-9.2 PPM	1.29873 V/g	0. PPM
	r_y	0.1^{0}	0.1003^{0}	1.3"	0.1^{0}	0."
	y_y	0.1^{0}	0.0996^{0}	-1.3"	0.0996^{0}	-1.3"
z–axis	b_z	0.003613 V	0.00360527 V	-6.1 ug	0.003613 V	0. ug
	S_z	1.26571 V/g	1.26568 V/g	-21.3 PPM	1.26571 V/g	0. PPM
	p_z	0.1^{0}	0.1005^{0}	1.9"	0.1005^{0}	1.9"
	r_z	0.1^{0}	0.1^{0}	0."	0.1^{0}	0."
Calibration Device (CD)						
CD Misalignments			1st Estimted	1st Error	2nd Estimted	2nd Error
	a	0.1^{0}	0.1002^{0}	0.6"	0.1^{0}	0."
	b	0.1^{0}	0.1003^{0}	1.2"	0.1^{0}	0."
	e	0.1^{0}	0.099^{0}	-3.8"	0.0991^{0}	-3.1"
	f	0.1^{0}	0.1005^{0}	1.9"	0.1009^{0}	3.1"
	k	0.1^{0}	0.1011^{0}	3.8"	0.1009^{0}	3.1"
	d	0.1^{0}	0.0988^{0}	-4.4"	0.099^{0}	-3.8"
	#^{0} number in degrees #" number in ArcSecs					

The results in Table G-5 show that the first estimates for the instrument coefficients are within tolerance except for the accelerometers *x* and *z*-axis sensitivities. The reason for these elements exceeding tolerance is due to the combination of misalignments present in the system. These misalignments do not place the accelerometers within tolerance in ±1g field. The second estimate in Table G-5 shows improvement when using the sensitivity and bias coefficients corrected for system misalignments as shown in Table G-6. Table G-6 Tabulates the sensitivity and bias corrected for system misalignments, this table shows the estimated pitch and roll angles required to place each accelerometer near the 1g and -1g fields.

Table G-6 Example 1, sensitivity and bias corrected for system misalignments.

Correct Sentivity and Bias (S & B) for Misalignments					
P_{sb}^{O}	R_{sb}^{O}	±1g	2nd Estimate [Error]		* 3rd Estimate [Error]
x-axis accelerometer					
89.617	-45.101	1.31752	b_x	0.00518 V [-3.05 ug]	N/A
-90.383	-45.101	-1.30716	S_x	1.31234 V/g [-3.05 PPM]	N/A
y-axis accelerometer					
0.100523	89.6988	1.29434	b_y	-0.004398 V [0. ug]	N/A
-0.300876	-90.3012	-1.30313	S_y	1.29873 V/g [0. PPM]	N/A
z-axis accelerometer					
-0.299654	-0.300872	1.26932	b_z	0.003613 V [0. ug]	N/A
0.0993	179.699	-1.2621	S_z	1.26571 V/g [0. PPM]	N/A
* No correction to b_x and S_x					

G.4.2: Example 2. CD misalignments to 0.1° and accelerometers' offset angles to 0.5°

Table G-7 The voltage output of a 3xAI for different p and r, and three mounting orientations

Output Using System Full Model						
Simulated 3xAI Voltage Output						
P^{o}	R^{o}	y^{o}	u^{o}	V_x(V)	V_y(V)	V_z(V)
Bottom Backwards						
0.	0.	180.	180.	-0.0108763	-0.0112254	-1.26199
0.	90.	180.	180.	-0.00621609	1.29427	-0.0030068
90.	0.	180.	180.	-1.30705	-0.00889597	0.0190253
Top Backwards						
0.	0.	180.	0.	0.0121072	0.0023505	1.26929
0.	90.	180.	0.	0.0166081	-1.30307	0.0102326
90.	0.	180.	0.	-1.30701	-0.0225665	0.0102899
Top Forwards						
0.	0.	0.	0.	0.0211641	0.0115193	1.26914
0.	90.	0.	0.	-0.00632017	1.29419	-0.0118576
90.	0.	0.	0.	1.3173	0.0136912	-0.0119149
Addtional Points						
0.	180.	0.	0.	-0.00622367	-0.020268	-1.26196
180.	0.	0.	0.	-0.0108521	-0.0157824	-1.26196

Table G-8 Example 2, first and second estimates of the 3xAI instrument coefficients and CD misalignments.

Algebra Method–3xAI

Input To Model			Output From Algorithm		After Correcting S & B	
Instrument Coefficients			1st Estimted	Error	2nd Estimted	Error
x–axis	b_x	0.005184 V	0.00514396 V	-30.5 ug	0.00518 V	-3. ug
	S_x	1.31234 V/g	1.31216 V/g	-141.6 PPM	1.31234 V/g	-3. PPM
	p_x	0.5^o	0.5018^o	6.4 "	0.5001^o	0.5 "
	y_x	0.5^o	0.4983^o	-6.1 "	0.4998^o	-0.7 "
y–axis	b_y	-0.004398 V	-0.00443763 V	-30.5 ug	-0.004398 V	0. ug
	S_y	1.29874 V/g	1.29863 V/g	-82.4 PPM	1.29873 V/g	0. PPM
	r_y	0.5^o	0.5018^o	6.3 "	0.5^o	-0.1 "
	y_y	0.5^o	0.4983^o	-6.2 "	0.4982^o	-6.4 "
z–axis	b_z	0.003613 V	0.00357434 V	-30.5 ug	0.003613 V	0. ug
	S_z	1.26571 V/g	1.26556 V/g	-118.7 PPM	1.26571 V/g	0. PPM
	p_z	0.5^o	0.5026^o	9.5 "	0.5026^o	9.3 "
	r_z	0.5^o	0.5^o	0.2 "	0.5^o	0. "
Calibration Device (CD)						
CD Misalignments			1st Estimted	1st Error	2nd Estimted	2nd Error
	a	0.1^o	0.1016^o	5.7 "	0.1^o	0. "
	b	0.1^o	0.1017^o	6.3 "	0.1^o	0. "
	e	0.1^o	0.0962^o	-13.8 "	0.0977^o	-8.2 "
	f	0.1^o	0.1005^o	1.9 "	0.1023^o	8.1 "
	k	0.1^o	0.1038^o	13.9 "	0.1023^o	8.1 "
	d	0.1^o	0.096^o	-14.5 "	0.0976^o	-8.8 "
	$\#^O$ number in degrees #" number in ArcSecs					

The results in Table G-8 show that the first estimate shows all the instrument coefficients are out of tolerance except for the *z*-axis accelerometer r_z offset. The errors are due to the larger than expected accelerometers' offset angles, which exceed the constraints presented in the paper. However, if the sensitivity and bias coefficients for the accelerometers are corrected for the system misalignments (CD misalignments and accelerometers offset angles) shown in Table G-9, then the second estimate shows an improvement for most of the accelerometers' coefficients, except for *y*-axis and *z*-axis accelerometers' offset angles, y_y offset and p_z offset, respectively. The reason why these two offsets end out of tolerance is related to second order elements not covered in this paper. This paper deems all second order terms negligible due to their small values. As demonstrated in this paper, the product of two system misalignments of magnitudes within ±0.1° (i.e., (0.0017(radians))^2 = 3E-6), which is a very small number. For clarification, the results are not in radians squared since the elements are the product of the first order Taylor Series for a Sine function, as explained at the end of this example.

What is the solution when the instrument accelerometers' offset angles, which are not adjustable, are outside the ±0.1° range? Examples 3 through 5 answer this question. The examples will show that as the magnitude of the CD misalignments are reduced, then the estimates for the instrument coefficients are improved or vice versa. Based on simulations when the CD misalignments are within ±0.02° (72" (arcsecs)), and the accelerometers' offset angles are within 0.2°, it is possible to estimate the instrument coefficients to within tolerance in the first estimate. Table G-2 shows that the minimum CD misalignments to perform a single mount least square regression are ±0.0005° (2") or 40 times smaller than the amount chosen for Example 4, which estimates the instrument coefficients within tolerance when using the method in the paper.

A potential second solution for correcting these second order terms is using the misalignments that affect the estimates of these two parameters. The following demonstration is outside the scope of the paper and has not been vetted for all combinations of CD misalignments magnitude and directions. However, it presents an interesting alternative to nullifying the CD misalignments, and for these examples, it showed improvement to these coefficients.

Converting all the parameters to radians, then the third estimate for y_y , Equation (G.1)

$$y_{y3rd} = y_{y2nd} + (\mathrm{a}_{2nd} + e_{2nd})r_{y2nd} \ \ (radians) \tag{G.1}$$

The third estimate for p_z , Equation (G.2)

$$p_{z3rd} = p_{z2nd} - (\mathrm{b}_{2nd} + d_{2nd} + k_{2nd})r_{z2nd} \ (radians) \tag{G.2}$$

The explanation for these terms is that the accelerometers, at the required angle position (pitch and roll) to estimate these coefficients rotates the accelerometer sensitive axis relative to itself. For instance, the *y*-axis accelerometer when the instrument is placed in 90° pitch and 0 roll, is rotated relative to its own axis (*y*-axis) by the system pitch angle, *a*, and pitch reference angle, *e*, then it is rotated again relative to *x*-axis in roll, r_y, forming a compound angle, Equation (G.1). The same can be described for p_z, which at the same angle position, 90° pitch and 0 roll, is rotated relative to its own axis (*z*-axis) by system roll, *b*, orthogonal angle, *d*, and reference yaw, *k*. Then it is rotated again relative to x-axis in roll, r_z, forming a compound angle, Equation (G.2). To reiterate, the second order terms are the product of two Sine functions and not of two angles in radians, for instance, the yaw offset angle second order elements are $(\mathrm{Sin}[a_{2nd}] + Sin[e_{2nd}])\ Sin[r_{y2nd}]$.

Table G-9 Example 2, sensitivity and bias corrected for system misalignments.

Correct Sentivity and Bias (S & B) for Misalignments					
$P_{sb}{}^{O}$	$R_{sb}{}^{O}$	±1g	2nd Estimate [Error]		⋆ 3rd Estimate [Error]
x–axis accelerometer					
89.0498	-45.101	1.31752	b_x	0.00518 V [-3.05 ug]	N/A
-90.9502	-45.101	-1.30716	S_x	1.31234 V/g [-3.05 PPM]	N/A
y–axis accelerometer					
0.500549	89.296	1.29434	b_y	-0.004398 V [0. ug]	N/A
-0.703702	-90.704	-1.30313	S_y	1.29873 V/g [0. PPM]	N/A
z–axis accelerometer					
-0.700378	-0.70231	1.26932	b_z	0.003613 V [0. ug]	N/A
0.497225	179.298	-1.2621	S_z	1.26571 V/g [0. PPM]	N/A
⋆ No correction to b_x and S_x					

G.4.3: Example 3. CD misalignments to 0.05^O and accelerometers' offset angles to 0.5^O

Table G-10 The voltage output of a 3xAI for different p and r, and three mounting orientations.

Output Using System Full Model						
Simulated 3xAI Voltage Output						
P^O	**R^O**	**y^O**	**u^O**	**$V_x(V)$**	**$V_y(V)$**	**$V_z(V)$**
Bottom Backwards						
0.	0.	180.	180.	-0.00857503	-0.0134812	-1.262
0.	90.	180.	180.	-0.00624518	1.29426	-0.00522144
90.	0.	180.	180.	-1.30706	-0.0123128	0.0168397
Top Backwards						
0.	0.	180.	0.	0.0143685	0.00464573	1.26926
0.	90.	180.	0.	0.0166192	-1.30305	0.0124474
90.	0.	180.	0.	-1.30704	-0.01915	0.0124759
Top Forwards						
0.	0.	0.	0.	0.018903	0.00922426	1.26919
0.	90.	0.	0.	-0.00629118	1.29422	-0.00964307
90.	0.	0.	0.	1.31737	0.0103144	-0.00967154
Addtional Points						
0.	180.	0.	0.	-0.00624675	-0.0179985	-1.26198
180.	0.	0.	0.	-0.00855901	-0.0157538	-1.26198

Table G-11 Example 3, first and second estimates of the 3xAI instrument coefficients and CD misalignments.

Algebra Method–3xAI

Input To Model			Output From Algorithm		After Correcting S & B	
Instrument Coefficients			1st Estimted	Error	2nd Estimted	Error
x–axis	b_x	0.005184 V	0.005164 V	-15.2 ug	0.005183 V	-0.8 ug
	S_x	1.31234 V/g	1.31221 V/g	-103.9 PPM	1.31234 V/g	-0.8 PPM
	p_x	0.5^0	0.5009^0	3.2 "	0.5^0	0.1 "
	y_x	0.5^0	0.4992^0	-3. "	0.4999^0	-0.2 "
y–axis	b_y	-0.004398 V	-0.0044178 V	-15.2 ug	-0.004398 V	0. ug
	S_y	1.29874 V/g	1.29863 V/g	-77.7 PPM	1.29873 V/g	0. PPM
	r_y	0.5^0	0.5009^0	3.2 "	0.5^0	-0.1 "
	y_y	0.5^0	0.4992^0	-3. "	0.4991^0	-3.2 "
z–axis	b_z	0.003613 V	0.0035937 V	-15.2 ug	0.003613 V	0. ug
	S_z	1.26571 V/g	1.26559 V/g	-94.4 PPM	1.26571 V/g	0. PPM
	p_z	0.5^0	0.5013^0	4.8 "	0.5013^0	4.6 "
	r_z	0.5^0	0.5^0	0.1 "	0.5^0	0. "
Calibration Device (CD)						
CD Misalignments			1st Estimted	1st Error	2nd Estimted	2nd Error
	a	0.05^0	0.0508^0	3. "	0.05^0	0. "
	b	0.05^0	0.0509^0	3.1 "	0.05^0	0. "
	e	0.05^0	0.0482^0	-6.6 "	0.049^0	-3.6 "
	f	0.05^0	0.0501^0	0.5 "	0.051^0	3.6 "
	k	0.05^0	0.0518^0	6.6 "	0.051^0	3.6 "
	d	0.05^0	0.0481^0	-6.8 "	0.049^0	-3.8 "
	$\#^O$ number in degrees #" number in ArcSecs					

Table G-11 shows an improvement relative to Example 2 since the CD misalignments are half of the magnitude used in that example. Except for the same two accelerometers' offset angles in Example 2, which are affected by the system roll, *b*, and orthogonal misalignment *d*.

The next example will reduce the CD misalignments by another factor of 2.5.

Table G-12 Example 3, sensitivity and bias corrected for system misalignments

Correct Sentivity and Bias (S & B) for Misalignments					
$P_{sb}{}^{O}$	$R_{sb}{}^{O}$	±1g		2nd Estimate [Error]	* 3rd Estimate [Error]
x–axis accelerometer					
89.1713	-45.05	1.31752	b_x	0.005183 V [-0.76 ug]	N/A
-90.8287	-45.05	-1.30716	S_x	1.31234 V/g [-0.76 PPM]	N/A
y–axis accelerometer					
0.500161	89.3981	1.29434	b_y	-0.004398 V [0. ug]	N/A
-0.601822	-90.6019	-1.30313	S_y	1.29873 V/g [0. PPM]	N/A
z–axis accelerometer					
-0.600326	-0.601041	1.26932	b_z	0.003613 V [0. ug]	N/A
0.498665	179.399	-1.2621	S_z	1.26571 V/g [0. PPM]	N/A
* No correction to b_x and S_x					

G.4.4: Example 4 CD misalignments to 0.02^O and accelerometers' offset angles to 0.2^O

Table G-13 The voltage output of a 3xAI for different p and r, and three mounting orientations

Output Using System Full Model						
Simulated 3xAI Voltage Output						
P^O	R^O	y^O	u^O	$V_x(V)$	$V_y(V)$	$V_z(V)$
Bottom Backwards						
0.	0.	180.	180.	-0.000315794	-0.00802741	-1.26208
0.	90.	180.	180.	0.000606752	1.29432	0.000078774
90.	0.	180.	180.	-1.30714	-0.0075684	0.00891043
Top Backwards						
0.	0.	180.	0.	0.0088524	-0.000774913	1.26931
0.	90.	180.	0.	0.00976221	-1.30312	0.00714722
90.	0.	180.	0.	-1.30714	-0.0102945	0.00715182
Top Forwards						
0.	0.	0.	0.	0.0106774	0.00104572	1.2693
0.	90.	0.	0.	0.000599394	1.29432	-0.00168908
90.	0.	0.	0.	1.3175	0.00149212	-0.00169368
Addtional Points						
0.	180.	0.	0.	0.000606459	-0.00983824	-1.26208
180.	0.	0.	0.	-0.000313234	-0.00893504	-1.26208

Table G-14 Results from applying the algebra method to Example 4

Algebra Method–3xAI

Input To Model			Output From Algorithm		After Correcting S & B	
Instrument Coefficients			1st Estimted	Error	2nd Estimted	Error
x-axis	b_x	0.005184 V	0.0051808 V	-2.4 ug	0.00518384 V	-0.1 ug
	S_x	1.31234 V/g	1.31232 V/g	-16.6 PPM	1.31234 V/g	-0.1 PPM
	p_x	0.2^0	0.2001^0	0.5 "	0.2^0	0. "
	y_x	0.2^0	0.1999^0	-0.5 "	0.2^0	0. "
y-axis	b_y	-0.004398 V	-0.00440117 V	-2.4 ug	-0.004398 V	0. ug
	S_y	1.29874 V/g	1.29872 V/g	-12.4 PPM	1.29873 V/g	0. PPM
	r_y	0.2^0	0.2001^0	0.5 "	0.2^0	0. "
	y_y	0.2^0	0.1999^0	-0.5 "	0.1999^0	-0.5 "
z-axis	b_z	0.003613 V	0.00360991 V	-2.4 ug	0.003613 V	0. ug
	S_z	1.26571 V/g	1.26569 V/g	-15.1 PPM	1.26571 V/g	0. PPM
	p_z	0.2^0	0.2002^0	0.8 "	0.2002^0	0.8 "
	r_z	0.2^0	0.2^0	0. "	0.2^0	0. "
Calibration Device (CD)						
CD Misalignments			1st Estimted	1st Error	2nd Estimted	2nd Error
	a	0.02^0	0.0201^0	0.5 "	0.02^0	0. "
	b	0.02^0	0.0201^0	0.5 "	0.02^0	0. "
	e	0.02^0	0.0197^0	-1.1 "	0.0198^0	-0.6 "
	f	0.02^0	0.02^0	0.1 "	0.0202^0	0.6 "
	k	0.02^0	0.0203^0	1.1 "	0.0202^0	0.6 "
	d	0.02^0	0.0197^0	-1.1 "	0.0198^0	-0.6 "
	$\#^O$ number in degrees #" number in ArcSecs					

Table G-14 shows that the results in the first estimate are within tolerance, when the CD misalignments are within ±0.02° or ±72". This is acceptable, and it is possible to improve the coefficient by correcting the sensitivity and bias estimates from Table G-15 as shown in the second estimate in Table G-14

The next example demonstrates how the CD residual (not nullified) misalignments can bias the instrument coefficients when the least square regression method is applied.

Table G-15 Example 4, sensitivity and bias corrected for system misalignments

Correct Sentivity and Bias (S & B) for Misalignments					
$P_{sb}{}^{O}$	$R_{sb}{}^{O}$	±1g	2nd Estimate [Error]		* 3rd Estimate [Error]
x-axis accelerometer					
89.6687	-45.02	1.31753	b_x	0.00518384 V [-0.12 ug]	N/A
-90.3313	-45.02	-1.30716	S_x	1.31234 V/g [-0.12 PPM]	N/A
y-axis accelerometer					
0.200023	89.7597	1.29434	b_y	-0.004398 V [0. ug]	N/A
-0.240288	-90.2403	-1.30313	S_y	1.29873 V/g [0. PPM]	N/A
z-axis accelerometer					
-0.24005	-0.240163	1.26932	b_z	0.003613 V [0. ug]	N/A
0.199785	179.76	-1.2621	S_z	1.26571 V/g [0. PPM]	N/A
* No correction to b_x and S_x					

G.4.5: Example 5-1 CD misalignments to 0.005° and accelerometers' offset angles to 0.2°

The goal for the following two examples (5-1 and 5-2) is to compare the results between the algebric method and the least square regression method. The CD misalignments are ten times larger than the max acceptable misalignments for the least square regression methiod.

Table G-16 The voltage output of a 3xAI for different p and r, and three mounting orientations

Output Using System Full Model						
Simulated 3xAI Voltage Output						
P^{O}	R^{O}	y^{O}	u^{O}	$V_x(V)$	$V_y(V)$	$V_z(V)$
Bottom Backwards						
0.	0.	180.	180.	0.000373286	-0.0087055	-1.26208
0.	90.	180.	180.	0.000603901	1.29432	-0.000584231
90.	0.	180.	180.	-1.30714	-0.00859065	0.0082509
Top Backwards						
0.	0.	180.	0.	0.00953669	-0.0000920866	1.26931
0.	90.	180.	0.	0.00976416	-1.30312	0.00781023
90.	0.	180.	0.	-1.30714	-0.00927222	0.00781136
Top Forwards						
0.	0.	0.	0.	0.00999311	0.000362893	1.26931
0.	90.	0.	0.	0.000602242	1.29432	-0.00102608
90.	0.	0.	0.	1.31751	0.000474634	-0.00102721
Addtional Points						
0.	180.	0.	0.	0.000603909	-0.00915808	-1.26208
180.	0.	0.	0.	0.000374046	-0.00893222	-1.26208

Table G-17 Example 5-1, first and second estimates of the 3xAI instrument coefficients and CD misalignments.

Algebra Method–3xAI

Input To Model			Output From Algorithm		After Correcting S & B	
Instrument Coefficients			1st Estimted	Error	2nd Estimted	Error
x–axis	b_x	0.005184 V	0.0051832 V	−0.6 ug	0.005184 V	0. ug
	S_x	1.31234 V/g	1.31232 V/g	−13.2 PPM	1.31234 V/g	0. PPM
	p_x	0.2^0	0.2^0	0.1 "	0.2^0	0. "
	y_x	0.2^0	0.2^0	−0.1 "	0.2^0	0. "
y–axis	b_y	−0.004398 V	−0.00439879 V	−0.6 ug	−0.004398 V	0. ug
	S_y	1.29874 V/g	1.29872 V/g	−12.2 PPM	1.29873 V/g	0. PPM
	r_y	0.2^0	0.2^0	0.1 "	0.2^0	0. "
	y_y	0.2^0	0.2^0	−0.1 "	0.2^0	−0.1 "
z–axis	b_z	0.003613 V	0.00361223 V	−0.6 ug	0.003613 V	0. ug
	S_z	1.26571 V/g	1.26569 V/g	−12.8 PPM	1.26571 V/g	0. PPM
	p_z	0.2^0	0.2001^0	0.2 "	0.2001^0	0.2 "
	r_z	0.2^0	0.2^0	0. "	0.2^0	0. "
Calibration Device (CD)						
CD Misalignments			1st Estimted	1st Error	2nd Estimted	2nd Error
	a	0.005^0	0.005^0	0.1 "	0.005^0	0. "
	b	0.005^0	0.005^0	0.1 "	0.005^0	0. "
	e	0.005^0	0.0049^0	−0.2 "	0.005^0	−0.1 "
	f	0.005^0	0.005^0	0. "	0.005^0	0.1 "
	k	0.005^0	0.0051^0	0.2 "	0.005^0	0.1 "
	d	0.005^0	0.0049^0	−0.3 "	0.005^0	−0.1 "
	$\#^O$ number in degrees #" number in ArcSecs					

The results in Table G-17 show that the instrument coefficients are within tolerance in the first estimate. In addition, by correcting sensitivity and bias coefficients for the instrument offset angle the second estimate results are much closer to the instrument coefficients true values.

Table G-18 Example 5-1, sensitivity and bias corrected for system misalignments

Correct Sentivity and Bias (S & B) for Misalignments					
P_{sb} O	R_{sb} O	±1g	2nd Estimate [Error]		* 3rd Estimate [Error]
x–axis accelerometer					
89.7051	-46.402	1.31753	b_x	0.005184 V [0. ug]	N/A
-90.2949	-46.402	-1.30716	S_x	1.31234 V/g [0. PPM]	N/A
y–axis accelerometer					
0.200003	89.7899	1.29434	b_y	-0.004398 V [0. ug]	N/A
-0.210072	-90.2101	-1.30313	S_y	1.29873 V/g [0. PPM]	N/A
z–axis accelerometer					
-0.210017	-0.210038	1.26932	b_z	0.003613 V [0. ug]	N/A
0.199948	179.79	-1.2621	S_z	1.26571 V/g [0. PPM]	N/A
* No correction to b_x and S_x					

G.4.6: Example 5-2 Repeat Example 5-1, solve with a least square regression

In this demonstration, a least square calibration is performed using the same inputs as before and with a different set of calibration setpoints. This subject was covered in Reference 1. The demonstration here is based on the current view that the CD misalignments are never nullified to zero. The absolute values (relative to gravity) for the CD misalignments are not known to a high accuracy. There are existing procedures to verify that the CD alignment with the gravity vector is within an acceptable range.

Table G-19 The voltage output of a 3xAI for different p and r, and one mounting orientation

Output Using System Full Model						
Simulated 3xAI Voltage Output						
P^O	R^O	y^O	u^O	$V_x(V)$	$V_y(V)$	$V_z(V)$
12	162	0	0	0.2723571	0.3846639	−1.176159
9	108	0	0	0.2047457	1.214801	−0.3877712
−12	54	0	0	−0.2685689	1.025105	0.7286128
21	72	0	0	0.4727707	1.151733	0.3629572
18	126	0	0	0.4045861	0.9935855	−0.7089124
−30	180	0	0	−0.6549454	−0.01080226	−1.090302
−24	−126	0	0	−0.5275322	−0.9687083	−0.6708100
−3	−90	0	0	−0.05869360	−1.301585	0.008476353
27	−108	0	0	0.6037564	−1.104100	−0.3429295
30	−72	0	0	0.6665701	−1.070399	0.3439388
15	−144	0	0	0.3439473	−0.7442807	−0.9839611
6	−54	0	0	0.1489960	−1.046041	0.7467554
0	−36	0	0	0.01185692	−0.7639135	1.030307
−18	−18	0	0	−0.3946111	−0.3832499	1.151230
3	18	0	0	0.07698958	0.4011467	1.204034
−6	36	0	0	−0.1308455	0.7581303	1.019749
−15	0	0	0	−0.3298253	−0.001027266	1.227380
−9	−162	0	0	−0.2029724	−0.4059712	−1.183211
24	90	0	0	0.5347691	1.183884	−0.002521421
−27	144	0	0	−0.5963410	0.6702884	−0.9091414

Table G-20 Results from applying the least square regression method to example 5-2

Least Square Regression Method–3xAl

Input To Model			Output From Algorithm			
Instrument Coefficients			Estimted Values		Error	
x–axis	b_x	0.005184	b_{xe}(V)	0.00529291	(ug)	-82.9897
	s_x	1.31234	s_{xe}(V/g)	1.31234	(PPM)	0.191466
	p_x	0.2	$p_{xe}{}^{O}$	0.20508	(ArcSecs)	18.288
	y_x	0.2	$y_{xe}{}^{O}$	0.20501	(ArcSecs)	18.036
y–axis	b_y	-0.004398	b_{ye}(V)	-0.00439869	(ug)	0.53237
	s_y	1.29874	s_{ye}(V/g)	1.29872	(PPM)	14.2003
	r_y	0.2	$r_{ye}{}^{O}$	0.2098	(ArcSecs)	35.28
	y_y	0.2	$y_{ye}{}^{O}$	0.20438	(ArcSecs)	15.768
z–axis	b_z	0.003613	b_{ze}(V)	0.00361102	(ug)	1.56058
	s_z	1.26571	s_{ze}(V/g)	1.26572	(PPM)	-10.8101
	p_z	0.2	$p_{ze}{}^{O}$	0.20337	(ArcSecs)	12.132
	r_z	0.2	$r_{ze}{}^{O}$	0.21092	(ArcSecs)	39.312
Calibration Device (CD)						
CD Misalignments			Estimted Values		Error	
	a^{O}	0.005	$a_e{}^{O}$	N/C	ArcSec	N/C
	b^{O}	0.005	$b_e{}^{O}$	N/C	ArcSec	N/C
	e^{O}	0.005	$e_e{}^{O}$	N/C	ArcSec	N/C
	f^{O}	0.005	$f_e{}^{O}$	N/C	ArcSec	N/C
	k^{O}	0.005	$k_e{}^{O}$	N/C	ArcSec	N/C
	d^{O}	0.005	$d_e{}^{O}$	N/C	ArcSec	N/C
	N/C Not-Computable with this method					

The results in Table G-20 show that most of the instrument coefficients are out of tolerance. The reference misalignments are transferred to the instrument coefficients with identical characteristics. For instance, the reference pitch misalignment, *e*, is transferred to the two accelerometers pitch offsets (*x*-axis p_x and *z*-axis p_z). The reference roll plus the system roll angle, *b*, is transferred to the two accelerometer roll offsets (*y*-axis r_y and *z*-axis r_z). The same goes for when the reference yaw misalignment is transferred to the two accelerometers' yaw offsets (*x*-axis y_x, and *y*-axis y_y). Finally, the system pitch, *a*, is transferred to the *x*-axis bias. Again, this is explained in Appendix A of Reference 1. Note that the instrument coefficient matrix in Reference 1 has a typo in the *z*-axis accelerometer bias, it should be zero.

Borrowing from the coefficient matrix in Reference 1, which uses a different set of calibration points to the ones shown in the example, the results shown above approximate the following matrix, Equation (G.3). Due to the calibration points chosen for the least square regression, a direct substitute will render a different result. This is mainly because the pitch setpoints are limited to +/-30°. If orthogonal setpoints identical to Appendix E for the top forward mount were used, then other dynamics occur, thus the matrix will remain the same except for the system misalignments, *a* and *b*, which will not show in the results.

$$\begin{bmatrix} b_x + a & b_y & b_z \\ S_x\left(1 - \frac{(y_x + k)^2}{2} - \frac{(p_x + e)^2}{2}\right) & (y_y + k)S_y & -(p_z + e)\, S_z \\ -(y_x + k)\, S_x & S_y\left(1 - \frac{(y_y + k)^2}{2} - \frac{(r_y + b + f)^2}{2}\right) & -(r_z + b + \mathrm{f})S_z \\ (p_x + e)\, S_x & (r_y + b + \mathrm{f})\, S_y & S_z\left(1 - \frac{(p_z + e)^2}{2} - \frac{(r_z + b + f)^2}{2}\right) \end{bmatrix} \tag{G.3}$$

G.4.7: Example 6 CD misalignments to 0.5° and accelerometers' offset angles to 0.5°

This example demonstrates it is possible to apply this method to a CD with misalignments of 0.5° and accelerometers' offset angles of 0.5°. This example requires that the two accelerometers' offset angles, as in Example 2, and the *x*-axis sensitivity and bias coefficients get corrected using the second order terms.

Table G-21 The voltage output of a 3xAI for different p and r, and three mounting orientations

Output Using System Full Model						
Simulated 3xAI Voltage Output						
P^O	R^O	y^O	u^O	$V_x(V)$	$V_y(V)$	$V_z(V)$
Bottom Backwards						
0.	0.	180.	180.	−0.0290644	0.00703563	−1.26162
0.	90.	180.	180.	−0.00576465	1.29424	0.0148452
90.	0.	180.	180.	−1.3065	0.0183661	0.0366424
Top Backwards						
0.	0.	180.	0.	−0.00576291	−0.016222	1.26923
0.	90.	180.	0.	0.016733	−1.30303	−0.0076242
90.	0.	180.	0.	−1.30631	−0.0498177	−0.0073376
Top Forwards						
0.	0.	0.	0.	0.0390275	0.0300851	1.26846
0.	90.	0.	0.	−0.0067682	1.29383	−0.0297063
90.	0.	0.	0.	1.31628	0.0406228	−0.0299929
Addtional Points						
0.	180.	0.	0.	−0.0059636	−0.0384907	−1.26161
180.	0.	0.	0.	−0.0292625	−0.0162254	−1.26161

Table G-22 Example 6, first and second estimates of the 3xAI instrument coefficients and CD misalignments.

Algebra Method–3xAI

Input To Model			Output From Algorithm		After Correcting S & B	
Instrument Coefficients			1st Estimted	Error	2nd Estimted	Error
x–axis	b_x	0.005184 V	0.00498242 V	-153.6 ug	0.0050898 V	-71.8 ug
	S_x	1.31234 V/g	1.31129 V/g	-799.5 PPM	1.31225 V/g	-71.9 PPM
	p_x	0.5^{0}	0.509^{0}	32.5 "	** 0.4998^{0}	-0.8 "
	y_x	0.5^{0}	0.4915^{0}	-30.6 "	** 0.5^{0}	-0.1 "
y–axis	b_y	-0.004398 V	-0.00459749 V	-153.6 ug	-0.00439785 V	0.1 ug
	S_y	1.29874 V/g	1.29843 V/g	-233.1 PPM	1.29873 V/g	-0.2 PPM
	r_y	0.5^{0}	0.5087^{0}	31.5 "	0.4998^{0}	-0.7 "
	y_y	0.5^{0}	0.4911^{0}	-32.2 "	0.4909^{0}	-32.6 "
z–axis	b_z	0.003613 V	0.00341773 V	-154.3 ug	0.00361297 V	0. ug
	S_z	1.26571 V/g	1.26504 V/g	-531. PPM	1.26571 V/g	-0.2 PPM
	p_z	0.5^{0}	0.513^{0}	47. "	0.5128^{0}	46. "
	r_z	0.5^{0}	0.5001^{0}	0.2 "	0.4998^{0}	-0.7 "
Calibration Device (CD)						
CD Misalignments			1st Estimted	1st Error	2nd Estimted	2nd Error
	a	0.5^{0}	0.5046^{0}	16.7 "	** 0.4954^{0}	-16.6 "
	b	0.5^{0}	0.5087^{0}	31.2 "	** 0.4997^{0}	-0.9 "
	e	0.5^{0}	0.4739^{0}	-94. "	** 0.4824^{0}	-63.5 "
	f	0.5^{0}	0.513^{0}	46.9 "	** 0.5217^{0}	78.2 "
	k	0.5^{0}	0.5266^{0}	95.6 "	** 0.5173^{0}	62.3 "
	d	0.5^{0}	0.4691^{0}	-111.1 "	** 0.4782^{0}	-78.6 "
	#^{O} number in degrees #" number in ArcSecs				** Computed after normalizing x-axis voltages with 3rd estimate for b_x and S_x	

Table G-22 shows that second estimates, which the sensitivity and bias coefficients are normally corrected for the system misalignments, is not sufficient to estimate the instrument coefficients.

To improve these estimates requires that the x-axis sensitivity and bias get corrected a third time for the two CD misalignments *b* and *d*, which were mentioned at the end of Section 2.4.2 and shown in Table G-23. The terms with the two asterisks are estimated using this third estimate for the x-axis sensitivity and bias coefficients. In addition, the errors in *y*-axis y_y and *z*-axis p_z are corrected the same way as demonstrated in Example 2.

What this example demonstrates is that it is possible to estimate the instrument coefficients using the algebraic method even when the CD and accelerometers' offset angles are much larger than 0.1°. It does require correcting the accelerometers sensitivity and bias coefficients for the system misalignments, including second order terms created by the system roll and the orthogonal angle, *b* and *d* respectively.

Table G-23 Example 6, Correcting the sensitivity and bias coefficients for the system misalignments, including the system roll and the orthogonal angle, *b* and *d* respectively.

Correct Sentivity and Bias (S & B) for Misalignments					
$P_{sb}{}^{O}$	$R_{sb}{}^{O}$	±1g	2nd Estimate [Error]		* 3rd Estimate [Error]
x–axis accelerometer					
88.0803	-46.659	1.31734	b_x	0.0050898 V [-71.78 ug]	0.00518519 [0.91 ug]
-91.9197	-46.659	-1.30716	S_x	1.31225 V/g [-71.91 PPM]	1.31234 [1.02 PPM]
y–axis accelerometer					
0.512984	88.4696	1.29434	b_y	-0.00439785 V [0.12 ug]	N/A
-1.52228	-91.5304	-1.30313	S_y	1.29873 V/g [-0.17 PPM]	N/A
z–axis accelerometer					
-1.49159	-1.52176	1.26932	b_z	0.00361297 V [-0.02 ug]	N/A
0.482295	178.478	-1.2621	S_z	1.26571 V/g [-0.17 PPM]	N/A
* $S_{x3rd} = S_{x2nd}/(1-\frac{b^2}{2}-\frac{d^2}{2})$; $b_{x3rd} = b_{x2nd} + S_{x3rd}*b*d$ Correcting the 2nd estimate of S_x and b_x with the first estimate for b and d					

A few clarification points to close this appendix. Equation (G.4) is the result of the least square regression for an unbiased 3xAI when the accelerometers' offset angles are > 0.1°. Equation B.6 in Appendix B.1.3 is a case for Equation (G.4) when the accelerometers' offset angles are < 0.1°, where the elements in the parenthesis for diagonal parameter are approximately equal to one.

$$\begin{bmatrix} b_x & b_y & b_z \\ S_x\left(1-\frac{y_x^2}{2}-\frac{p_x^2}{2}\right) & y_y S_y & -p_z\, S_z \\ -y_x\, S_x & S_y\left(1-\frac{y_y^2}{2}-\frac{r_y^2}{2}\right) & -r_z\, S_z \\ p_x\, S_x & r_y\, S_y & S_z\left(1-\frac{p_z^2}{2}-\frac{r_z^2}{2}\right) \end{bmatrix} \tag{G.4}$$

The estimate for the accelerometers' sensitivity coefficient for the least square regression method is the root mean square for each of the lower 3x3 matrix column vectors, Equation (G.5).

$$\begin{aligned} x-axis\ sensitivity &= \hat{S}_x\sqrt{\left(1-\frac{y_x^2}{2}-\frac{p_x^2}{2}\right)^2+y_x^2+p_x^2} \cong \overline{S}_x \\ y-axis\ sensitivity &= \hat{S}_y\sqrt{\left(1-\frac{y_y^2}{2}-\frac{r_y^2}{2}\right)^2+y_y^2+r_y^2} \cong \overline{S}_y \\ z-axis\ sensitivity &= \hat{S}_z\sqrt{\left(1-\frac{p_z^2}{2}-\frac{r_z^2}{2}\right)^2+p_z^2+r_z^2} \cong \overline{S}_z \end{aligned} \tag{G.5}$$

Note, when the accelerometers' offset angles are > 0.1°, the coefficient matrix for the instrument has a different representation. This new representation shown in Equation (G.6) adjusts the diagonal elements for accelerometers' offset angles, therefore it requires substituting the last two matrices in Equation (A.3.5) with Equation (G.6) when the offset angles are > 0.1°. This representation is not new since it was presented as Equation (A.1.24) in Appendix A.1.4.2 without using a small angle approximation. The elements in Equation (A.1.25) can be substituted with the Taylor series resulting in Equation (G.6) with the diagonal elements from Equation (A.1.26).

$$\begin{bmatrix} \left(1-\frac{y_x^2}{2}-\frac{p_x^2}{2}\right) & y_y & -p_z \\ -y_x & \left(1-\frac{y_y^2}{2}-\frac{r_y^2}{2}\right) & -r_z \\ p_x & r_y & \left(1-\frac{p_z^2}{2}-\frac{r_z^2}{2}\right) \end{bmatrix}\begin{bmatrix} S_x & 0 & 0 \\ 0 & S_y & 0 \\ 0 & 0 & S_z \end{bmatrix} \tag{G.6}$$